Evaluating nuclear magnetic resonance (NMR) as a robust absolute reference method for water holding capacity (WHC) of pork meat

Evaluering av kjernemagnetisk resonans (NMR) som en robust absolutt referansemetode for vannbindingsevne (VBE) i svinekjøtt

Philosophiae Doctor (PhD) Thesis

Han Zhu

Department of Chemistry, Biotechnology and Food Science
Norwegian University of Life Sciences

Ås 2016

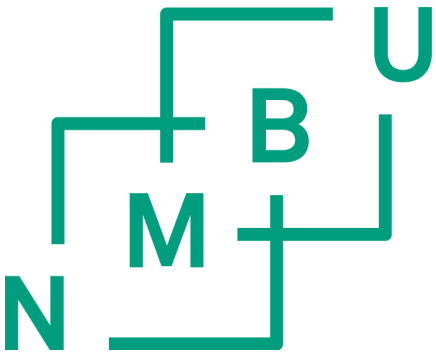

Thesis number 2016:64
ISSN 1894-6402
ISBN 978-82-575-1383-2

Preface

This thesis reports the work carried out during the period from 2013 to 2016. The project was funded through the industrial PhD scheme by the Research Council of Norway and Nortura SA. Project partners included University of Oslo, SINTEF and Norwegian University of Life Sciences (NMBU).

First and foremost, I want to express my sincere gratitude to my supervisors, Bjørg Egelandsdal, Eddy Walther Hansen and Marion O'Farrell for all their valuable help and continuous support throughout this project. I am grateful for their patience, motivation and immense knowledge. Furthermore, I would like to thank Per Berg from Nortura SA for giving me the opportunity to start this project and all the assistance.

For their great cooperation, I would like to thank Frøydis Bjerke, André Backer, Kathrine Lunde and Ole Alvseike from Animalia, Petter Vejle Andersen, Frank Lundby, Jens Petter Wold and Eva Veiseth-Kent from Nofima. Eli Gjerlaug-Enger from Norsvin is acknowledged for her help and discussion during the project. I would also like to thank Kari Anne Hestnes Bakke, Jon Tschudi and Gregory Bouquet from SINTEF for their kind support during my visits to SINTEF. For his valuable comments of this thesis, I would like to thank Pedro Araujo from NIFES. I wish to thank my former and current colleges at the environmental chemistry group at the Department of Chemistry (UiO), Cathrine, Emilie, Frøydis, Lena, Liang and others for their company and nice lunch breaks.

I am also deeply indebted to my family and friends for their patience and encouragement. Finally, thanks to Stian, for being there and always supporting me.

Han Zhu

Oslo, June 2016

Summary

Water holding capacity (WHC) is among the most important quality traits of meat. However, the mechanism behind WHC continues to be poorly understood and online measurement has yet to be achieved in the meat industry. The overall objectives of this thesis were to advance the understanding of WHC in meat (specifically the changes of different water domains during drip production process) using nuclear magnetic resonance (NMR) proton T_2 relaxometry, and to investigate the suitability of NMR as a reference method for faster, online spectroscopic methods to measure WHC. Visible/near infrared spectroscopy (Vis/NIR spectroscopy) and X-ray spectroscopy were investigated as potential online methods. NMR was compared with the traditional reference method for WHC in pork, EZ-DripLoss method, and the error magnitudes and sources were discussed. NMR was also investigated as a method to predict purge in vacuum packages in early post mortem (p.m.).

The results show that NMR is an accurate and quantitative method for measuring small changes of water content in a controlled system (H_2O and D_2O mixtures). NMR can also separate the T_2 values well in another controlled system ($CuSO_4$ solutions of varying concentrations) consists of three different known T_2 values, that are similar to the T_2 values found in meat. The complexity of sample inhomogeneity and sample handling introduces errors in NMR measurements of meat, and standardized procedures need to be considered. Regarding meat samples, the three, decomposed spin-spin relaxation time components corresponding to water domains of different mobility were seen to change during drip production. For relatively shorter periods of dripping (45 hours), the migration of water and larger molecules from the meat to the drip domain was irreversible, and governed by molecules from the slowest relaxation domain (contains free water). In addition, it was found that NMR T_2 relaxometry could be considered as an improved reference method for spectroscopic techniques when compared with EZ-DripLoss method to measure WHC, i.e. the relaxation time of the slowest relaxation component (T_{22}) correlated better with both Vis/NIR and X-ray spectra than EZ-DripLoss values. Two different approaches of model fitting (discrete and continuous model) were applied to the NMR data and directly compared. It was found that the two fitting methods gave different results for both relaxation rates and intensity for all three components, which might cause different interpretation of water activity in meat during drip. Finally, the ability of predicting purge from pork muscle after 9-day vacuum-packed storage using NMR parameters measured early post mortem was explored. Results

show that NMR had limited prediction ability. This was investigated further and it was found that it could be an effect of muscle structural changes during storage, which affect WHC, but could also be due to the substantial errors in NMR and purge measurements relative to the variation in purge.

In summary, it was concluded that NMR proton relaxometry is a very informative method for WHC measurement. However, careful and standardized sample handling is required, and errors caused by this issue should be further assessed. Furthermore, it seems that there is a need for NMR instrument can be adapted for WHC measurement in meat samples, with a larger sample holder size than the common ~2.8 gram for intact meat measurement. This can increase robustness towards sample inhomogeneity and reduce sampling errors.

Sammendrag

Kjøttets evne til å binde vann er blant dets viktigste kvalitetsegenskaper. Mekanismen for vannbinding er langt fra forstått og online målinger er fortsatt en drøm for kjøttbransjen. De overordnede målene for denne avhandlingen var å fremme forståelsen av vannbindingsevnen (VBE) til kjøtt (spesielt endringer i domener av vann under dannelse av drypp) ved hjelp av kjernemagnetisk resonans (NMR) proton T_2 relaksasjon, samt å undersøke NMR sin egnethet som referansemetode for å gi for raskere, online spektroskopiske metoder for måling av VBE. Synlig/nær infrarød og røntgen spektroskopi ble undersøkt som potensielle online metoder. NMR ble sammenlignet med den tradisjonelle EZ-DripLoss metoden med tanke på at denne kunne bli en ny referansemetode for vannbindingsevnen til svinekjøtt. Størrelse og kilder til målefeil ble diskutert. NMR sin evne til å forutsi drypp i lagrede vakuum pakninger ble undersøkt tidlig post mortem (*p.m.*).

Resultatene viste at NMR var en nøyaktig og kvantitativ metode for å måle små forandringer i vanninnhold i enkle system (H_2O og blandinger D_2O). NMR gir tre ulike T_2-verdier i $CuSO_4$ løsninger av varierende konsentrasjoner, og disse tre T_2-verdiene ligner på de tre som finnes i kjøtt. Reproduserbarheten til NMR-målinger av kjøttprøver kompliseres av prøvenes inhomogenitet og av prøvehåndteringen, og standardiserte måleprosedyrer er derfor nødvendig. Når det gjelder kjøttprøver, så gjennomgår de tre spin-spin relaksasjonskomponentene endringer i tidsrommet hvor dryppet produseres. Etter relativt korte perioder med dryppdannelse (45 timer), vil migrasjon av vann og større molekyler fra kjøttet i drypp domene være irreversible, og styres av molekyler fra det langsomste relaksasjons domenet (inneholder fritt vann). NMR-T_2 relaksasjon ansees som en forbedret referansemetode for spektroskopiske teknikker relativt til EZ-DripLoss metodens mål for vannbindingsevne, dvs. relaksasjonstiden til den tregeste relaksasjonskomponenten (T_{22}) er korrelert bedre med synlig lys / NIR og røntgen spektra enn til EZ-DripLoss målinger. To ulike tilnærminger til modellbygging (diskret og kontinuerlig modell) ble sammenlignet, og resultatene indikerte at de ulike modellene ga forskjellige resultater både for relaksasjons hastigheter og intensitet for alle tre komponenter for vann. Valg av modell kan således gi ulike tolkninger av vannamobiliteten i kjøttet under dryppdannelsen. Til slutt, ble evnen til å predikere drypp fra svine muskel etter 9 dagers lagring i vakuumpakning forsøkt predikert fra NMR målinger som ble utført tidlig post mortem. Resultatene viste at NMR hadde begrenset evne til å predikere drypp 8 dager fram i tid. Dette kan være forårsaket av strukturelle

endringer i kjøttet som påvirker vannbindingsevnen under lagring, men også de betydelige feil i NMR og drypp-målinger som eksisterer i forhold til variasjonen i drypp.

NMR proton relaksasjon er en informativ metode for vannets status i kjøtt. Imidlertid må man være forsiktig ved prøvehåndtering, og feil forårsaket av dette problemet bør vurderes nærmere. Det ser ut til at det er et behov for NMR-instrument med en større prøveholder enn den som vanligvis bruker ~2,8 gram intakt kjøtt. Kjøttprøvenes inhomogenitet og utvalgsfeil kan da reduseres og NMR-metoden tilpasses måling og prediksjon av vannbindingsevnen til kjøttprøver.

List of papers

Paper I

Hansen, E.W., Zhu, H., (2015). New insight into the dynamics of water and macromolecules in meat during drip as probed by proton CPMG NMR. International Journal of Research and Reviews in Applied Sciences, 23(3), 207-220.

Paper II

Zhu, H., O'Farrell, M., Bouquet, G., Lunde, K., Egelandsdal, B., Alvseike, O., Berg, P., Gjerlaug-Enger, E., Hansen, E.W., (2016). Evaluating nuclear magnetic resonance (NMR) as a robust reference method for online spectroscopic measurement of water holding capacity (WHC). Journal of Food Engineering, 175, 51-57.

Paper III

Hansen, E.W., Zhu, H., (2016). Discrete and continuous spin-spin relaxation rate distributions derived from CPMG NMR response curves — a comparative analysis exemplified by water in meat. Accepted by Applied Magnetic Resonance. Accepted version is slightly amended.

Paper IV

Zhu, H., Hansen, E.W., O`Farrell, M., Andersen, P.V., Berg, P., Egelandsdal, B., (2016). The potential for predicting purge in packaged meat using low field NMR. Submitted to Journal of Food Engineering.

Abbreviations

ATP	Adenosine triphosphate
CPMG	Carr-Purcell-Meiboom-Gill
DFD	Dark, firm and dry
LD	*Longissimus dorsi*
NMR	Nuclear magnetic resonance
pI	Isoelectric point
PLSR	Partial least squares regression
p.m.	Post mortem
PSE	Pale, soft and exudative
RF	Radio frequency
RMSD	Root mean square error of linear regression
SG	Savizky-Golay
S/N	Signal-to-noise
SNV	Standard normal variate
Vis/NIR	Visible/near infrared
WHC	Water holding capacity

Contents

List of Errata

	Written	**Should be**
Page 3, Line 19	softs	soft
Page 8, Line 12	uses allows	allows
Page 10, Line 3	result	results
Page 12, Line 5	faster	shorter
Page 12, Line 8	faster	shorter
Page 13, Line 4	─ the	─ fits the
Page 19, Line 9	Comparing	Compare
Page 19, Line 9	determining	determine
Page 19, Line 11	Identifying	Identify
Page 19, Line 11	minimizing	minimize
Page 19, Line 12	Exploring	Explore
Page 25, Line 17	of	,
Page 28, Line 4	One	One of the three chosen
Page 31, Line 9	+	±
Page 31, Line 10	+	±
Page 31, Line 14	+	±
Page 32, Line 3	+	±
Page 32, Table 2	+	±
Page 34, Line 21	+	±
Page 36, Figure 11d, y axis	I_{21} (%)	I_{22} (%)
Page 37, Line 8	23(+8)	23 (±8)
Page 40, Line 4	intra-and	intra- and
Page 46, Line 12	and showed	and the results showed
Page 46, Line 13	domain	domain on day 9 compared to day 1 *p.m.*
Page 47, Line 8	measured,	,
Page 50, Line 7	before	taken before
Page 51, Line 28	T(2)	T_2
Page 53, Line 5	D(2)O	D_2O
Page 54, Line 4	1H	^1H

Page 59, Line 22	myowater	Myowater
Page 59, Line 24	1H	^{1}H
Paper I, page 208, Line 1	T_2s	T_2 values
Paper I, page 208, Line 31	carcass	carcasses
Paper I, page 212, Line 6	*long-T2*	*long-T_2*
Paper I, page 219, Line 12	R_2^X/I_X	R_2^X/I_T^X
Paper I, page 220, Line 45	T. J. Phys.Chem.	J. Phys.Chem.
Paper I, page 220, Line 48	M.J.A.D. Hertog-Meischke	M.J.A. den Hertog-Meischke
Paper I, page 220, Line 49	M.J.A.D. Hertog-Meischke	M.J.A. den Hertog-Meischke
Paper I, page 212, Line 7	*"Corrected"*	*"corrected"*
Paper II, page 52, Line 39	longissimus dorsi	*longissimus dorsi*
Paper II, page 52, Line 84	is interest	are interests
Paper II, page 52, Line 56	Ersen	Andersen
Paper II, page 52, Line 75	Ersen	Andersen
Paper II, page 56, Figure 5a	a) (in smaller font)	(should be deleted)
Paper II, page 57, Line 10	i+1	i+1,
Paper II, page 57, Line 54	Ersen	Andersen
Paper III, page 2, Line 39	show	shows
Paper III, page 5, Line 180	Fig 2a	Fig 2b
Paper III, page 6, Line 209	the	three
Paper III, page 6, Line 220	are	is
Paper III, page 6, Line 222	5	1
Paper III, page 8, Line 268	combing	combining
Paper III, page 8, Line 278	increase	increases
Paper III, page 10, Line 318	F_i's	F_i
Paper III, page 11, Line 362	half height	half maximum height
Paper III, page 11, Line 376	components,	components.
Paper III, page 13, Line 409	(A2.3)	A2.3
Paper III, page 13, Line 411	A2.3	A2.4
Paper IV, page 3, Line 64	myofibrils	myofibrillar
Paper IV, page 3, Line 79	p.m.	*p.m.*
Paper IV, page 4, Line 109	studied using	tried to use
Paper IV, page 5, Line 174	p. m.	*p.m.*

Paper IV, page 5, Line 187	parameter	parameters
Paper IV, page 6, Line 226	Hanne Christine Bertram	Bertram
Paper IV, page 9, Line 2	H. C. Bertram	Bertram
Paper IV, page 10, Line 57	p. m.	post mortem
Paper IV, page 11, Line 99	study;	study
Paper IV, page 14, Line 236	postmortem	post mortem
Paper IV, page 16, Line 271	intra-and	intra- and

1 Introduction

1.1 Distribution and function of water in post mortem muscle

Water is one of the main constituents of meat. Water functions as a lubricant between the muscle fibers, as medium for metabolite transportation and determines the plasticity, rigidity and gelatinization of the insoluble proteins (myofibrillar proteins, cytoskeletal proteins and connective tissue) (Hughes et al., 2014; Puolanne and Halonen, 2010). The content, location and mobility of water in muscle (myowater) change as a function of several mutual interacting factors, including age, sex, breed, muscle type, stress level, cooling rate, aging time, temperature, etc. (Honikel, 2004; Pearce et al., 2011). In general, lean muscles (e.g. *longissimus dorsi* (LD) muscle) contain about 75% of water and 22% of proteins (Honikel, 2004; Kauffman, 2001). Based on the structure and mobility of water, three classes of water are commonly recognized in intact muscle, and are illustrated in Figure 1.

● Bound water

This type of water is attracted to polar or ionic groups of macromolecules like proteins (Aubin et al., 1980). Due to the dipolar property of water and the hydrophilicity of some proteins, water is bond to the protein structure. From a biochemical point of view, water molecules are very important for the three-dimensional structure and activity of proteins. Bound water is reported to make up less than a tenth of total myowater, and it has reduced mobility and changes very little in post-rigor muscle (Huff-Lonergan and Lonergan, 2005).

● Entrapped (or immobilized) water

Entrapped water might be retained by steric effects and/or by attraction to bound water. The location of entrapped water is much debated in the literature. Some works mentioned that entrapped water is located within myofibrils (intra-myofibrillar) and between myofibrils (inter-myofibrillar) (Pearce et al., 2011), others concluded that entrapped water resides within muscle structure (e.g. water held in myofiber by cell membrane), bound partly (Aubin et al., 1980) or not to proteins (Huff-Lonergan, 2002; Huff-Lonergan and Lonergan, 2005; Powrie and Tung, 1975). This portion of water makes up about 80% of the total myowater in living muscle or pre-rigor muscle, and does not flow freely within muscle (Huff-Lonergan, 2002; Huff-Lonergan and Lonergan, 2005).

● Free water

This type of water is unimpeded and is held by weak intermolecular forces between the liquid and the surrounding matrix, e.g. between myofibers in the inter-fascicular space or between the muscle bundles in the extra-fascicular space (Pearce et al., 2011). Free water makes up less than 10% of the total myowater found in pre-rigor meat (Huff-Lonergan, 2002), but the amount can increase when muscle structure changes and entrapped water flows out (Huff-Lonergan and Lonergan, 2005).

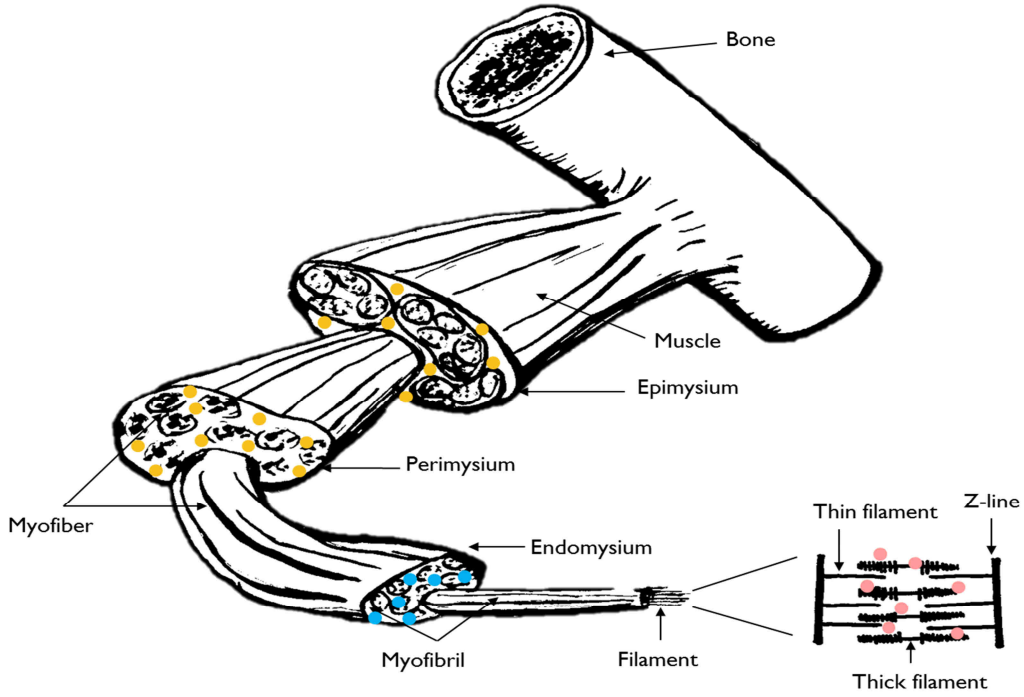

Figure 1. Schematic representation of skeletal muscle organization and water distribution based on mobility, including bound water (●), entrapped (or immobilized) water (●) and free water (●).

1.2 Water holding capacity

Today's consumers and manufacturers are increasingly aware of meat quality and this has increased demands on the meat sector to provide products with certified quality (Damez and Clerjon, 2013). Among the most important quality traits of meat is water holding capacity (WHC), which refers to the meat's ability to retain inherent moisture during cutting, heating, grinding, pressing, etc. (Fennema, 1990; Warner, 2014). WHC should be discriminated from another similar term ─ water binding capacity, which refers to the same ability while extrinsic

water, phosphates and salt are added (Warner, 2014). To the industry, it is important to understand WHC, since it affects salable weight, sensory properties, consumer perception, eating quality, recipe and yield in further processing of other meat products (den Hertog-Meischke et al., 1997; Schäfer et al., 2002).

The complexity of the water holding capacity of meat is determined by its complex structure, and more than one simple model for how water is held in the myofibrillar protein system should be expected (Puolanne and Halonen, 2010). As reviewed by Puolanne and Halonen (2010), several hypotheses for how water is held have been presented, including electrostatic force, osmotic force, capillary force, etc. More recent research focuses on the structure of water, as low (or high) density water is induced by cosmotropic effects (or chaotropes) (Puolanne and Halonen, 2010). However, there is still a lack of theoretical understanding of how bulk water is held in the meat. Water loss is affected by evaporation, in particular when carcasses are warm (e.g. 37 degrees) and unwrapped. In addition, numerous factors have been proven to influence WHC, including animal genetics, post mortem handling, rate of pH decline, pre-rigor temperature, processing (cutting, grinding, heating, pressing and freezing), etc. (Gunenc, 2007; Huff-Lonergan and Lonergan, 2005; Mason et al., 2016; Rosenvold and Andersen, 2003). pH, for example is often measured in fresh meat (Gunenc, 2007) to ensure higher quality of meat. The combination of a fast decline in pH and low ultimate pH results in low WHC, causing high drip loss. An extreme example of this case is pale, softs and exudative (PSE) meat. The post mortem glycolysis rate of PSE meat is accelerated when the carcass temperature is still high, which leads to a lower pH at high temperature and significant protein denaturation. Water loss is increased due to the breakdown of the structural (myofibrillar) proteins (Bowker et al., 2000). In a recent study, a new hypothesis is proposed regarding the role of sarcoplasmic proteins in heat-induced protein denaturation (i.e. PSE). Sarcoplasmic proteins were found to form a network between myofibril filaments which improved WHC (Liu et al., 2015).

1.3 Drip loss

Drip is the red aqueous solution of proteins (sarcoplasmic proteins, glycolytic enzymes and myoglobin) flowing out of the cut surface of a carcass (Offer and Cousins, 1992). Drip loss results in an undesirable appearance (e.g. unnaturally pale color), weight loss and poorer nutritive value, reducing the meat value both economically and nutritionally (den Hertog-Meischke et al., 1997; Offer and Cousins, 1992). In addition, drip is an excellent culture

medium for certain micro-organisms, resulting in a shorter shelf life for safety reasons (den Hertog-Meischke et al., 1997). Drip loss from meat is a time-dependent process, which requires driving force or pressure. Drip loss is significantly influenced by the following factors: 1) temperature post mortem; 2) the degree of myofibrillar shrinkage during rigor and myofibrillar interfilamentous spacing; 3) the permeability of the cell membrane to water; 4) the degree of cytoskeletal protein degradation and the development of drip channels and extracellular space (Hughes et al., 2014; Schäfer et al., 2002).

1.3.1 Drip loss at early post mortem

The process of drip formation remains unclear. However, there are several processes that are known to be linked to the amount of drip, including early post mortem pH drop mechanism. The decline in pH can partially explain the myofibril shrinkage. Reduction of pH causes the reduction of negative electrostatic repulsion between the myofibril filaments, thus the space between the filaments for water decreases (den Hertog-Meischke et al., 1997). As pH has reached the isoelectric point (pI) of the major proteins (e.g. for myosin, pI =5.4), proteins carry no net electrical charge. Less water binding groups on proteins are available at pI when oppositely charged groups tend to attract each other (Huff-Lonergan and Lonergan, 2005). At pI, meat is believed to have the least water holding capacity (Texas A&M AgriLife Extension Service). In the meantime, as the ATP level reaches a critically low value, the formation of permanent cross-bridges between myosin and actin, i.e. actomyosin, takes place, and causes the muscle to become stiff (den Hertog-Meischke et al., 1997; Pearce et al., 2011). The process causes the shrinkage of myofibrils and reduces the space for water in myofilaments (Pearce et al., 2011). Denaturation of myosin further increases shrinkage (den Hertog-Meischke et al., 1997). The charge and head length of myosin are reduced, which in return stimulates myofibril shrinkage. Myofibril shrinkage may force water within myofibril filaments to the extra-myofibrillar space (Huff-Lonergan and Lonergan, 2005). Sarcomeres shrink while myofibril shrinkage occurs, and studies have shown that drip loss increases linearly with a decrease in the length of sarcomeres (Honikel et al., 1986). Myofibrillar shrinkage contributes to the contraction of myofiber via proteinaceous linkages, and further creates water channels between myofibers and muscle bundles (Huff-Lonergan and Lonergan, 2005). Offer and Cousins studied the structural changes of beef *sternomandibularis* muscle by light microscopy and scanning electron microscopy (Offer and Cousins, 1992). Their results showed that gaps (channels) between myofiber bundles started to appear from 4 to 6 h *p.m.*,

and gaps between myofibers appeared until 24 to 48 h *p.m.* These gaps have been documented by Bertram et al., who studied changes of water distribution within rabbit muscles by non-invasive NMR micro-imaging (Bertram et al., 2004b). T_2 maps in a total of 24 h post mortem indicated the formation of water channels close to the connective tissue network.

1.3.2 Drip loss at later post mortem and drip production during storage

Drip loss at a later time post mortem has been reported to be controlled by different processes compared to early stage. Changes in WHC have been reported from 24 h *p.m.* up to 10 days *p.m.*, when measured using 48 h Honikel bag method and 24 h centrifugation method (Joo et al., 1999; Kristensen and Purslow, 2001; Moeseke and Smet, 1999). The measured drip loss in percentage (%) peaked at around 48 h post mortem and decreased subsequently. Two hypotheses exist to explain the decrease in drip loss (increase in WHC): 1) The reduction in drip loss with sampling time post mortem is a result of "leaking out", i.e. the meat with poor WHC will lose relatively more water early post mortem, leaving limited water available for dripping in later stages (Joo et al., 1999; Moeseke and Smet, 1999). 2) Cytoskeleton proteins (vinculin, desmin, talin, etc.) degrade gradually during storage, and the inter-myofibrillar linkages and costameric connections are removed (Kristensen and Purslow, 2001), making myofibril shrinkage energetically less favorable and ceasing the flow of water into the extracellular spaces. The previously expelled water may be taken up again to some degree, causing swelling of myofibrils (Huff-Lonergan and Lonergan, 2005; Kristensen and Purslow, 2001; Straadt et al., 2007).

The development of WHC during storage may account for different rates of drip production that have been observed during storage. Zarate and Zaritzky studied the effect of storage conditions (different packing films and temperatures) on purge production in packaged beef during a storage period of 22 days (Zarate and Zaritzky, 1985). During the first 20 hours (induction period), the purge in percentage (%) increased nonlinearly initially, followed a reduced but constant increase rate. In another work, Taylor and Dant (1971) reported that much of the drip was generated in the first 2 days of storage in pork.

1.3.3 Effect of sample location/size on drip loss

It has been reported that the absolute amount and percentage of drip are related to sample surface area and sample volume, since most drip comes from the cut surface (Christensen, 2003). Taylor and Dant (1971) studied the effect of sample thickness (= 0.7, 1.2 and 2.5 cm) on drip loss in percentage (%) using 12 porcine *longissimus dorsi* muscles, and found that drip loss in percentage (%) was less dependent on sample thickness and weight as the thickness was increased. The distribution of drip (weight of drip per unit area or weight of drip per unit weight) in pig was also determined by a method similar to Honikel bag method (Honikel, 1998; Taylor and Dant, 1971). The drip percentage was found to be linearly correlated to the equivalent area/unit volume ratio of the sample, assuming that the rate of drip loss was proportional to the equivalent area of sample (Taylor and Dant, 1971; Zarate and Zaritzky, 1985). Water that turned into drip during storage was located extracellularly or extra-myofibrillarly, and the drip was mainly produced by gravitational force (Zarate and Zaritzky, 1985). Joo et al. reported that the percentage of drip loss and shrinkage in porcine *longissimus thoracis et lumborum* increased over time for bigger pieces ($\bar{x}$ = 5937 g), and decreased for smaller pieces ($\bar{x}$ = 373-777 g) (Joo et al., 1999). It was concluded that smaller pieces release drip more quickly than bigger pieces early post mortem, since drip production follows a certain path (myofilament lattice → interfibrillar sarcoplasm → interfiber space → interfascicular space) (Joo et al., 1999; Swatland et al., 1989). When different sample sizes are used for WHC studies, drip rate difference should be considered if results are compared. For instance, an offset of 1.2% was found between the drip loss in percentage (%) measured using two WHC methods (Honikel bag method and EZ-DripLoss method), which suggested that surface area/weight ratio and drip loss are positively correlated (Christensen, 2003). These results were expected since the sample size (weight) difference of the two methods was big (~100 g sample for Honikel bag method and ~3-4 g sample for EZ-DripLoss method).

1.4 Methods for WHC measurement

Several methods have been used to measure WHC. They can be categorized into 3 groups as summarized by Honikel (2004): 1) methods that apply no external force, including evaporation and drip loss; 2) methods that apply external force, including centrifugation, capillary forces, pressure, etc. and 3) methods that apply thermal force (e.g. cooking/heating). The different techniques have been also reviewed elsewhere (Trout, 1988; Kauffman et al.,

1986; Offer et al., 1989; Gunenc, 2007). There is no definitive absolute approach for WHC due to the variety of available methods (Gunenc, 2007), which unfortunately hinders the direct comparison of the results from different methods. Therefore, information regarding the applied method and the history of meat needs to be included for result comparison.

Gravitational methods are simple, inexpensive, sensitive and reproducible, yet they are slow and require destructive sampling, animal information and sample processing history (Q-PorkChains, 2007-2011). Other methods applying external forces including the filter paper method can speed up the gravitational methods (several minutes to an hour), but still require sample history (post mortem time, pH, etc.) (Q-PorkChains, 2007-2011). Unfortunately, all the methods mentioned above are too slow for online application for meat industry. Almost all the existing methods used for WHC prediction begin either at or after 24 h post mortem chilling due to temperature regulations to avoid hot boning, and this is too late for carcass sorting (Kapper et al., 2014). Norwegian meat industry has shown that 1.8-2% of pork carcasses are classified as PSE in Norwegian pig breeds, and these should be sorted out. For the meat processing industry, the suggested optimal time for measuring, in order to classify, screen and sort raw meat efficiently, is before cutting, while the actual time for measuring is after cutting, i.e. 24, 72 or 96 h p.m.

New methodologies, including fast spectroscopic methods do not require sample preparation and have the potential to be implemented online. However, most spectroscopic methods need to be calibrated against other more accurate and absolute methods. A faster and more accurate reference method is thus in need for WHC, if online methods will eventually be applied. In this thesis, three methods namely EZ-DripLoss, NMR and Vis/NIR spectroscopy are explored and discussed. The two former techniques (EZ-DripLoss and NMR) are assessed as reference methods for calibrating Vis/NIR spectroscopy. In addition, some X-ray scattering results were also included, however it must be mentioned that this particular technique, while showing potential, is out of the scope of the present thesis.

1.4.1 EZ-DripLoss method

The EZ-DripLoss method was developed at the Danish Meat Research Institute in 1996 (Danish Meat Research Institute, 2010). The sampling procedure includes coring two cylindrical samples (25ø × 25 mm) using a sharp cork borer (Figure 2 b) from a slice of 3-5 cm *posterior* to the last rib curvature, and placing samples in specially designed containers

(Figure 2 c), in which the drip can flow down freely to the bottom of the holder, with no contact to the meat sample. Samples are stored at 4 ˚C for 24 or 48 h, and drip loss percentage is calculated as the ratio between the drip weight and the initial meat weight. The EZ-DripLoss percentage of the loin is obtained by averaging the drip loss percentage of the two samples taken from the same slice.

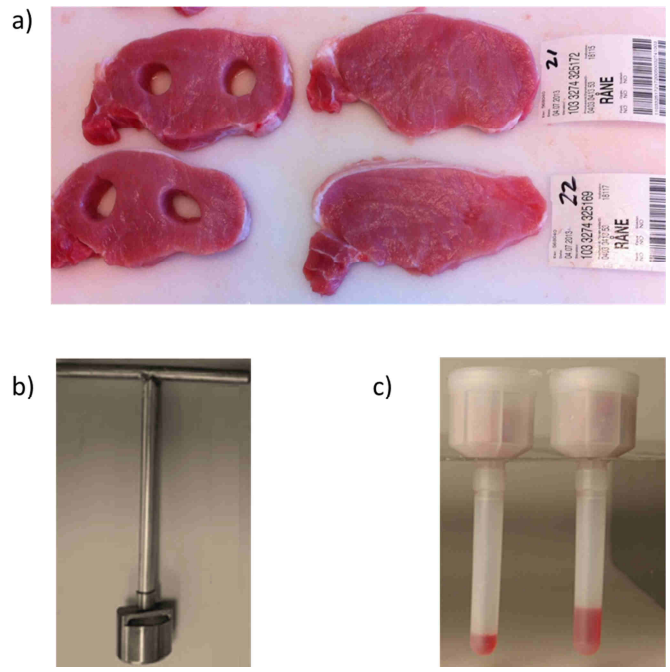

Figure 2. a) Sampling locations for EZ-DripLoss method, one towards the cranial end and another towards the caudal end of the muscle. b) Cork borer (ø 25 mm). c) Sample holders for EZ-DripLoss method with meat samples on the top and drip fluid in the bottom of the specially designed containers.

The relatively small sample size used in the EZ-DripLoss method uses allows for the detection of local PSE spot (Christensen, 2003). EZ-DripLoss method has been preferred in many labs and implemented in the routine analysis for pork quality worldwide (Correa et al., 2007). The EZ-DripLoss method has produced relatively high heritability values in the Norwegian pig breeding program (Norsvin, Hamar, Norway, 2006-present) and has been reported to have high sensitivity and reproducibility, as well as correlating well with the Honikel bag method (Christensen, 2003).

The EZ-DripLoss method is, however, time consuming, labor intensive and operator dependent. In addition, the EZ-DripLoss method is known to depend on slice number along

the LD muscle and sampling position within one slice, which makes the sampling procedure less flexible (Christensen, 2003). The reliability of the standard methodology of EZ-DripLoss method has been questioned by Correa et al. (2007), who argued that the samples that are not dabbed/mopped dry before final weighing result in the underestimation of the amount of drip, especially if drip adheres on the meat surface. The EZ-DripLoss method has been investigated in this thesis as one of the reference methods for WHC measurement.

1.4.2 Nuclear magnetic resonance proton relaxometry

1.4.2.1 Theory

Nuclear magnetic resonance (NMR) is a phenomenon that occurs when immersing nuclei of certain atoms in a static magnetic field and exposing them to a second oscillating magnetic field (Hornak, 1997-2014). For instance, hydrogen atoms in a water molecule have a nucleus composed of a proton. The spin property of protons causes protons to behave like a magnet. The hydrogen proton has a spin quantum number of I = ½, and in the presence of a large magnetic field, the nuclear energy levels split into 2I+1 states. Therefore the hydrogen proton spin has two possible orientations (spin up and spin down). A sample (e.g. meat) contains many spins, and when there is no external magnetic field, the two populations (spin up and spin down) are degenerated. However, when an external magnetic field is applied, spins align themselves either with or against the external magnetic field (Figure 3 a). The orientation of these spins regarding the external field causes them to have different energy levels, and the difference between the energy levels (ΔE, Figure 3 b) depends linearly on the strength of the external magnetic field according to:

$$\Delta E = h\gamma B_0 = h\nu \qquad (1)$$

where h is Planck's constant (h = 6.626x10^{-34} J·s), γ is the gyromagnetic ratio of the particle (for hydrogen, γ = 42.58 MHz/T), B_0 is the strength of the external magnetic field and ν is the resonance frequency (Larmor frequency).

At thermal equilibrium, the number of spins in either lower energy level (N^+ corresponds to spin up) or higher energy level (N^- corresponds to spin down) follows the Boltzmann equation:

$$\frac{N^-}{N^+} = \exp(\frac{-\Delta E}{kT}) \qquad (2)$$

where *k* is Boltzmann constant (1.3805×10^{-23} J/K) and T is the temperature in Kelvin. At room temperature, N^+ is slightly higher than N^-, which result in the net magnetization has the same direction as the external magnetic field.

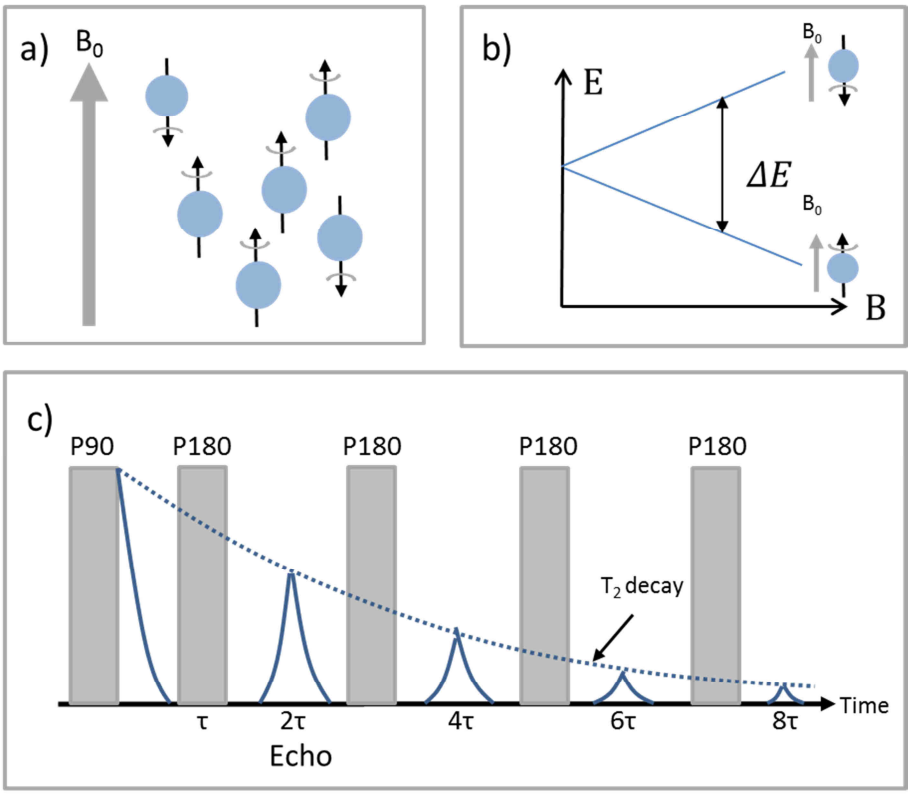

Figure 3. a) Spins align with or against the external magnetic field (B_0). b) Energy level difference of spins that have lower and higher energy levels. c) The CPMG pulse sequence, radio frequency pulses (P90 and P180) are shown in grey, and T_2 decay is shown in dotted curve.

The spins can undergo a transition between the two energy levels by absorbing a photon. The energy of the photon is related to its frequency *v* (Eq 1) and must be equal to the energy difference between the two energy levels (*ΔE*) (Hornak, 1997-2014). By applying the correct radio frequency (RF) pulse (same as Larmor frequency *v*), transitions can occur between the two energy levels. Protons are perturbed from their initial equilibrium state when they are excited, but they will subsequently return to the equilibrium state (governed by the Boltzmann distribution) by a process called relaxation when the RF pulse is turned off. There are two

types of relaxation processes involved, longitudinal relaxation (T_1) and transverse relaxation (T_2). The T_1 relaxation describes the longitudinal magnetization (M_z) returns to its equilibrium state, governed by the effect of the environment on the spin (Guðjónsdóttir, 2011). The T_2 relaxation characterizes the transverse magnetization (M_{xy}) returns to its equilibrium state, which shows the effect of other neighboring nuclei on a nucleus, and indicates the phase and state of the atoms (Guðjónsdóttir, 2011). Both T_1 and T_2 are affected by molecular motions. For fast molecular motion (e.g. in pure water), T_1 and T_2 values are very long. Restricted motion (in dense solids, e.g. proteins) shortens the T_2 value.

To detect T_2 relaxation, a Carr-Purcel-Meiboom-Gill (CPMG) pulse sequence (Meiboom and Gill1, 1958) was used. A CPMG pulse sequence includes an initial 90˚ pulse follows by a $(\tau\text{-}180^{\circ}\text{-}\tau)_n$ pulse sequence (Figure 3 c), in which the 90˚ pulse flips the magnetic vector to the transverse plane, hereafter the diphase of net magnetization occurs due to field inhomogeneities and/or spin-spin interactions. At $t = \tau$, an 180˚ pulse applied in the transverse plane can reverse the dephasing due to field inhomogeneities. At $t = 2\tau$, the frequencies can refocus and form a spin echo, follows by a signal diffuse until the next 180˚ pulse applied at $t = 3\ \tau$ (Guðjónsdóttir, 2011). The repeated applied 180˚ pulse produces a train of echoes, with reduced net magnetization one after another. T_2 can be calculated by the following equation:

$$M_{xy} = M_0 e^{-t/T_2} \qquad (3)$$

where M_0 is the equilibrium magnetization. Only protons from mobile compounds (i.e. water and non-crystallized fat) contribute to the relaxation signal in low field NMR (Thybo et al., 2004). The T_2 relaxation was extensively discussed in current thesis.

1.4.2.2 Application

NMR proton relaxometry is a powerful tool for quantitatively studying the physical (distribution, compartmentalization) and chemical (mobility, interactions with macromolecules) properties of water molecules in biological materials, and has been widely used in understanding meat structure and WHC. NMR proton relaxometry has been used for the quantitative measurement of different components in meat. Sørland et al. (2004) developed a method to accurately determine the total content of fat and moisture in meat using low field NMR, using a simple calibration procedure, where only a 100 % oil is needed (Sørland et al., 2004). As mentioned previously, water in meat can be grouped into 3 classes,

and NMR proton relaxometry is able to provide direct information on the quantity and mobility of each class based on the T_2 relaxation properties (Bertram and Andersen, 2004). The T_2 relaxation curve of meat samples is recognized as very different from the single exponential T_2 relaxation curve of bulk water. The relaxation time of water from meat samples is much faster, and appears to be multi-exponential (Hazlewood et al., 1974). The multi-exponential behavior of muscle was found to be caused by the overall structural organization of meat rather than intra/extra- cellular compartmentalization caused by cell membranes (Bertram et al., 2001b). The faster relaxation time is due to fast exchange between hydrated water and bulk like water (Tornberg et al., 1993). Three relaxation populations were assigned to different proton relaxation pools in meat according to their relaxation time magnitude: a fast component (T_{20}, 0-10 ms) represents bound water, an intermediate component (T_{21}, 35-50 ms) signifies entrapped water and a slow component (T_{22}, 100-250 ms) corresponds to free water (Bertram and Andersen, 2004). The relationship between individual T_2 parameters and microstructural water distribution in meat is confirmed by several studies (Venturi, 2008), including an investigation that found a correlation between T_{21} and sarcomere length, which supported the hypothesis that the T_{21} reflects water located within myofibrils (Bertram et al., 2002b).

There is a general interest in the meat industry to know the total, immobilized and free water in meat products (Q-PorkChains, 2007-2011). The ability of NMR to determine these previously mentioned parameters is assessed in this thesis. Compare to EZ-DripLoss method, NMR relaxation measurement is much faster (in the scale of minutes), which is a distinct advantage for NMR as a reference method in large-scale analysis. Regarding WHC, the first correlation to NMR relaxometry was reported by Renou et al. (1985), who observed that the population of T_{21} ($r = 0.54$) and T_1 ($r = 0.59$) were positively correlated to WHC measured using the pH paper imbibition technique. Later on, various correlations ($r = 0.46$-0.77) between NMR relaxation parameters (T_1 or T_2) and WHC (determined by different methods) were found and reported by Bertram and Andersen (2004). Among all the various NMR parameters that were correlated to WHC, the slowest relaxation component (T_{22}) was the most interesting and straight forward in explaining the correlation. It has been suggested that the water, that is represented by the T_{22} component is the most likely to drip (Tornberg et al., 1993). In this thesis, the T_{22} time constant has been investigated as reference value for WHC.

1.4.2.3 Processing methods of NMR relaxation data

The meat samples are heterogeneous, and a distribution of relaxation times is expected (Menon and Allen, 1991). Mainly two approaches have been investigated in the literatures regarding the elucidation of spin-spin relaxation of water in tissue/muscle: firstly, the discrete model ─ the CPMG response curve to a predefined number of exponential decaying functions (Belton et al., 1972; Belton and Packer, 1974; Burnell et al., 1981; Hazlewood et al., 1974; Renou et al., 1985); and secondly, the continuous model ─ where a continuous distribution of relaxation times was assumed (Bertram et al., 2002a; Bertram et al., 2001b; Bertram et al., 2002b; Bertram et al., 2003; Li et al., 2012; McDonnell et al., 2013; Micklander et al., 2005; Renou et al., 1989; Renou et al., 1985; Sørland et al., 2004; Straadt et al., 2011; Straadt et al., 2007).

The discrete model (D) composed of three exponential functions can be written as:

$$I(t) = \sum_{i=0}^{2} I_{2i}^{D} \cdot \exp\left[-t / \overline{T}_{2i}^{D}\right] \quad (4)$$

Where I_{2i}^{D} and $\overline{T}_{2i}^{D}$ represent the signal intensity and the mean relaxation time of component *i*, respectively. $\overline{R}_{2i}^{D}$ (=$1/\overline{T}_{2i}^{D}$) is the mean relaxation rate of component *i*.

Using the discrete model to analyze T_2 relaxation data in meat is considered restricted (Bertram et al., 2002a). A fixed number of relaxation components may only represent an approximation due to sample heterogeneities, caused by distribution of pore shapes, pore sizes and surface relaxation sites (Menon and Allen, 1991). The continuous distribution of exponentials is described elsewhere (Bertram et al., 2002a; Bertram et al., 2002b). Briefly, the continuous distribution can be expressed as:

$$g_i = \sum_{j=1}^{m} I(T_{2j}) \exp[-t_i/T_{2j}] \quad (5)$$

where g_i is the intensity of the exponential distribution at time t_i and $I(T_{2j})$ is the amplitude of the component that has a relaxation time T_{2j}. The software RI Win-DXP (version 1.2.3, Resonance Instruments, Witney, UK) was used in this thesis to solve Eq 5 by minimizing:

$$(g_i - \sum_{i=1}^{m} f_x \exp\left[-\frac{t_i}{T_x}\right])^2 + \lambda \sum_{i=1}^{m} f_x^2 \quad (6)$$

where λ is the weight and $\lambda \sum_{i=1}^{m} f_x^2$ is a linear combination of functions, added to overcome the ill-imposed problem by performing a zeroth order regularization (Bertram et al., 2002a). RI Win-DXP software then returns the continuous log(T_2)-relaxation time distribution *dI/dlog(T_2).*

A spin-spin relaxation rate distribution F(R_2) can be transformed from *dI/dlog(T_2)* as:

$$F(R_2) = \frac{dI}{dR_2} = \frac{dI}{d(LogT_2)} \cdot \frac{d(LogT_2)}{dR_2} = -\frac{T_2}{\ln 10} \cdot \frac{dI}{d(LogT_2)} \qquad \text{with } R_2 = 1/T_2 \qquad (7)$$

For instance, three peaks are most commonly observed in meat samples, thus an overall relaxation distribution can be written as:

$$F(R_2) = \sum_{i=0}^{2} I_i^C F_i(R_2) \qquad (8)$$

where I_i^C represents the signal intensity and $\overline{R}_{2i}^C$ represents the "mean" relaxation rate of component "*i*", i.e.:

$$\overline{R}_{2i}^C = \int_0^\infty R_2 F_i(R_2) dR_2 \Big/ \int_0^\infty F_i(R_2) dR_2 \qquad (9)$$

Both the discrete model and continuous model have been widely used regarding relaxation in meat, and the two methods have been reported to correlate differently to WHC determined using Honikel bag method (Bertram et al., 2002a). Higher correlation was found between WHC (determined using Honikel bag method) and T_2 relaxation data obtained using the continuous model (r = -0.85) than using the discrete model (r = -0.77, 2-exponential function). The different correlation may lead to different physical interpretation of the relaxation data.

1.4.2.4 Commercial NMR equipment and suitability for industrial use

Commercially available low field NMR equipment has various magnetic field strength (0.11 – 1.41 T, corresponding to operating frequency of 5-60 MHz), with varying sample holder sizes (ø 5-60 mm, volume 0.2-100 mL) (Bruker BioSpin, 2012; Oxford Instruments, 2013). The instrument that holds a bigger sample size normally operates at a lower frequency, e.g. the MQC5 model from Oxford instrument (Abingdon, United Kingdom) that operates at 5 MHz can hold a sample with a diameter of 60 mm (100 mL). A larger sample size is presumed

better suited for inhomogeneous sample measurements, but can compromise the instrument sensitivity. As mentioned in Eq 1, the energy difference between two levels (ΔE) depends on the external magnetic field strength. Higher magnetic field strength creates higher energy difference between the two states, hence higher signal intensity can be achieved which enhances the sensitivity of the technique. To guarantee the sensitivity of the NMR measurements, equipment with certain level of external magnetic field strength should be chosen, while the maximum sample volume should be considered. For instance, the MQC23 model from Oxford instrument (Abingdon, United Kingdom) might be considered for industrial use, which operates at 23 MHz and can hold a sample as large as 14 mL (ø 26 mm).

Various instruments have been used for WHC measurements in meat. However, instruments with operating frequencies of around 20 MHz have been chosen by the majority of the reported studies (Bertram et al., 2002a; Bertram et al., 2002b; Bertram et al., 2004a; McDonnell et al., 2013; Straadt et al., 2007; Tornberg et al., 1993; Wu et al., 2007). In addition, different sample sizes and handling procedures have also been investigated, e.g. 10 × 10 × 50 mm, 35mm^2 × 7mm, 7ø × 30 mm, 8cm in length, etc. (Bertram et al., 2002a; Bertram et al., 2003; Straadt et al., 2007; Tornberg et al., 1993). The intact meat samples could be sensitive to applied pressure during sample treatment, and different sample handling (including sample cutting, sample transferring, etc.) may result in different measurement errors. Sample heterogeneity might also differ depending on the size, handling or presentation of samples. To the best of our knowledge, the different sources of errors (e.g. different sample sizes) in NMR measurements have not been discussed yet. Such studies are of great importance to understand and ensure method accuracy and comparability. In this thesis, the effect of sample size on the error of NMR measurement of meat was investigated using two NMR instruments operating at the same frequency (23 MHz) but hold different sample sizes (8ø × 10 mm and 16ø × 22 mm). Although ideally a third instrument that can hold an even larger sample (e.g. MQC23 that hold a sample of 14 mL) might be included, unfortunately such an instrument was not accessible.

1.4.3 Vis/NIR spectroscopy

Visible/near infrared (Vis/NIR) spectroscopy involves the region of electro-magnetic spectrum between 390-2500 nm. Vis/NIR spectroscopy measures the compositional difference between the light source from the instrument and the light after it has been exposed

to a sample (Abdullah et al., 2014). The Vis/NIR spectra of foods relate to overlapping absorptions corresponding mainly to overtones and combinations of chemical bonds such as C-H, O-H and N-H.

Vis/NIR spectroscopy has been applied to food analysis since its development (Alander et al., 2013). The concentration of water, fat, protein and carbohydrate in samples can be determined using Vis/NIR spectroscopy (Büning-Pfaue, 2003; Forrest et al., 2000; Prieto et al., 2008; Ripoll et al., 2008; Savenije et al., 2006; Wählby and Skjöldebrand, 2001). However, in food matrices, complex physical properties can cause changes of spectra and mask the chemical information, which makes Vis/NIR spectroscopy a secondary method dependent on calibration of reference method using multivariate data analysis (Firtha et al., 2011).

The measurement modes of Vis/NIR spectroscopy include transmission, reflection, transflection, contact and non-contact interaction (interactance) (O'Farrell et al., 2011). The selection among those methods depends on sample types, installment location, etc. (Alander et al., 2013). The technique is fast, sensitive, non-destructive and has the potential to be applied for online monitoring. Vis/NIR spectroscopy has been widely applied for meat quality prediction. As reviewed by Prevolnik et al. (2004), NIR has shown good predicting ability regarding chemical composition of meat and assessing meat in terms of categorization. However, technological and sensory attributes including WHC are poorly predicted by Vis/NIR spectroscopy, which might be attributable to the low precision of reference methods and the heterogeneous characteristic of meat samples and the sample preparation for the reference methods (Prieto et al., 2009). Efforts have been made to predict WHC using Vis/NIR spectroscopy, and various results were obtained regarding predictability (Brøndum et al., 2000; De Marchi et al., 2007; Forrest et al., 2000; Geesink et al., 2003; Hoving-Bolink, 2005; Leroy et al., 2003; Pedersen et al., 2003; Prevolnik et al., 2010; Prieto et al., 2008; Savenije et al., 2006). Table 1 summarizes studies that have used Vis/NIR spectroscopy for WHC prediction. Only works measured WHC as drip loss were considered for comparison. As shown in Table 1, reflectance and transmission were among the most selected measurement modes in such studies. In this thesis, the chosen measurement configuration was interatcance, which is similar to transmission except light needs to be scattered to reach the detector. The predictability of Vis/NIR spectra regarding WHC varied in a large range (R^2cal[a]

[a] Coefficient of determination in calibration.

= 0.004-0.71, SE_{CV}[b] = 0.36 – 3.5%), which indicates that the current reference methods lack robustness. In this thesis, Vis/NIR spectroscopy was investigated as a potential online method for WHC determination, using EZ-DripLoss and NMR as reference methods.

[b] Standard error of cross validation.

Table 1. Prediction of drip loss in meat by Vis/ NIR spectroscopy.

Wavelength range (nm)	Measuring mode	Muscle type	Time *p.m.* (spectra collection)	WHC method	R^2cal	SE_{CV} (%)	Reference
280-980	Internal reflectance	Pork, *longissimus dorsi* and ham muscle	24 h	Honikel bag method	0.37	2.53	(Brøndum et al., 2000)
400-800	Reflectance	Pork, *longissimus dorsi* and ham muscle	48-54 h	Honikel bag method	0.52	2.14	(Brøndum et al., 2000)
802-2500	Reflectance	Pork, *longissimus dorsi* and ham muscle	48-54 h	Honikel bag method	0.41	2.43	(Brøndum et al., 2000)
900-1800	Transmission	Pork, *longissimus* muscle	30 min post exsanguination	EZ-DripLoss method	0.71	1.8	(Forrest et al., 2000)
833-2500	Reflectance and transmission	Beef, *longissimus thoracis* muscle	2 or 8 days	Barton-Gade method	0.38-0.54	0.82-0.99	(Leroy et al., 2003)
380-1700	Reflectance	Pig carcass	24 h	Honikel bag method	0.004	1	(Hoving-Bolink, 2005)
400-800	Reflectance	Pork, *longissimus* muscle	24 h	Horizontal drip method	0.31-0.55	1.24-1.35	(Savenije et al., 2006)
1100-2498	Reflectance	Freeze-dried / fresh minced beef	-	Hanging method	0.1/0.04	3.5/3.44	(De Marchi et al., 2007)
1100-2500	Reflectance	Beef, *longissimus thoracis* muscle	7 or 3 days	Honikel bag method	0.20/0.26	0.36/0.55	(Prieto et al., 2008)
1000-2500	Reflectance	Pork, *longissimus* muscle	48 h	Tray drip loss method	0.51-0.55	1-1.1	(Geesink et al., 2003)
400-2500	Reflectance	Pork, *longissimus dorsi* muscle	48 h	Tray drip loss method	0.39-0.58	0.81-0.96	(Prevolnik et al., 2010)
400-2500	Reflectance	Pork, *longissimus dorsi* muscle	48 h	EZ-DripLoss method	0.37-0.66	0.95-1.31	(Prevolnik et al., 2010)

*Note: R^2cal: coefficient of determination in calibration, SE_{CV} (%): standard error of cross validation.

2 Objectives

Improve the understanding of the drip production process and investigate the suitability of NMR as a reference method for faster, online spectroscopic methods.

In particular, the present thesis aims to:

1). Use NMR as a tool to gain information on the irreversible and slow transport or migration of water and macromolecules from the sample during short-term drip production.

2). Access the accuracy of NMR in measuring small changes of water in a model system and in meat.

3). Comparing NMR and EZ-DripLoss methods and determining whether NMR relaxometry could be a suitable reference method for measuring WHC in meat.

4). Identifying and minimizing different sources of error in T_2 measurement.

5). Exploring the ability of NMR to predict purge from pork muscle after vacuum-packed storage post mortem.

3 Methodological considerations

3.1 Study materials

Two simple model systems were investigated before implementing NMR to meat samples, including $CuSO_4$ solution of different concentrations and a series of H_2O/D_2O mixtures. The solutions were selected due to their simple and homogeneous characteristics compared to meat samples. Copper (II) sulfate (anhydrous, ≥99.0%) and deuterium oxide (99.9 atom % D) were purchased from Sigma-Aldrich Co (St Louis, MO, USA).

Studies designed for method comparison consisted of animals with a variation of WHC and were selected according to several factors including breeds, meat percentage/back fat thickness, chilling methods and early pH (6 h *p.m.*). Breeds used in this thesis included Landrace, Duroc, Noroc (50% Duroc, 25% Landrace and 25% Yorkshire) and LYLL (25 % Yorkshire and 75 % Landrace). The porcine *longissimus dorsi* muscle was selected as the study material due to its lean and homogeneous nature. It has very low intramuscular fat (~ 1%, averaged from 710 pigs of Landrace breed, courtesy of Norsvin, Harmar, Norway), but heterogeneity still exists throughout the muscle, and has been reported to increases towards the cranial end (Christensen, 2003). This heterogeneity was studied in **paper II**. In addition, the LD muscle has been studied extensively regarding WHC, thus was considered suitable for result comparison purposes.

3.2 Sampling protocols

The sampling procedure for NMR measurements is shown in Figure 4 a-c. A slice of approx. 1 cm in thickness was cut off from the *longissimus dorsi* muscle. A cylindrical sample (8ϕ × 10 mm, ~0.459 g) was cored using a sharp cork borer without pressing the muscle. Since there is a distance of around 12.5 cm between the top of the NMR instrument and the homogeneous magnetic field where the sample should be placed during measurement, the sample holder should be long enough (Figure 4 d). The sample was then gently pushed to the bottom of the glass tube with a glass rod, while maintaining the fiber direction parallel to the cylindrical axis. A layer of parafilm was placed on the top of the muscle to prevent water evaporation. It should be mentioned that although care was taken during transferring the meat sample into the glass tube, the glass rod may have unavoidably caused small amount of unwanted liquid loss, which may be a source of error. The glass sample holder was used in **paper I-IV**. Another

bigger, detachable Teflon sample holder was also used in **paper IV** (Figure 4 d-e), where samples could be inserted into the bottom of a Teflon sample holder, which was the same size as the meat samples, and a long Teflon rod could be attached to the top of the sample holder. This sample setup eliminates possible errors caused by sample squeezing. In addition, the effect of sample holder size on sampling errors was considered. Bigger samples have smaller surface-to-volume ratio, and likely to be less affected by sample handling. The sample irregularity was also expected to be lower on bigger samples. The bigger sample holder is shown in Figure 4 e and was used in **paper IV**.

Another sample setup was used in **papers I, III** and **IV** to document the changes of the sample during dripping. The sample was suspended above the bottom of the glass tube, where the drip fluid can flow down freely as shown in Figure 4f. A layer of parafilm was placed on the top of the sample to avoid water evaporation.

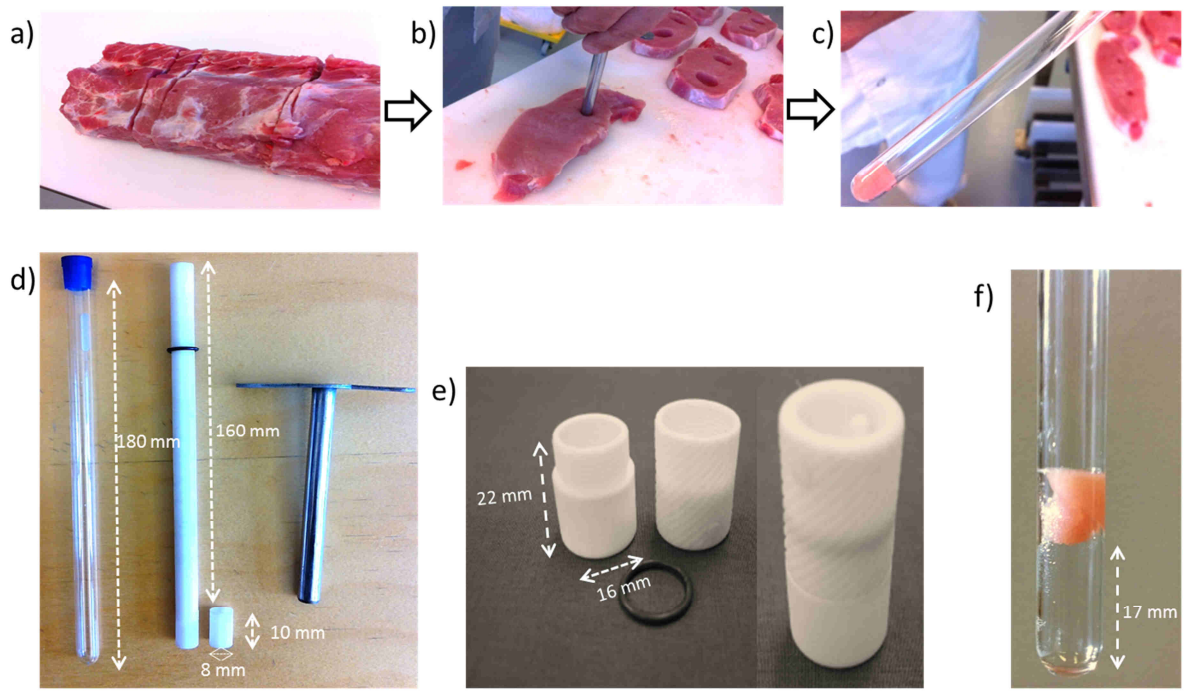

Figure 4. a) Trimmed *longissimus dorsi* muscle. b) Sampling on a thin slice of LD muscle using a sharp cork borer. c) An NMR tube with a meat sample in the bottom. d) Glass NMR sample holder (left), detachable Teflon sample holder (middle) and cork borer (right). e) Larger Teflon sample holders, detached (left) and attached (right). f) Suspended sample in an NMR tube, with parafilm on the top.

When different techniques (EZ-DripLoss, NMR, Vis/NIR spectroscopy and X-Ray spectroscopy) were compared, the LD muscle was divided into different sizes and assigned to different techniques accordingly. Slices of defined thickness at the cranial and caudal ends were discarded to avoid potentially extreme drip loss.

3.3 NMR measurements

Transverse relaxation was measured by applying a traditional CPMG pulse sequence (Meiboom and Gill1, 1958). Different parameters were used based on the materials and instruments. Further details can be found in the Experimental part of **papers I-IV**. Other experiments not considered in **papers I-IV** comparing the two NMR instruments (with the same magnetic field strength, 0.54 T, Maran Ultra NMR instrument, Resonance Instruments, Witney, UK) that have different sample holder sizes were conducted, in order to compare the measurement errors. The instruments had sample holder sizes of 8ø × 10 mm and 16ø × 22 mm.

3.4 Vis/NIR measurements

Figure 5a shows the instrumental setup for Vis/NIR measurement for meat samples. The UV/Vis/NIR spectra were collected using a USB2000 spectrometer (Ocean optics, Dunedin, FL) in the range 350-1025 nm. The two optical fibers (one fiber for illumination (400 µm) and another fiber (200 µm) for detection) separated by a set distance of 8 mm, were inserted into meat samples (~1 cm under sample) resulting in a Vis/NIR interactance signal with more increased absorption features than a reflectance configuration would give. The incoming light propagated through myofibers and was transmitted back to the detection optical fiber. The interactance configuration requires that light is scattered through the muscle before it reaches the detection fiber and the resulting interactance spectra contains both the scatter effects and strong absorption peaks since the light travels a relatively long distance before it is detected. This setup was used in **paper II**.

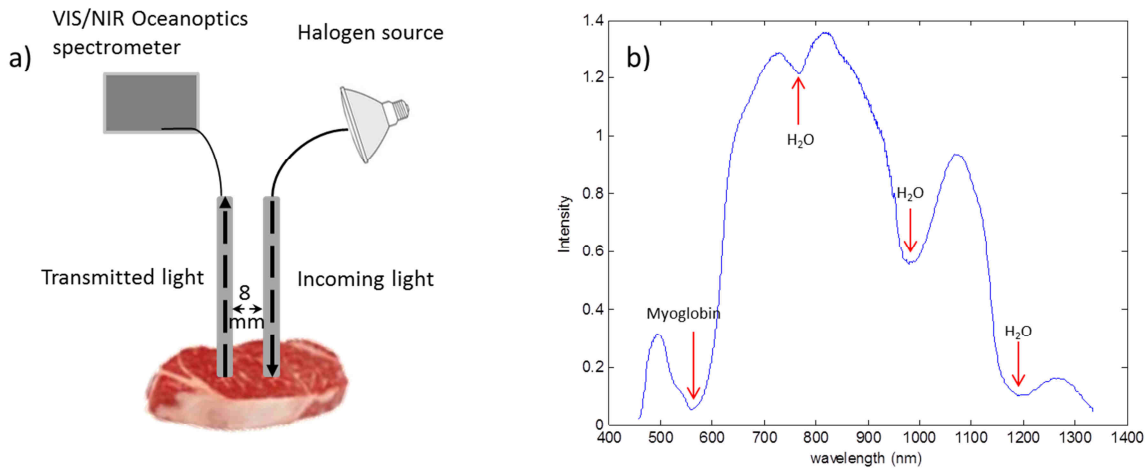

Figure 5. a) Set up of Vis/NIR for WHC measurement. b) A typical Vis/NIR transmission spectra of meat samples.

4 Data Analysis

4.1 NMR relaxation data analysis

The two approaches used for T_2 relaxation data analysis were discussed in section 1.4.2.3, namely the discrete and the continuous models. The discrete model fitting includes three exponential functions (Eq 4) was performed using Origin 9.0 (OriginLab Corporation, MA, USA). One fitted curve and its three exponential components are shown in Figure 6 a as an example. The residue plot showing the difference between observed data and fitted curve is shown in Figure 6 b. The residuals were small and randomly distributed except for a slight effect of non-randomness in the early part of the CPMG curve.

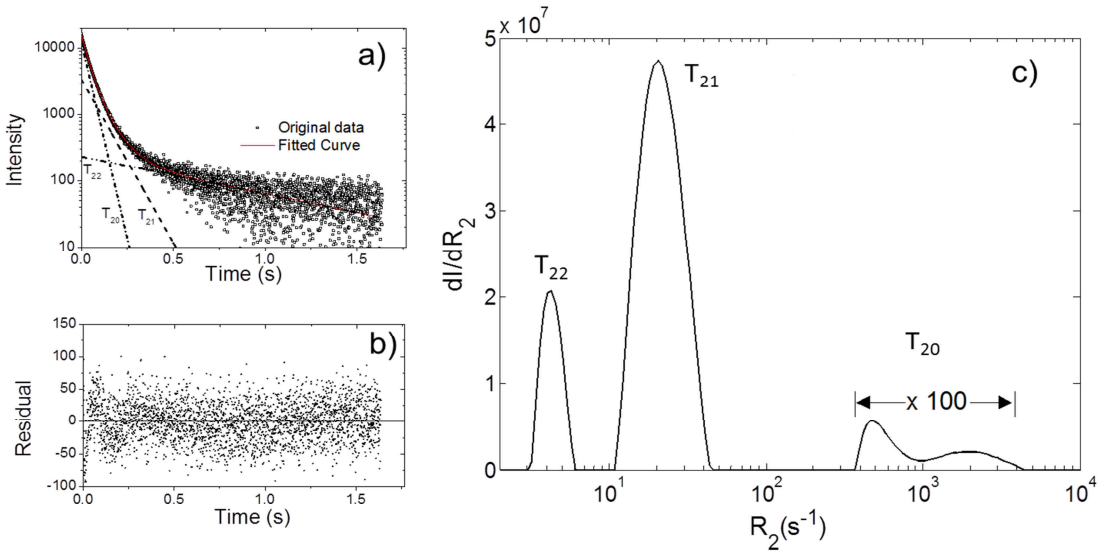

Figure 6. a) Observed CPMG response curve of a meat sample shown in black dots, fitted to a sum of three (T_{20}, T_{21} and T_{22}) exponential functions model (Eq 4) and b) residual plot between the observed CPMG curve and the model fitted curve (3-exponential function). c) The relaxation rate distribution $F(R_2)$ of water in the same meat sample as Figure 6 a-b. The intensity of the fast R_2-distribution component $F_0(R_2)$ with $R_2 > 300$ s^{-1} was multiplied by a factor of 100 for clarity. The three distribution components are shown as T_{20}, T_{21} and T_{22}.

As described in section 1.4.2.3, a distributed exponential fitting of the T_2 relaxation data was performed and a continuous $\log(T_2)$-relaxation time distribution $dI/d\log(T_2)$ was acquired. The R_2-distribution $F(R_2) = dI/dR_2$ was then computed, as shown in Figure 6 c. Three distribution

peaks were observed (shown as T_{20}, T_{21} and T_{22}), in which the fastest relaxation component (T_{20}) is represented by a rather complex shape, indicating deviation from a pure exponential decay. This may explain the initial oscillation behavior of the residue curve shown in Figure 6 a. Two of the relaxation distribution components (T_{21} and T_{22}) were also closely fitted based on a three-parameter function (more details refer to **paper III**), where excellent fit was obtained for all samples.

The discrete model was used to fit the NMR data in **papers I-III**, and the continuous model was used in **papers III and IV**. Direct comparison was made between water relaxation rates and their corresponding mole fractions obtained by the two approaches, and discussed in **paper III**.

4.2 Vis/NIR spectra analysis

The Vis/NIR transmission spectra were corrected by source and background spectra (Eq 10), measured by inserting the optical fibers into glass beads (ø1 mm) in a lightproof case when the source was turned on (as I_{Source}) and off (as $I_{Background}$).

$$\text{Vis/NIR spectrum} = \frac{I_{Meat} - I_{Background}}{I_{Source} - I_{Background}} \quad (10)$$

Figure 5 b shows a typical transmission spectrum (460-1350 nm) of where the absorptions (indicated by arrows) are mainly due to water. The absorption at 578 nm is due to myoglobin (Brøndum et al., 2000), the absorptions observed at 760 nm, 970 nm and 1190 nm were due to third overtone O-H stretching in water, the second overtone of the O-H stretching, and the combination of the first overtone of O-H stretching and the O-H bending respectively (O'Farrell et al., 2011).

Savizky-Golay smoothing was applied to the spectra. Pre-processing methods including mean normalization and Standard Normal Variate method (SNV) (Rinnan et al., 2009) were also assessed.

4.3 Statistical analysis

Linear least-squares regression was used for calibration purposes, to establish the relationship between the NMR proton signal response and mass of water molecules. Linear least-squares

regression minimizes the sum of squares of residuals to find the best line. Coefficient of determination (R^2) was computed and compared for goodness of fit of a model. The root mean square error of linear regression (RMSD) estimates the average deviation from the regression line, and was used to calculate confidence intervals (Burke, 2001). Origin 8.6 (OriginLab Corporation, MA, USA) was used for the linear regression analysis.

To assess if the correlation between quality parameters was statistically significant or not ($P < 0.05$), Pearson correlation coefficient (r) was calculated using OriginPro 2016 (OriginLab Corporation, MA, USA).

The X-variables from data obtained from modern instruments (e.g. Vis/NIR spectra) tend to be numerous and can be strongly correlated, thus the traditional multiple linear regression is not effective (Wold et al., 2001). Partial least square regression (PLSR) enables the analysis of more complex problems. PLSR is a calibration method based on finding the model relating matrix **X** (predictor variables) and **Y** (response variables), in which the PLS components are calculated to find the maximum variation of **X** related to **Y**. PLSR with full internal cross-validation (leave one out) was computed using the Unscrambler (version X 10.3, CAMO Software AS, Oslo, Norway). Statistical parameters including coefficient of determination of cross validation in calibration (R^2_{CV}) and standard error of cross validation in calibration (se_{CV}) were obtained for model comparison.

5 Results and Discussion

5.1 Accuracy of T_2 relaxation analysis

The accuracy of NMR, while separating different T_2 values in a controlled system was analyzed. The T_2 relaxation time of water in the presence of paramagnetic ions differs from pure water, and the scale of T_2 depends on the concentration of the paramagnetic ion. Paramagnetic ions, e.g. copper (II) ions, can reduce the T_2 of water by interacting with hydrogen nuclei, providing additional oscillating field that resonates at the Larmor frequency of the protons (Melville, 2014). Thus, different T_2 values can be observed on $CuSO_4$ solutions of varying concentrations. The T_2 relaxation was measured on a series of $CuSO_4$ solutions ($CuSO_4$, g/L = 0.67, 1.06, 1.94, 4.73 and 14.24), and a linear relation was found between relaxation rates ($1/T_2$) and the concentration of copper (II) ions (Figure 7a), which agreed with early reports (Köylü et al., 2009). As mentioned previously, the T_2 relaxation decay of meat is multi-exponential, and most studies have reported three exponential functions. In order to simulate the multiple exponential behavior of T_2 relaxation in meat, three T_2 values similar to the ones reported in meat samples (1.30, 45.00 and 110.00 ms) were chosen, and the concentrations of $CuSO_4$ solutions (128.17, 3.67 and 1.48 g/L) were calculated based on Figure 7 a. Each of the three solutions was then prepared and measured using NMR in a glass tube separately, and the relaxation curve was fitted to a single exponential function, which resulted in the following T_2 values (1.13, 44.85 and 108.58 ms). Specially designed three-layered cylindrical glass tubes were filled with the three selected $CuSO_4$ solutions, each solution having its own layer (Figure 7 b-c). A single replicate of each tube system was included, and the T_2 relaxation was measured on the 6 tubes with 3 repeated measurements for each tube.

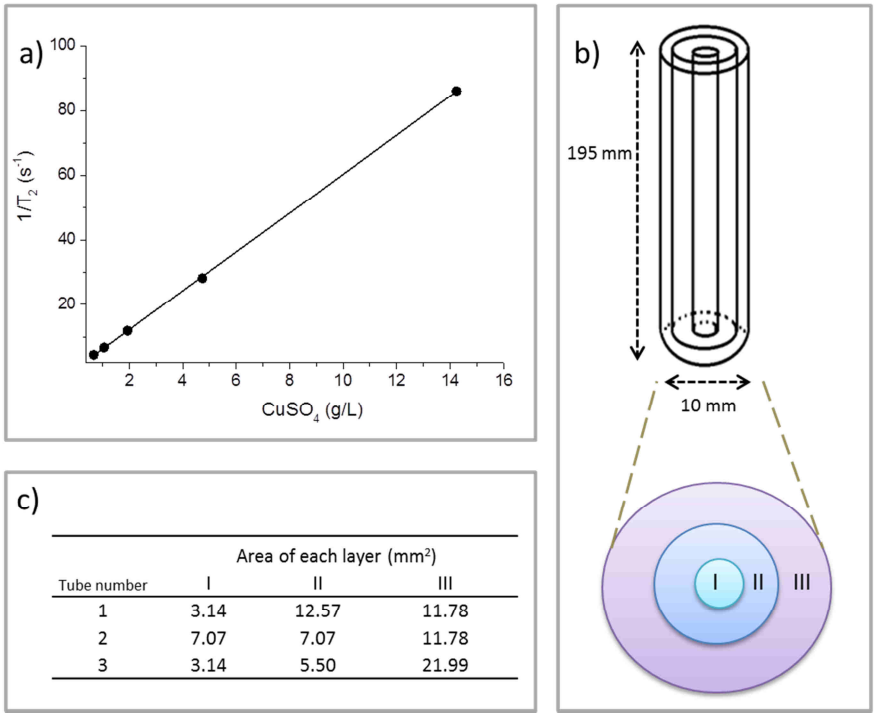

c)

	Area of each layer (mm²)		
Tube number	I	II	III
1	3.14	12.57	11.78
2	7.07	7.07	11.78
3	3.14	5.50	21.99

Figure 7. a) Relationship between the concentration of $CuSO_4$ (g/L) and $1/T_2$ (s^{-1}). b) Three-layer glass tube system labeled based on layers (I-III). c) Three different tube systems (1-3 in the embedded table) of different layer area/unit volume. One $CuSO_4$ solutions was added to each layer of the glass tube system, based on the concentration of the $CuSO_4$ solutions and the area of each layer in the tube (e.g. in tube number 1, the $CuSO_4$ solution of concentration 1.48 g/L was filled in layer I, the $CuSO_4$ solution of concentration 3.67 g/L was filled in layer II and the $CuSO_4$ solution of concentration 128.17 g/L was filled in layer III, according to the embedded table).

The relaxation curve was then decomposed using a three-exponential discrete model, and the average of the three T_2s (n = 6) was computed as 1.17 ms, 45.13 ms and 110.49 ms with relative errors of 10%, 0.3% and 0.4% respectively. Compare to the theoretical values, the relative errors were much smaller on the components with more protons (bigger layer area/unit volume).

Another model system (H_2O and D_2O mixtures) was tested to determine the absolute accuracy of NMR when measuring small changes of water (**paper II**). The relaxation signal intensity is proportional to the number of protons in ^1H NMR. Since deuterium has a different magnetic moment and spin, it is invisible to ^1H NMR. A series of H_2O/D_2O mixtures then had a different number of protons in a fixed volume, which served as a calibration set for water mass based on the NMR proton intensity. The results showed that NMR was able to measure

small water changes accurately in the model system, and the NMR proton intensity had a good correlation to the mass of water in the H_2O/D_2O mixtures (R^2 = 0.9989, 2.6% prediction error in 99% probability).

A similar study was then conducted on meat. It was shown that water content can be predicted from the NMR proton intensity, using the correlation obtained between water mass and proton intensity. Based on 20 samples (8ø × 10 mm, ~0.5 g) from the same porcine LD muscle, the samples mass and the estimated water mass had a slightly poorer correlation (R^2 = 0.9765) than in the model system, where the root mean square error of linear regression (RMSD) was 0.0139 g (~0.375 g H_2O in meat). The results were presented in **paper II**.

5.2 Understanding drip production using NMR

In order to understand the formation of drip and gain information on the gross transport or migration of water and macromolecules during drip, one meat sample (sample setup shown on Figure 4 f) was monitored, without being disturbed, for 45 hours continuously using CPMG NMR at 25 ˚C. The results were reported in **paper I**. Each relaxation curve was decomposed to three relaxation components after subtracting a long T_2 component (t > 0.5s) using the discrete model. The relaxation rates and their respective intensities obtained by the discrete model (section 1.4.2.3) was highly reproducible due to the very distinct relaxation rates (different by a factor of more than 3) and high signal-to-noise (S/N) ratio (>200). Based on the magnitude of the spin-spin relaxation rates, a fast relaxation component (F), an intermediate relaxation component (I), and a slow relaxation component (S) were identified. Both the relaxation rates and their relative intensities during the 45-hour drip experiment fit very well to the second order polynomials within experimental error (Figure 8). No observable changes in signal intensity or relaxation rate within domain F were noted, thus the F domain was considered as not changing during drip/aging, and was excluded for further investigation. The proton relaxation rates of I and S domains revealed a monotonic increase with drip time (t_d). The shortest spin-spin relaxation rate was found to be larger than 8 s^{-1}, which is much large than the relaxation rate of pure water (0.3-1 s^{-1}), and indicated interactions dominating the relaxation of water.

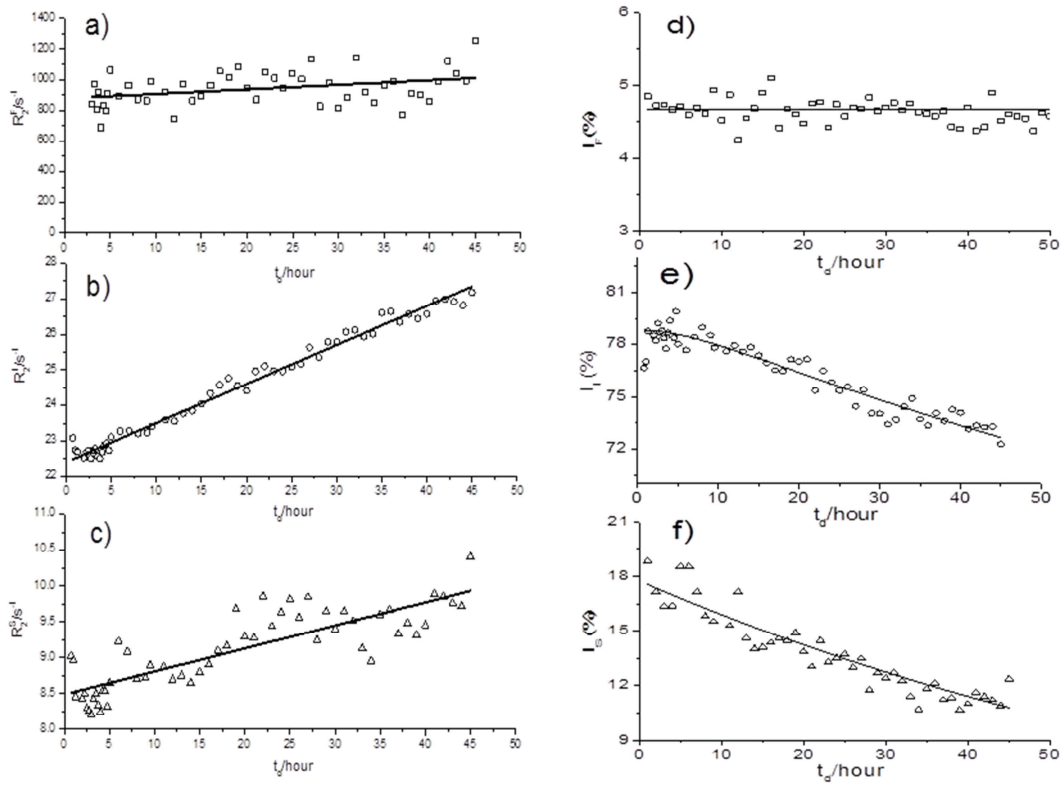

Figure 8. a-c) Observed spin-spin relaxation rates (R_2) within domain F (□), I (○) and S (Δ) as a function of drip time (t_d). d-f) Normalized proton signal intensity of the resolved components F (□), I (○) and S (Δ) as a function of drip time (t_d). The initial sum of intensities of F, I, S and the long-T_2 component was set to 100%.

A simple first order dynamic model (Figure 9), composed of two spatial domains in meat (I and S) and the drip domain (P), was used to describe the migration of water and macromolecules from the inner to the outer part of a sample. The model also assumed that the molecular migration was irreversible from I to S then to P during the 45-hour drip experiment. The rate constants were determined by a simultaneous fit to a number of equations and were presented in Table 2. Neither k_1^E nor k_2^E could be reliably determined which is most probably caused by their rather small intensities of less than 2%. The migration of water from domain S to the drip fluid domain was approximately 4 – 5 times faster than the migration of water from domain I to S, indicating that the drip is strongly governed by migration of water from domain S during the experiments.

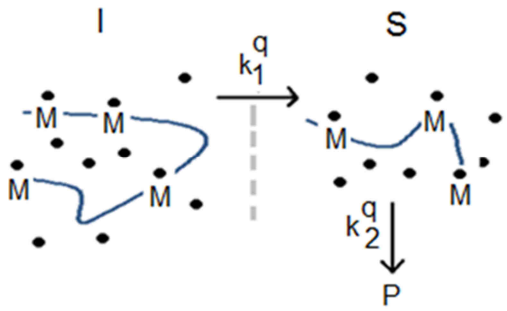

Figure 9. Schematic view of the distribution of water molecules (W: ●) and macromolecules $\dot{M}$ within domains I and S in which $\dot{M}$ contains functional groups possessing a proton E (●) that can exchange with protons in water molecules. The parallel dotted line (— —) is introduced to illustrate the spatial difference between domains I and S. The parameters k_1^q and k_2^q define the rate constants of migration of q (= W and E) between the domains. P represents the drip fluid outside the meat.

The number of water molecules represented by the signal intensity decreased by 8.5% (+ 0.1%) in domain I and by 37% (+2%) in domain S during 45 hours of drip. By assigning domain I and S to the intra- and extra-myofibrillar space respectively, the intensity changes might be a result of myofibrillar shrinkage and longitudinal contraction which “forces” free water from I and subsequently into S, and subsequently out into P (Figure 9). At the end of the experiment, the relaxation rates of domain I (13.1 + 0.3%) and S (21.3 + 0.3%) increased. Under the condition of fast exchange of adsorbed and "free" water within one domain, R_2 is proportional to the surface-to-volume ratio (S/V) of the domain. For spherical or cylindrical geometries it follows that the inverse diameter or the inverse length of the cylinder becomes proportional to the water relaxation rate (R_2^X). According to the data presented in Figure 8 (a-c) an increase in relaxation rates would correspond to a decrease in the diameter/length of domains (I and S) of the order of 10 – 15%, which can be explained by water being expelled from the domain and a reduction in the volume of the domain as the drip progresses (Bertram et al., 2002b).

The drip solution was analyzed at the end of experiment (t_d =45 h), and three distinct components were observed, where one of the R_2 components was comparable to bulk water. The multi-exponential behavior of the relaxation curve of drip solution support previous

results where it was stated that macromolecules migrate from the meat and into drip solution. The number of macromolecules (probably small) migrated into the drip solution was estimated based on the decrease in the number of exchangeable protons in domain S (25% + 2%).

Table 2. Rate constants k_1^W , k_2^W , k_1^E and k_2^E as determined by a simultaneous fit and their respective errors.

Rate constant	Value
k_1^W	$(1.7 + 0.8)\cdot10^{-6}$ s^{-1}
k_2^W	$(7.5 + 0.2)\cdot10^{-6}$ s^{-1}
k_1^E	$(3 + \ ?\ )\cdot10^{-8}$ s^{-1}
k_2^E	$(1 + \ ?\ )\cdot10^{-6}$ s^{-1}

5.3 Assessing NMR as a reference method for WHC compared to EZ-DripLoss method

In order to assess and compare the NMR and EZ-DripLoss methods as potential reference methods for faster, online spectroscopic techniques, LD muscles from forty pigs with a large variation of WHC were measured. Vis/NIR and X-ray spectroscopy were investigated as potential online spectroscopic techniques and the spectra were obtained on the same LD muscles. The results are presented in **paper II**. Of the NMR parameters, the slowest component (T_{22}, 100-250 ms, ~10 % of signal intensity) corresponds to extra-myofibrillar water (Bertram and Andersen, 2004) and was selected as the potential reference value for WHC. This water group has been suggested as the most susceptible to dripping (Tornberg et al., 1993). In this thesis, the Pearson correlation coefficient between T_{22} and EZ-DripLoss values was determined as 0.64 ($P < 0.05$), which was consistent with previous works, where T_{22} was reported to correlate with WHC determined by gravimetrical and centrifugal methods (Bertram et al., 2001a; Brøndum et al., 2000; Tornberg et al., 1993).

PLSR models using Vis/NIR or X-ray spectra as response parameters, and T_{22} or EZ-DripLoss values as “design” variables were summarized in Table 3. In contrast to EZ-

DripLoss values, the Vis/NIR and X-ray spectroscopies exhibited good correlations (R^2_{CV}) between both spectra and T_{22} values. It should be noted that the standard error of cross validation of the two reference values (T_{22} and EZ-DripLoss) are not directly comparable as they have different units. Only a few works have attempted to correlate Vis/NIR spectra and EZ-DripLoss values, and good correlations were reported (r = 0.79-0.84, se_{CV} = 1%) (Forrest et al., 2000; Prevolnik et al., 2010). However, other similar approaches, especially those concerned with reference methods for WHC (e.g. Honikel bag method, tray drip loss and Barton-Gade method) for Vis/NIR spectra have shown unstable correlation coefficients (R^2cal = 0.004-0.71, SE_{CV} = 0.36 – 3.5%, Table 1), which indicated the current WHC techniques lack robustness and predictability as reference methods.

Table 3. Statistical evaluation of potential reference methods for WHC measurement in meat using PLSR.

	T_{22}		EZ-DripLoss	
	R^2_{CV} [a]	se_{CV} [b]	R^2_{CV} [a]	se_{CV} [b]
X-ray	0.76	0.0047 s	0.3	1.667%
Vis/NIR	0.66	0.0055 s	0.04	1.933%

a: coefficient of determination of cross validation; *b*: standard error of cross validation.

Figure 10 shows the average Vis/NIR and X-ray spectra of samples characterized by more extreme T_{22} values. The Vis/NIR spectral characteristics that related to short and long T_{22} times agreed with differences in light scattering due to protein aggregation, which relate to differences in WHC. It has been reported that meat with extremely low WHC (i.e. PSE) had high reflectance and vice versa (Greaser, 2001; Monroy et al., 2010). In the current study, samples with long T_{22} (susceptible higher drip) have shown higher transmission. Of samples that had short T_{22} (< 0.08 s), the X-ray spectrum was shifted towards higher energy levels (showed by arrows, Figure 10 b). The shift indicated repeated patterns with shorter spacing and changes in the myofilament spacing, which correlated to WHC. In addition, longer T_{22} has been reported to correlate to larger extrafibrillar (fluid) space by microscopy (Bertram et al., 2002c; Pearce et al., 2011). These results highlight the potential application of NMR as a reference method for WHC, as well as the necessity to evaluate other spectroscopic techniques, especially the not widely explored energy dispersive X-ray as an online technique.

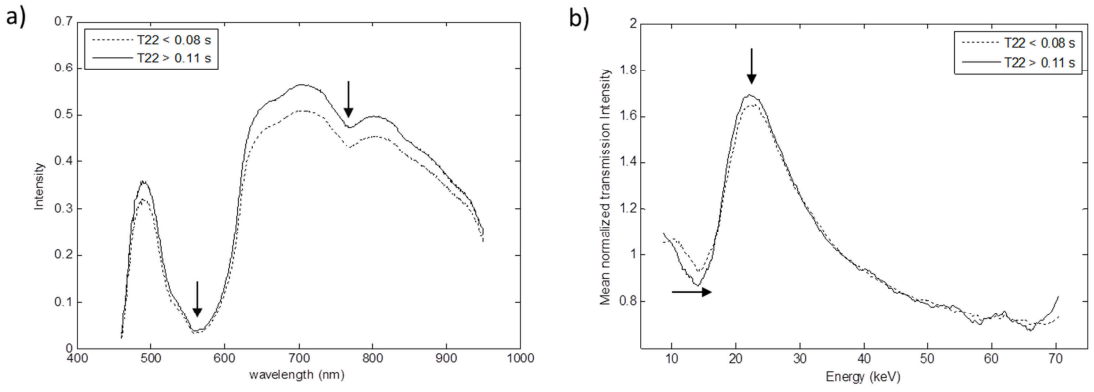

Figure 10. a) Averaged Vis/NIR transmission spectra and b) averaged mean normalized X-ray spectra based on the short (dotted line) and long (solid line) T_{22} relaxation time.

5.4 Errors regarding reference methods for WHC

As mentioned in section 1.4.1, the EZ-Driploss percentage of a loin is calculated as the average of two samples from the same slice. However, the correlation between the two presumed identical samples of EZ-DripLoss method was low (R^2 = 0.39, RMSD = 0.14%, assessed on 710 porcine LD muscles), and the EZ-DripLoss value is known to depend on the position along the LD muscle (Christensen, 2003). The similar error in NMR measurements due to sampling positions was analyzed along one LD muscle. T_2 relaxation was measured against slice numbers (10 slices in total) at two locations (towards dorsal or ventral ends, similar to the EZ-DripLoss positions) on both left and right loins from one pig at the same time. The left loin was measured using a smaller sample size (8ø × 10 mm), and the right loin was measured using a bigger sample size (16ø × 22 mm). After fitting each T_2 relaxation curve to the discrete model composed of three exponential components, the obtained T_2 relaxation parameters are plotted along slice number (Figure 11).

For the suggested reference value of WHC, T_{22} measured on smaller samples (8ø × 10 mm) was reported in **paper II**. After excluding 3 samples for each position (R and B), the mean $\overline{T}_{22}$ at position R (towards dorsal end) and B (towards ventral end) within any slice was calculated to be $\overline{T}_{22}(R)$= (0.145 + 0.002) s and $\overline{T}_{22}(B)$ = (0.149 + 0.001) s, corresponding to a relative error of less than 1%, which is of the same order as the inherent NMR error. Interestingly, the T_{22} values of bigger samples had less variation between R and B (indicated by two red lines in Figure 11 b) compared to the smaller samples (indicated by two black lines

in Figure 11 b). The T_{22} values measured using those two sample sizes had different magnitudes, showing samples taken from different sides (left and right) of the carcass had different characteristics. Regarding other NMR parameters (T_{21}, I_{21} and I_{22}), less variation between R and B was observed when bigger samples were used, i.e. that the variation between NMR parameters of R and B of any slice was much smaller (comparing the difference between red lines and black lines at each slice number in Figure 11 a, c and d).

The big variation between R and B position on the same slice reflected errors from different sources. One inherent error is caused by the signal-to-noise (S/N) ratio in the NMR signal intensity. The error in the total signal intensity of H_2O/D_2O mixtures of the smaller sample was determined to be 1.2%, and the same error on larger samples appeared to be 1.61%, indicating a small difference that was caused by sample sizes regarding model system. Concerning meat samples, the S/N ratio of the bigger samples was about 5.5 times larger than of the smaller samples. The S/N ratio can be further increased if a larger number of scans are used, enabling a smaller inherent NMR error, but the experiment time will increase accordingly. Other sources possibly contribute to the error including non-separable sample heterogeneity and sample treatment errors, e.g. errors due to the sharpness of the sampling tools or weighing and transferring of a sample into a sample holder may result in moisture loss. However, when bigger samples were used, sampling errors might become less important and fewer outliers were recognized (Figure 11). Standardization of either manual or mechanical sample handling procedures is crucial to minimize the errors regardless of the sample size.

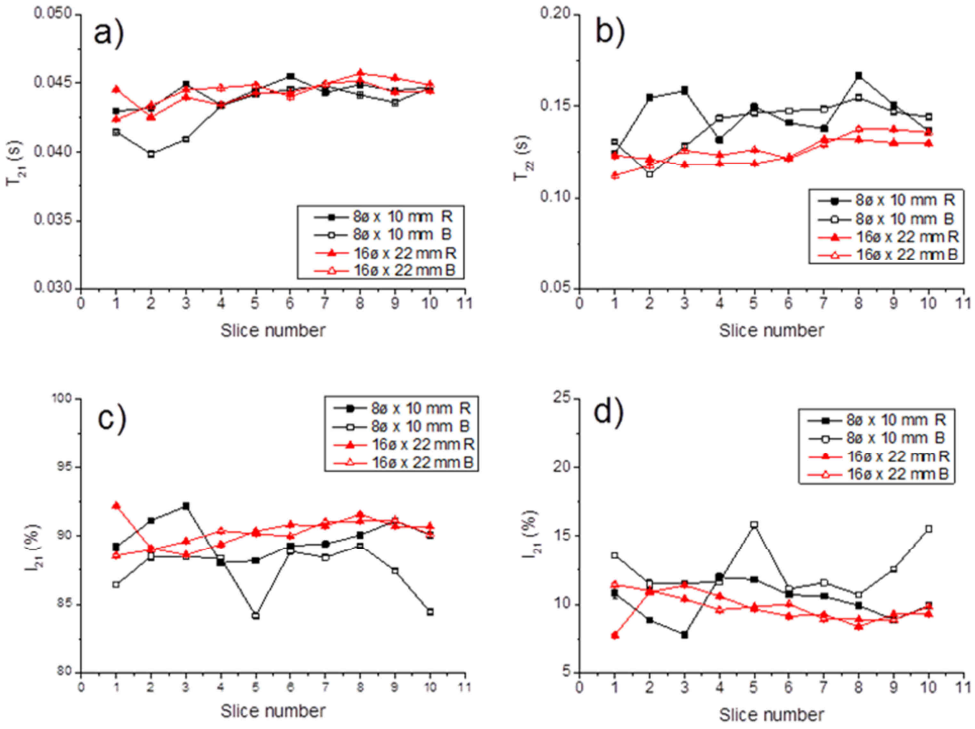

Figure 11. The resolved T_2 time constants (a-b) and their intensities in percentage (c-d) (%, the summation of component I_{21} and I_{22} was set to 100%) for sampling position R (towards dorsal end) and B (towards ventral end) against slice number. The thickness of neighboring slices is 32 mm, of which a certain slice (22 mm for the smaller sample, and 10 mm for the bigger sample) was discarded to avoid drip loss caused by cutting between measurements. The left LD loin of a randomly selected pig measured by NMR with a smaller sample size (8ø × 10 mm, shown in black), while the right LD loin of the same animal was measured by NMR of the same frequency but with a bigger size (16ø × 22 mm, shown in red).

5.5 Comparison of discrete and continuous spin-spin relaxation rate models

Regarding T_2 relaxation response measured on tissue/meat samples, very few works have compared the two methods for data analysis directly ─ the discrete and the continuous models (Bertram et al., 2002a; Menon and Allen, 1991). In **paper III**, the T_2 relaxation response in a meat sample (cut at 96 h *p.m.*) suspended in an NMR tube was measured every hour during a 49-hour drip period at 25 ˚C. Each relaxation response was fitted to a three-component discrete model as well as continuous relaxation model. The continuous model included deriving a distribution $dI/dlog(T_2)$ from the CPMG signal response, and then the obtained

distribution was fitted perfectly to the distribution function (Figure 12 a), as described in **paper III**.

Three parameters calculated from two models (continuous model, X = C and discrete model, X = D) — $\overline{R}_{2i}^{X}$ (mean relaxation rate of the fast (i=0), intermediate (i=1) or slow component (i= 2)) and f_i^X (mole fraction of the fast (i=0), intermediate (i=1) or slow component (i= 2)) were directly compared. Interestingly, the intensity (or area) of fastest relaxing component calculated by both models revealed to be constant, although the discrete model predicted a somewhat larger amount compared to the continuous model, by about 23(+8) %. This again proved that the fastest relaxing component representing bound water does not contribute to drip loss, as presented in **paper I**. Regarding relaxation rate of the fastest component ($\overline{R}_{20}$), the continuous model predicted an increasing molecular motional constraint of the bound water whereas the discrete model did not reveal any such change with time during the 49-hour experiment. Fitting methods seemingly affected the slowest relaxing component ($\overline{R}_{22}$, < 10% in fraction) more dramatically. Both ratios f_2^D / f_2^C and $\overline{R}_{22}^D / \overline{R}_{22}^C$ increased with decreasing f_2^C (calculated by the continuous model, Figure 12 b-c) which reflected the inconsistency between the two model approaches C and D. When the magnitude of f_2^C was smaller than 5%, $\overline{R}_{22}^D$ became larger than $\overline{R}_{22}^C$ by nearly 25%, while f_2^D became larger than f_2^C by nearly a factor of 3. These differences should be highlighted since rather different biophysical interpretations of the relaxation results can be obtained when the two model fitting methods are used. Finally, the relative error in $\overline{R}_{2i}$ and f_i (i = 1 or 2) were found to depend strongly on the S/N of the T_2 relaxation data.

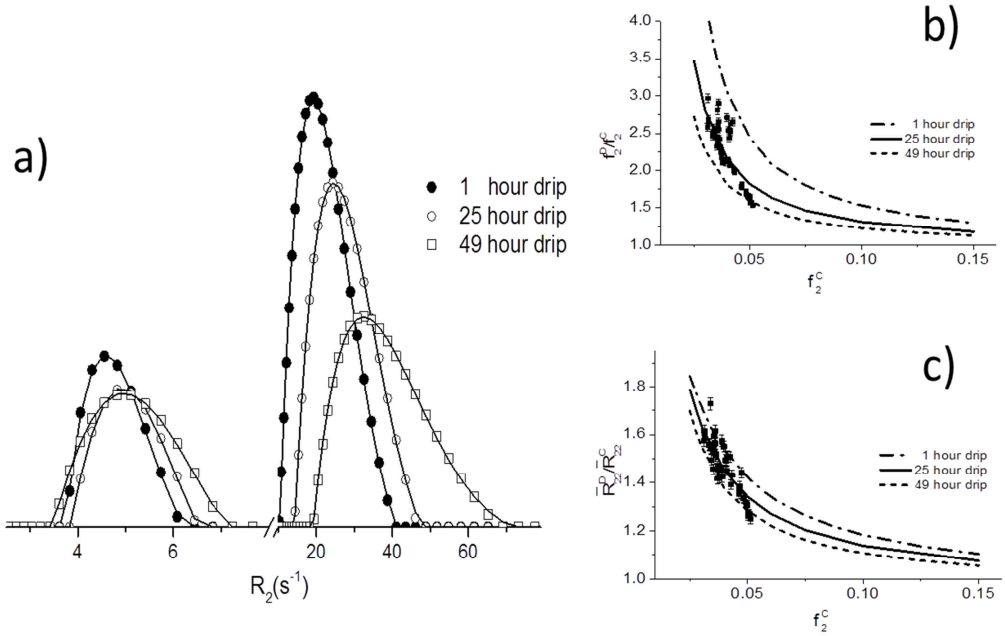

Figure 12. a) Model fitted (─) and observed (dots or squares) relaxation distributions acquired at 1 hour (●), 25 hours (○) and 49 hours (□). b-c) Experimental (■) and model calculated (dotted curved lines) ratios f_2^D / f_2^C and $\overline{R}_{22}^D / \overline{R}_{22}^C$ against f_2^C. The superscripts "C" and "D" represent the continuous and discrete model approaches, respectively. The continuous curves were obtained by model calculations.

5.6 Prediction of purge in meat packages

Purge is referred to as the accumulation of a red aqueous solution of proteins in packaged, refrigerated meat, and relates to what would be visible to a consumer. In **paper IV**, NMR and other quality parameters were assessed on LD muscles from 18 pigs to correlate with purge after vacuum-packed storage at chilled temperature for 9 days. Pearson correlation coefficients (r) was calculated and showed that purge (%) measured on day 9 *p.m.* correlated significantly ($P < 0.05$) to a number of parameters. However, NMR parameters measured at 24 h *p.m.* showed very limited prediction ability ($|r| = 0.37\text{-}0.52$), which suggested that the distribution and mobility of water in meat on day 1 *p.m.* may be of limited relevance for purge production after storage. The prediction error for purge by different parameters can be

estimated from the RMSD, e.g. the prediction error for purge using the relaxation time of the intra-myofibrillar water domain (T_{21}) measured on day 1 *p.m.* was ±2.6% (2 x RMSD with 95% probability, r = -0.46). By comparing the NMR parameters measured on day-1 *p.m.* and after 9-day storage, T_{21} and T_{22} decreased, suggesting lower mobility in both intra- and extra-myofibrillar domains. An increase in the normalized area of T_{21} was observed, which suggested possible uptake of extra-myofibrillar water.

In order to understand the poor predictability, NMR measurements of water mobility and distribution was conducted on one meat sample (cut at 96 h *p.m.*) daily during a 9-day storage period. The sample setup in Figure 4 f was used. Results shown in Figure 13 indicated complex water movement during the 9-day storage period, which can be divided into three phases (shown as 1-3 in Figure 13):

1). Water exchange between intra- and extra-myofibrillar domains (from day 1 to day 5), that the increase in the area of the T_{22} domain accounted for 63% of decrease in area of T_{21} domain on the day 5 of storage (Δ in Figure 13 a-b). The water exchange did not result in significant purge, as can be seen from the slow decrease in the total area loss (Figure 13 c).

2). Water release from the extra-myofibrillar water being as drip (day 5-7). Continuous decrease of T_{21} and T_{22} area was observed (Figure 13 a-b), which resulted in significant drip (indicated by the decrease in the total area in Figure 13 c).

3). Water inflow from extra-myofibrillar domain to intra-myofibrillar domain. An increase in T_{21} area was observed on day 8-9 of storage (Δ in Figure 4 a), presumed due to the degradation of cytoskeletal structure enabled water flowing back from extra-myofibrillar domain. The decrease in total area loss slowly decreased on day 8 and day 9. The relaxation distribution of the drip fluid in the bottom of the NMR tube was analyzed on day 9. The T_2 value of the drip fluid was of the same order as the T_{22} values. Thus it is reasonable to suggest that the some intake of water from drip fluid into myofibril water compartment is possible.

The experiments verified the complexity of the water redistribution between domains, and explained that it is not straightforward to predict purge after storage from NMR parameters measured on day 1 *p.m.* In addition, the purge and NMR measurement errors make it difficult to predict purge. Although the measurement error of purge using the current method is unknown, the error of purge loss on beef steaks (~0.23 kg) has been reported and estimated to be 3-4 % (Elam et al., 2002).

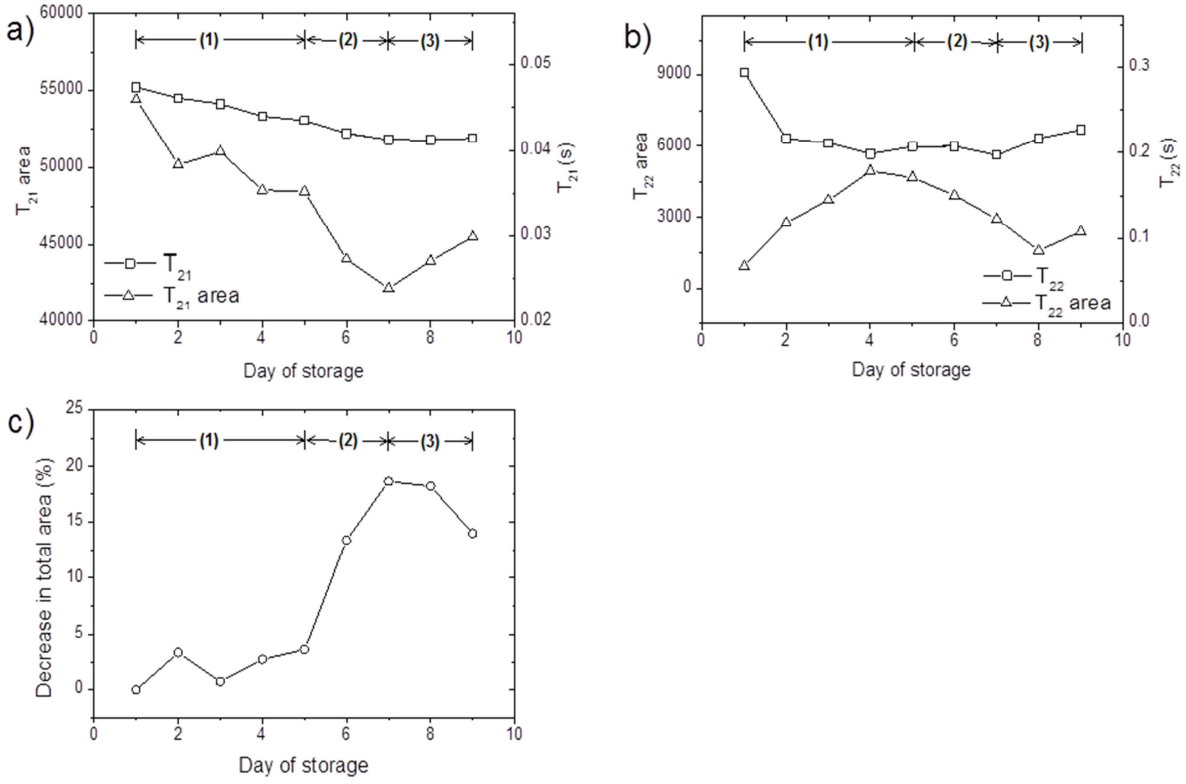

Figure 13. a) T_{21} and its area, b) T_{22} and its area along storage time. c) Decrease in total area (%) of storage on each day compare to storage on day 1. In each figure, three phases are marked according to water movement: (1). exchange between intra-and extra-myofibrillar water; (2). extra-myofibrillar water moves out as drip; (3). water inflow from extra-myofibrillar domain to intra-myofibrillar domain.

6 Advances beyond state of art

Proton NMR T_2 relaxometry has been used for muscle/meat studies for a few decades (Cope, 1969; Hazlewood et al., 1969). The T_2 relaxation of muscle/meat was found to be multi-exponentially behaved, and the T_2 relaxation time was much shorter than bulk water. Several hypotheses have been proposed to explain the multi-exponential behavior (Bertram et al., 2001b), including 1) physical compartmentalization of water, where cell membranes act as physical barriers, 2) contraction of muscle/meat results in the structuration of intracellular water and 3) fast exchange between free water and the wall of differently sized pores. One study of Bertram et al. (2001b) based on processed meat and other protein matrices did not support the physical compartmentalization hypothesis, but reported that the multi-exponential behavior of meat indicates the state of protein integrity and morphology. Three distinct relaxation time domains reflect the degree of water bound to macromolecules (proteins): tightly bound, intra-myofibrillar or extra-myofibrillar.

The drip loss in meat accounts for large economical losses for the meat industry, e.g. according to the data obtained from 2009 in Norway, a 1% increase in drip loss would result in 738 fewer tons of meat (Gjerlaug-Enger, 2011). The formation of drip is still not fully understood, but NMR can assist the understanding of the drip production process. The water and macromolecules transport among different domains in meat during drip loss are informative for understanding drip production, but has rarely been addressed in the literature. Thus in **paper I**, an in situ drip-loss study (45 hours) on a *longissimus dorsi* muscle was performed using proton NMR in order to understand the molecular transport among domains. A simple first order kinetic model was set up in order to interpret proton transverse relaxation in terms of water/small macromolecules in different dynamic regimes, and of their kinetics of exchange during drip-loss. To be more specific, the exchange of “free” water and water molecules temporarily bonded to the functional groups of macromolecules on a biopolymer is a local process, restricted to smaller and individual domains as compared to the much slower and irreversible water transport between and out of domains. The latter transport process involves a net transport of water/macromolecules between domains during drip, and was the focus in **paper I**. It should be noted that the experiments were performed at 25 ˚C, which increased the rate and amount of drip loss compared to experiments performed at lower temperatures. The increased drip rate and amount at a higher temperature were documented on 2 samples (25ø × 25 mm) measured at 2 different temperatures (4 and 25 ˚C) using EZ-

DripLoss setup (Figure 14) during 120 hours after sampling. This effect might be more pronounced on the current smaller NMR sample (8ϕ × 10 mm) than the EZ-Driploss samples (Figure 14) due to the increased surface to volume ratio.

A short T_1 component of minor intensity was found which corresponded to the bound water domain. Further T_2 analysis indicated that the fastest T_2 domain representing bound water did not change as a function of drip time. This complies with what has been reported in the literature, that bound water is less mobile and changes very little in post-rigor muscle (Huff-Lonergan and Lonergan, 2005). The exchange rate constants of water between the domains showed that the irreversible migrating rate of water from the slowest relaxation domain (extra-myofibrillar, contains free water) to drip domain is around 4-5 times faster than the rate of water moving from the intermediate relaxation domain (intra-myofibrillar, contains immobilized water) to the slowest domain. This indicated that the drip production at early storage/drip time is governed by migration of water from the extra-myofibrillar domain, which is consistent with a previous work (Zarate and Zaritzky, 1985). Myofibrillar shrinkage and longitudinal contraction may provide force for the water transport from intra- to extra-myofibrillar space and further out of the meat, this has been already reported (Bertram et al., 2002b), and supported by the increase of relaxation rates in both domains in current experiments. The migration rate of the macromolecules could not be reliably estimated due to the rather small fraction of exchangeable protons (< 2% of the total proton intensity), but the relative ratio of macromolecules in intra-/ extra-myofibrillar space was estimated to be around 11.

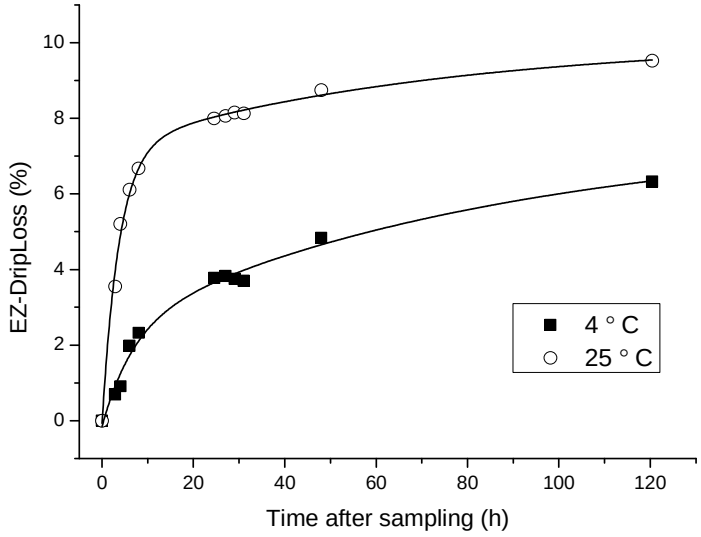

Figure 14. EZ-DripLoss values of two meat samples (sampling at 96 h *p.m.*) of size 25ø x 25 mm stored at 4 or 25 ˚ C as a function of time.

The majority of methods for WHC prediction are slow, tedious and time consuming (e.g. EZ-DripLoss method, ≥ 24 hours) which indicate the need for a faster, accurate and robust reference method for WHC measurement. NMR transverse relaxometry is a relatively faster technique (measurements within several minutes) that has been gradually accepted and applied as a tool to analyze WHC in meat products, as it provides information on the physical and chemical properties of myowater (Bertram and Andersen, 2004). Some of the relaxation parameters obtained from the NMR relaxation curve showed certain correlation to early post mortem WHC measured using e.g. Honikel bag method (rT_{21} = 0.72 and rT_{22} = 0.77) and centrifugation (rT_{21} = 0.50 and rT_{22} = 0.75) at 24 h *p.m.* (Bertram et al., 2001a). The distribution of both intra- and extra-myofibrillar water were found important for WHC determination (Bertram et al., 2001a). Regardless of the numerous studies reported, the measurement error of WHC using NMR has not been clearly addressed. This is actually surprising bearing in mind its economic importance. This topic was assessed in **paper II**, and NMR was found to accurately measure water mass in a controlled model system (H_2O/D_2O mixtures), but the measurement error increased on meat samples. Except random error that may be caused by temperature etc., other error sources regarding NMR measurement include the inherent NMR error and non-NMR error (caused by sample heterogeneity, sampling

handling, etc.). The inherent NMR error depends on S/N ratio, and using the current experimental settings, this error of the total proton signal intensity was determined as 1.2% on the H_2O/D_2O model system (of size 8ø × 10 mm). The error can be further decreased when the S/N ratio is increased (by increasing the number of scans), but the time of analysis will be increased as well.

Various sizes of NMR samples (10 × 10 × 50 mm, $35mm^2$ × 7mm, 7ø × 30 mm, 8cm in length etc.) and different sample handling procedures have been used when WHC was studied on meat in the literature (Bertram et al., 2002a; Bertram et al., 2003; Straadt et al., 2007; Tornberg et al., 1993). However, as sample heterogeneity and sample handling will affect the NMR method by changing water distribution in meat samples, errors caused by sample treatment and sample heterogeneity can vary accordingly. This topic is of great importance regarding method accuracy and result comparison, but has been seemingly omitted. When bigger samples are used, sample heterogeneity and water loss due to sampling might decrease, which affect measuring errors. Although the errors from these two sources (sample heterogeneity and sample handling) cannot be separated, these errors can be reflected on samples of different sizes. The inherent error of NMR is similar on samples with small (8ø × 10 mm) or big size (16ø × 22 mm) investigated in this thesis using the H_2O/D_2O model system, both below 2 %. However, as shown in Figure 11, difference between paired measurements on each slice of all the NMR parameters was smaller when the measurements were done using the bigger sample size. In other words, there were fewer outliers when bigger sample size was used, and these outliers were most likely caused by sample heterogeneity and sample handling. In order to achieve smaller errors, the present thesis suggests confirming and then implementing the NMR instrument with a bigger sample holder size (16ø × 22 mm) over the instrument with a smaller sample holder size (i.e. 8ø × 10 mm) for industrial use for intact meat measurements. In addition, compared with EZ-DripLoss method, NMR was independent on slice number and also had lower absolute error.

In **paper II**, the potential of using NMR relaxometry as a reference method for fast spectroscopic methods of WHC in pork *longissimus dorsi* muscle was assessed. Although the T_2 relaxation time of the slowest relaxation component (T_{22}, corresponding to extra-myofibrillar/extra-cellular water and is most susceptible to dripping (Tornberg et al., 1993)) has been found to correlate with WHC (Bertram et al., 2001a), T_{22} has not been investigated as a reference value for WHC previously. In **paper II**, T_{22} values showed higher correlation (assessed by PLSR analysis) with both Vis/NIR and X-ray spectra than drip loss values

measured using the EZ-DripLoss method, indicating the potential T_{22} has as a reference value for WHC.

Two approaches (the discrete and the continuous model) have been used to assess the T_2 relaxation data, as summarized in section 1.4.3.2. The continuous model has been suggested to be more appropriate for water relaxation in complex heterogeneous samples (e.g. muscle) (Lillford et al., 1980). However, very few works have compared the two methods (Bertram et al., 2002a; Menon and Allen, 1991), in which Bertram et al. (2002a) performed an indirect comparison. There has been no direct comparison between these two methods in the literature. The correlation between WHC (determined using Honikel bag method) and T_2 relaxation data on water in meat fitted using different methods were reported to be different, and a higher correlation was obtained when the continuous model (r = -0.85) was compared to the discrete model (r = -0.77, 2-exponential function) (Bertram et al., 2002a). This indicated that the two fitting methods provided different results regarding NMR parameters. Although the true values of the T_2 are not known, the difference regarding the two models may result in rather different biophysical interpretations regarding water activity in meat during drip, which is of significance in understanding WHC. Thus in **paper III**, the "discrete" and "continuous" relaxation rate models were directly compared and revealed significant differences in both relaxation rates and corresponding mole fractions, as derived from the same experimental CPMG response, and was confirmed by analyzing synthetic CPMG data. The differences showed that cares must be taken when data fitting methods are selected for complex meat samples, especially when the acquired results are to be compared with other works that used different data fitting methods.

In the last manuscript (**paper IV**), the predictability of quality parameters, especially NMR parameters measured early post mortem (before or at 24 h) were discussed regarding 9-day storage purge. The purge produced during storage reflects the visibly accumulated red aqueous solution of proteins in packaged refrigerated meat, which is important for consumer acceptance, but to the best of knowledge, very few works have predicted purge using data obtained early post mortem and none of the works used NMR data. As summarized in a published investigation (Huff-Lonergan and Lonergan, 2005), desmin degradation at day 1 *p.m.* was a reasonable predictor for purge loss, in addition, desmin degradation accounted for 24.1% variation of purge loss over 7 days by using stepwise regression models. The purge production process follows different rates post mortem (Zarate and Zaritzky, 1985), which depends on the meat structure changes (which causes WHC changes). If purge is to be

predicted early post mortem, a method with high precision is needed. A number of parameters measured before or at 24 h *p.m.* correlated with purge, in which T_{21} measured on day 1 *p.m.* correlated negatively to purge (r = -0.46, RMSD = 1.31% of 1.15-7.69% purge). However, it corresponded to a large prediction error i.e. ±2.6% (2 × RMSD, 95% probability). The low correlation between NMR parameters on day 1 and day-9 purge suggests that it was difficult to predict purge early post mortem. A closer investigation of the T_2 characteristics on both day 1 and day 9 showed that both T_{21} and T_{22} have decreased on day 9 *p.m.*, indicating the decreased mobility in intra- and extra-myofibrillar water. A decrease in T_{21} on day-7 and day-14 storage has been reported elsewhere (Straadt et al., 2007). The decrease in T_{22} also indicated a decrease in drip loss (increase in WHC), as T_{22} has been reported to reflect the width of gaps between meat fiber bundles and to correlate positively with drip loss (Tornberg et al., 1993). The area of each domain reflects the amount of water, and showed that there was an average increase of about 2.4% in the T_{21} domain, which might be a result of water inflow based on the hypothesis, that during storage, the cytoskeleton proteins degraded, and water flows into extracellular space ceases, and previously expelled water can to some degree reverse (Huff-Lonergan and Lonergan, 2005; Kristensen and Purslow, 2001; Melody et al., 2004; Straadt et al., 2007). The water uptake will cause swelling of the myofibrils, which has been recorded by confocal laser scanning microscopy and changes in T_{21} width during storage (Straadt et al., 2007). The effect of storage time (9 days) on continuous purge production was studied on one meat sample (taken at 96 h *p.m.*) suspended in an NMR tube. Decrease in T_2 time constants was observed during storage and area analysis showed water exchange between domains was dominant during the first 5 days of storage. Major drip was produced on day-6 storage. An increase in T_{21} area showed possible water intake from extracellular area. The complexity of the water movement between domains during storage, together with the error in the NMR and purge measurement determined the poor prediction of purge.

7 Conclusions

CPMG NMR can provide valuable information regarding water mobility and distribution in meat. The NMR relaxation-rate data on an in situ drip loss study (45 hours) suggested that information regarding the exchange of water and larger molecules between the distinct domains can be extracted to assist the understanding of meat structural changes during drip. The studies presented in this thesis have shown that NMR accurately measured small changes of water content in a homogeneous model system (D_2O and H_2O mixtures), and the inherent error of NMR method was rather low (1.2%). When this was repeated on meat samples measured, the water content was slightly less accurately predicted as expected, due the heterogeneity and complexity of the meat. The spin-spin relaxation curve of meat could be decomposed into three components, each of which has distinct mobility. T_2 values can be accurately separated in homogeneous model system ($CuSO_4$ solutions of varying concentrations), but when meat samples were measured, the errors in the T_2 value, especially of the smaller component (T_{22}) was higher, which can be a result of sample heterogeneity and sample handling etc. By increasing sample size, the detected error decreased as the result of increased S/N and possibly decreased sample handling/inhomogeneity error. Of the same operating frequency (e.g. 23 MHz), the NMR instrument can measure a larger sample volume is thus preferred for water measurement in intact meat samples for industrial use.

NMR showed potential as a reference method for predicting WHC and correlated better to both Vis/NIR and X-ray spectra compared to the traditional methods, i.e. EZ-DripLoss. It is thus suggested that NMR has potential as a reference method for faster spectroscopic methods of WHC in meat. In the storage experiments, NMR measured on day 1 *p.m.* had limited prediction ability of purge produced during longer storage time (9-day) in packaged meat, due to the complexity of WHC changes during storage and the error in the NMR and purge measurements. Purge production is a combination of water redistribution and dripping, which is closely related to the meat structural changes. Fitting methods of T_2 relaxation data should be carefully chosen. Analysis of T_2 showed differences in decomposed T_2 relaxation rates and their proton intensities when different models (discrete and continuous) were used.

8 Future approaches

1) The ability of NMR to predict purge after vacuum-packed chill storage was not satisfactory. Although changes in WHC is a complex process during storage and this partly accounts for the poor correlation. The prediction may, however, be improved if more measurements are done at the start of the purge production process. Zarate and Zaritzky (1985) have reported a fast release of drip (nonlinear increase of drip upon time) during day 1 *p.m.* on beef, followed at a slower and constant drip rate. The trend of purge production against storage time should be further studied for pork. The correlation might be improved by measuring the meat sample twice at early post mortem using NMR, and the two measurements should be performed after the drip rate has stabilized and can be calculated.

2) Since sample heterogeneity and sample handling were recognized as part of the error sources, further investigation on this matter should be carried out. Sample heterogeneity naturally exists and is unavoidable, but sample handling errors need to be minimized. Water distributions in meat are sensitive to any pressure including vacuum. In the current thesis, NMR samples had a diameter of either 8ø × 10 mm or 16ø × 22 mm. Manual coring was done using a sharp cork borer. Although care was taken when coring samples, it is not guaranteed that the applied pressure was the same for every sample, which might cause increased errors in reproducibility. To study the effect of force/pressure on error in sampling, a mechanical sample coring machine of which the applied force/pressure can be controlled and changed is suggested to be investigated. In order to avoid any differences caused by animals, one loin (e.g. the left loin) from one animal can be divided into 10 slices, and 5 samples are to be cored using the same force/pressure level from the same slice. Different force/pressure shall be applied for coring samples from the respective slice (Figure 15). All samples should be measured by NMR right after cutting, and the decomposed T_2 relaxation parameters can be compared. Since sample handling errors can be minimized by using larger samples, NMR machines with even larger sample holder sizes should be investigated (e.g. MQC23 model, sample size 14 mL from Oxford instrument, Abingdon, United Kingdom).

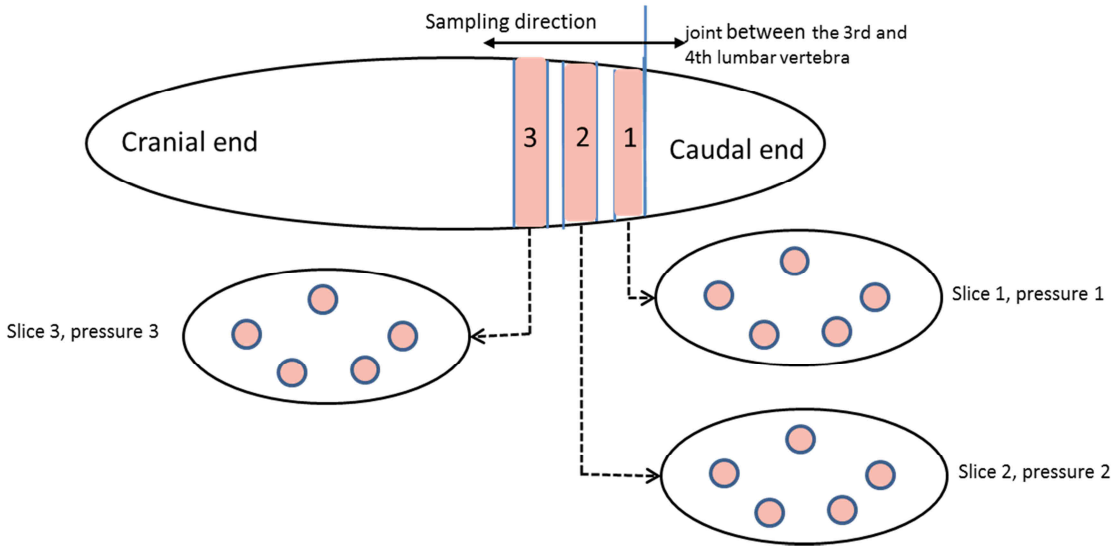

Figure 15. One left *longissimus dorsi* loin is divided for NMR measurement. Sampling starts from the joint between the 3rd and 4th lumbar vertebra. The first three slices are shown (slice 1-3, in light orange), thin white stripes between slices indicate slices to be discarded to avoid dripping caused by cutting. On each slice, five samples are cored using the same force/pressure level. Different force/pressure levels are used for different slices (shown as pressure 1, 2 and 3).

3) In this thesis, studying the changes of the same sample as a function of time during drip/storage was used as a tool to explore the water/macromolecule exchange among domains against time, in order to further understand the mechanism of drip loss. Promising results were obtained. Similarly, as suggested in Figure 16, experiments can be performed on the drip solution produced during storage as a function of time using proton NMR spectroscopy. Proton NMR spectra has rich information regarding metabolite profile, and can thus provide changing patterns of certain metabolites which might be informative for WHC mechanism interpretation.

Due to the high proton content of meat samples, proton NMR spectroscopy has very high sensitivity when meat samples are studied. Proton NMR has been used in metabolic studies (e.g. lactate) for meat quality, when a water suppression technique was used (Bertram and Andersen, 2004). Metabolite profiling of meat is a relatively new research topic, that only a few works have been focused on (Brescia et al., 2002; Graham et al., 2012; Graham et al., 2010; Straadt et al., 2011; Straadt et al., 2014). Straadt et al. have investigated the potential of proton NMR for assessing quality of meat from different breeds, using freeze exudate and

meat extracts and revealed difference in their metabolite profile (Straadt et al., 2011). Another study has analyzed beef LD samples over a 21-day period using proton NMR spectroscopy, and found 12 of the identified amino acids increased using freeze extracts (Graham et al., 2010). They concluded that the increase was a result of increased proteolysis during aging.

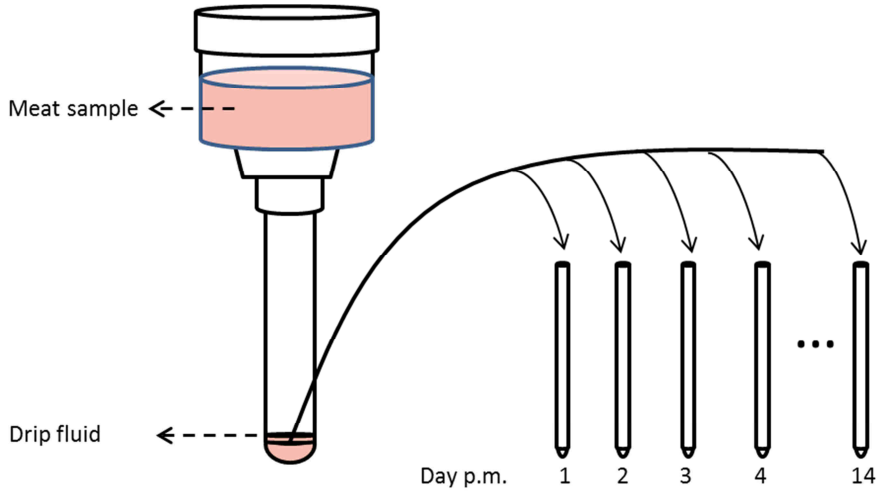

Figure 16. One meat sample before 24 h *p.m.* is stored in the container used in the EZ-DripLoss method at chilled temperature (e.g. 4 ˚C). The drip fluid is collected every day for proton NMR spectroscopic profiling during the storage period (e.g. 14 days).

9 References

Abdullah, B.M., Cullen, J.D., Korostynska, O., Mason, A., Al-Shamma'a, A.I., (2014). Assessing water-holding capacity (WHC) of meat using microwave spectroscopy, in: Mason, A., Mukhopadhyay, S.C., Jayasundera, K.P., Bhattacharyya, N. (Eds.), *Sensing Technology: Current Status and Future Trends I*. Springer International Publishing, pp. 117-140.

Alander, J.T., Bochko, V., Martinkauppi, B., Saranwong, S., Mantere, T., (2013). A review of optical nondestructive visual and near-infrared methods for food quality and safety. International Journal of Spectroscopy 2013, 1-36.

Aubin, M., Prud'Homme, R.E., Pézolet, M., Caillé, J.-P., (1980). Calorimetric study of water in muscle tissue. Biochimica et Biophysica Acta (BBA) - General Subjects 631(1), 90-96.

Belton, P.S., Jackson, R.R., Packer, K.J., (1972). Pulsed NMR studies of water in striated muscle: I. Transverse nuclear spin relaxation times and freezing effects. Biochimica et Biophysica Acta (BBA) - General Subjects 286(1), 16-25.

Belton, P.S., Packer, K.J., (1974). Pulsed NMR studies on water in striated muscle III. The effects of water content. Biochimica et Biophysica Acta (BBA) - General Subjects 354(2), 305-314.

Bertram, H.C., Andersen, H.J., (2004). Applications of NMR in meat science. Annual Reports on NMR Spectroscopy 53, 157-202.

Bertram, H.C., Andersen, H.J., Karlsson, A.H., (2001a). Comparative study of low-field NMR relaxation measurements and two traditional methods in the determination of water holding capacity of pork. Meat Science 57(2), 125-132.

Bertram, H.C., Dønstrup, S., Karlsson, A.H., Andersen, H.J., (2002a). Continuous distribution analysis of T_2 relaxation in meat—an approach in the determination of water-holding capacity. Meat Science 60(3), 279-285.

Bertram, H.C., Karlsson, A.H., Rasmussen, M., Pedersen, O.D., Donstrup, S., Andersen, H.J., (2001b). Origin of multiexponential T(2) relaxation in muscle myowater. Journal of Agricultural and Food Chemistry 49(6), 3092-3100.

Bertram, H.C., Purslow, P.P., Andersen, H.J., (2002b). Relationship between meat structure, water mobility, and distribution: a low-field nuclear magnetic resonance study. Journal of Agricultural and Food Chemistry 50(4), 824-829.

Bertram, H.C., Rasmussen, M., Busk, H., Oksbjerg, N., Karlsson, A.H., Andersen, H.J., (2002c). Changes in porcine muscle water characteristics during growth—an in vitro low-field NMR relaxation study. Journal of Magnetic Resonance 157(2), 267-276.

Bertram, H.C., Schäfer, A., Rosenvold, K., Andersen, H.J., (2004a). Physical changes of significance for early post mortem water distribution in porcine M. longissimus. Meat Science 66(4), 915-924.

Bertram, H.C., Whittaker, A.K., Andersen, H.J., Karlsson, A.H., (2003). pH dependence of the progression in NMR T_2 relaxation times in post-mortem muscle. Journal of Agricultural and Food Chemistry 51(14), 4072-4078.

Bertram, H.C., Whittaker, A.K., Andersen, H.J., Karlsson, A.H., (2004b). Visualization of drip channels in meat using NMR microimaging. Meat Science 68(4), 667-670.

Bowker, B.C., Grant, A.L., Forrest, J.C., Gerrard, D.E., (2000). Muscle metabolism and PSE pork. Proceedings of the American Society of Animal Science, 1-8. Accessed: 13/01/2016. http://www.ars.usda.gov/SP2UserFiles/Place/12657300/pubsFTSL/2000BowkerASAS1-8.pdf

Brescia, M.A., Jambrenghi, A.C., Martino, V.d., Sacco, D., Giannico, F., Vonghia, G., Sacco, A., (2002). High resolution nuclear magnetic resonance spectroscopy (NMR) studies on meat components: potentialities and prospects. Italian Journal of Animal Science 1(2), 151-158.

Bruker BioSpin, (2012). The minispec mq series TD-NMR Analyzers. Accessed: 10/06/2016. https://www.bruker.com/fileadmin/user_upload/8-PDF-Docs/MagneticResonance/TD-NMR/minispec_mqseries_T137089.pdf.

Brøndum, J., Munck, L., Henckel, P., Karlsson, A., Tornberg, E., Engelsen, S.B., (2000). Prediction of water-holding capacity and composition of porcine meat by comparative spectroscopy. Meat Science 55(2), 177-185.

Burke, S., (2001). Regression and Calibration. LC•GC Europe Online Supplement, Accessed: 12/04/2016. http://images.alfresco.advanstar.com/alfresco_images/pharma/2014/08/22/f96fa516-d36f-4554-b891-9af3f75322fc/article-4500.pdf.

Burnell, E.E., Clark, M.E., Hinke, J.A., Chapman, N.R., (1981). Water in barnacle muscle. III. NMR studies of fresh fibers and membrane-damaged fibers equilibrated with selected solutes. Biophysical Journal 33(1), 1-26.

Büning-Pfaue, H., (2003). Analysis of water in food by near infrared spectroscopy. Food Chemistry 82(1), 107-115.

Christensen, L.B., (2003). Drip loss sampling in porcine *m. longissimus dorsi*. Meat Science 63(4), 469–477.

Cope, F.W., (1969). Nuclear magnetic resonance evidence using D(2)O for structured water in muscle and brain. Biophysical Journal 9(3), 303-319.

Correa, J.A., Méthot, S., Faucitano, L., (2007). A modified meat juice container (EZ-DripLoss) procedure for a more reliable assessment of Drip Loss and related quality changes in pork meat. Journal of Muscle Foods 18(1), 67-77.

Damez, J.-L., Clerjon, S., (2013). Quantifying and predicting meat and meat products quality attributes using electromagnetic waves: an overview. Meat Science 95(4), 879-896.

Danish Meat Research Institute, (2010). Instruction manual: EZ Driploss Accessed: 22/03/2015. www.dti.dk/_root/media/58882_EZ_Driploss_instruction.pdf.

De Marchi, M., Berzaghi, P., Boukha, A., Mirisola, M., Gallo, L., (2007). Use of near infrared spectroscopy for assessment of beef quality traits. Italian Journal of Animal Science 6, 421-423.

den Hertog-Meischke, M.J., van Laack, R.J., Smulders, F.J., (1997). The water-holding capacity of fresh meat. Veterinary Quarterly 19(4), 175-181.

Elam, A.T., Brooks, J.C., Morgan, J.B., Ray, F.K., (2002). Yield and fabrication time for value added beef from the chuck and round. Accessed: 01/06/2016. http://www.ansi.okstate.edu/research/research-reports-1/2002/2002-4%20Elam%20Research%20Report.pdf

Fennema, O.R., (1990). Comparative water holding properties of various muscle foods. Journal of Muscle Foods 1(4), 363-381.

Firtha, F., Jasper, A., Friedrich, L., (2011). Spectral and hyperspectral inspection of beef ageing state. Chinese-European cooperation for a long-term sustainability. Accessed: 13/04/2016. http://korny.uni-corvinus.hu/cneucoop_fullpapers/s3/ferencfirtha.pdf

Forrest, J.C., Morgan, M.T., Borggaard, C., Rasmussen, A.J., Jespersen, B.L., Andersen, J.R., (2000). Development of technology for the early post mortem prediction of water holding capacity and drip loss in fresh pork. Meat Science 55(1), 115-122.

Geesink, G.H., Schreutelkamp, F.H., Frankhuizen, R., Vedder, H.W., Faber, N.M., Kranen, R.W., Gerritzen, M.A., (2003). Prediction of pork quality attributes from near infrared reflectance spectra. Meat Science 65(1), 661-668.

Gjerlaug-Enger, E., (2011). Genetic analyses of meat, fat and carcass quality traits measured by rapid methods. Norwegian University of Life Science, Phd thesis.

Graham, S.F., Farrell, D., Kennedy, T., Gordon, A., Farmer, L., Elliott, C., Moss, B., (2012). Comparing GC–MS, HPLC and 1H NMR analysis of beef *longissimus dorsi* tissue extracts to determine the effect of suspension technique and ageing. Food Chemistry 134(3), 1633-1639.

Graham, S.F., Kennedy, T., Chevallier, O., Gordon, A., Farmer, L., Elliott, C., Moss, B., (2010). The application of NMR to study changes in polar metabolite concentrations in beef *longissimus dorsi* stored for different periods post mortem. Metabolomics 6(3), 395-404.

Greaser, M.L., (2001). Postmortem Muscle Chemistry, in: Hui, Y.H., Nip, W.K., Rogers, R., Young, O.A. (Eds.), *Meat Science and Applications*. CRC Press, pp. 21-35.

Guðjónsdóttir, M., (2011). Quality changes during seafood processing as studied with NMR and NIR spectroscopy. Department of Biotechnology, Norwegian University of Science and Technology, PhD thesis.

Gunenc, A., (2007). Evaluation of pork meat quality by using water holding capacity and vis-spectroscopy. Department of Bioresource Engineering, McGill University, Master thesis.

Hazlewood, C.F., Chang, D.C., Nichols, B.L., Woessner, D.E., (1974). Nuclear magnetic resonance transverse relaxation times of water protons in skeletal muscle. Biophysical Journal 14(8), 583-606.

Hazlewood, C.F., Nichols, B.L., Chamberlain, N.F., (1969). Evidence for the existence of a minimum of two phases of ordered water in skeletal muscle. Nature 222(5195), 747-750.

Honikel, K.O., (1998). Reference methods for the assessment of physical characteristics of meat. Meat Science 49(4), 447-457.

Honikel, K.O., (2004). Water holding capacity of meat, in: Pas, M.F.t., Everts, M.E., Haagsman, H.P. (Eds.), *Muscle development of livestock animals: physiology, genetics and meat quality*. CABI Publishing, Cambridge pp. 389–400.

Honikel, K.O., Kim, C.J., Hamm, R., Roncales, P., (1986). Sarcomere shortening of prerigor muscles and its influence on drip loss. Meat Science 16(4), 267-282.

Hornak, J.P., (1997-2014). The Basics of NMR. Accessed: 25/03/2016. https://www.cis.rit.edu/htbooks/nmr/inside.htm.

Hoving-Bolink, A.H., Vedder, H. W., Merks, J. W. M., de Klein, W. J. H., Reimert, H. G. M., Frankhuizen, R., (2005). Perspective of NIRS measurements early post mortem for prediction of pork quality. Meat Science 69(3), 417-423.

Huff-Lonergan, E., (2002). Water-Holding Capacity of Fresh Meat. Fact sheet (04669), National Pork Board, Des Moines, IA.

Huff-Lonergan, E., Lonergan, S.M., (2005). Mechanisms of water-holding capacity of meat: The role of postmortem biochemical and structural changes. Meat Science 71(1), 194-204.

Hughes, J.M., Oiseth, S.K., Purslow, P.P., Warner, R.D., (2014). A structural approach to understanding the interactions between colour, water-holding capacity and tenderness. Meat Science 98(3), 520-532.

Joo, S.T., Kauffman, R.G., van Laack, R.L.J.M., Lee, S., Kim, B.C., (1999). Variations in rate of water loss as related to different types of post-rigor porcine musculature during storage. Journal of Food Science 64(5), 865-868.

Kapper, C., Walukonis, C.J., Scheffler, T.L., Scheffler, J.M., Don, C., Morgan, M.T., Forrest, J.C., Gerrard, D.E., (2014). Moisture absorption early postmortem predicts ultimate drip loss in fresh pork. Meat Science 96(2, Part A), 971-976.

Kauffman, R.G., (2001). Meat Composition, in: Y.H. Hui, W.K. Nip, Rogers, R., Young, O.A. (Eds.), *Meat Science and Applications*. CRC Press: New York, pp. 1-18.

Kauffman, R.G., Eikelenboom, G., van der Wal, P.G., Engel, B., Zaar, M., (1986). A comparison of methods to estimate water-holding capacity in post-rigor porcine muscle. Meat Science 18(4), 307-322.

Köylü, M.Z., Asubay, S., Yilmaz, A., (2009). Determination of proton relaxivities of Mn(II), Cu(II) and Cr(III) added to solutions of serum proteins. Molecules 14(4), 1537.

Kristensen, L., Purslow, P.P., (2001). The effect of ageing on the water-holding capacity of pork: role of cytoskeletal proteins. Meat Science 58(1), 17-23.

Leroy, B., Lambotte, S., Dotreppe, O., Lecocq, H., Istasse, L., Clinquart, A., (2003). Prediction of technological and organoleptic properties of beef *longissimus thoracis* from near-infrared reflectance and transmission spectra. Meat Science 66(1), 45–54.

Li, C., Liu, D., Zhou, G., Xu, X., Qi, J., Shi, P., Xia, T., (2012). Meat quality and cooking attributes of thawed pork with different low field NMR T_{21}. Meat Science 92(2), 79-83.

Lillford, P.J., Clark, A.H., Jones, D.V., (1980). Distribution of water in heterogeneous food and model systems, in: Rowland, S.P. (Ed.), *Water in Polymers*. American Chemical Society, Washington, D.C., pp. 177-195.

Liu, J., Puolanne, E., Ertbjerg, P. (2015). A new hypothesis explaining the influence of sarcoplasmic proteins on the water-holding of myofibrils In *61st International Congress of Meat Science & Technology*, Clermont-Ferrand, France.

Mason, A., Abdullah, B., Muradov, M., Korostynska, O., Al-Shamma'a, A., Bjarnadottir, S., Lunde, K., Alvseike, O., (2016). Theoretical basis and application for measuring pork loin drip loss using microwave spectroscopy. Sensors 16(2), 182.

McDonnell, C.K., Allen, P., Duggan, E., Arimi, J.M., Casey, E., Duane, G., Lyng, J.G., (2013). The effect of salt and fibre direction on water dynamics, distribution and mobility in pork muscle: A low field NMR study. Meat Science 95(1), 51-58.

Meiboom, S., Gill1, D., (1958). Modified spin-echo method for measuring nuclear relaxation times. Review of Scientific Instruments 29, 688-691.

Melody, J.L., Lonergan, S.M., Rowe, L.J., Huiatt, T.W., Mayes, M.S., Huff-Lonergan, E., (2004). Early postmortem biochemical factors influence tenderness and water-holding capacity of three porcine muscles. Journal of Animal science 82(4), 1195-205.

Melville, J., (2014). Pulse NMR Spectroscopy. University of California, Berkeley. Accessed : 15/03/2016
https://www.ocf.berkeley.edu/~jmlvll/lab-reports/pulseNMR/pulseNMR.pdf

Menon, R.S., Allen, P.S., (1991). Application of continuous relaxation time distributions to the fitting of data from model systems and excised tissue. Magnetic Resonance in Medicine 20(2), 214-227.

Micklander, E., Christine Bertram, H., Marnø, H., Søvad Bak, L., Jørgen Andersen, H., Balling Engelsen, S., Nørgaard, L., (2005). Early post-mortem discrimination of water-holding capacity in pig longissimus muscle using new ultrasound method. LWT - Food Science and Technology 38(5), 437-445.

Moeseke, W.V., Smet, S.D., (1999). Effect of time of deboning and sample size on drip loss of pork. Meat Science 52, 151–156.

Monroy, M., Prasher, S., Ngadi, M.O., Wang, N., Karimi, Y., (2010). Pork meat quality classification using Visible/Near-Infrared spectroscopic data. Biosystems Engineering 107(3), 271-276.

O'Farrell, M., Bakke, K.A.H., Tschudi, J., Wold, J.P., (2011). Near-infrared (NIR) interactance system for non-contact monitoring of the temperature profile of baked liver pâté. Applied Spectroscopy 65(12), 1372-1379.

Offer, G., Cousins, T., (1992). The mechanism of drip production: formation of two compartments of extracellular space in muscle post mortem. Journal of the Science of Food and Agriculture 58(1), 107-116.

Offer, G., Knight, P., Jeacocke, R., Almond, R., Cousins, T., Elsey, J., Parsons, N., Sharp, A.S., Roger;, Purslow, P., (1989). The structural basis of the water-holding, appearance and toughness of meat and meat products. Food Structure 8, 151-170.

Oxford Instruments, (2013). MQC Benchtop QA systems from the NMR specialists. Accessed: 10/06/2016. http://www.oxford-instruments.com/OxfordInstruments/media/industrial-analysis/magnetic-resonance-pdfs/MQC-Brochure-April-2013.pdf.

Pearce, K.L., Rosenvold, K., Andersen, H.J., Hopkins, D.L., (2011). Water distribution and mobility in meat during the conversion of muscle to meat and ageing and the impacts on fresh meat quality attributes — A review. Meat Science 89(2), 111-124.

Pedersen, D.K., Morel, S., Andersen, H.J., Engelsen, S.B., (2003). Early prediction of water-holding capacity in meat by multivariate vibrational spectroscopy. Meat Science 65(1), 581–592.

Powrie, W.D., Tung, M.A., (1975). Electron microscopy in the study of immobilized water, in: Duckworth, R.B. (Ed.), *Water Relations of Foods*. Academic Press, pp. 249-269.

Prevolnik, M., Čandek-Potokar, M., Škorjanc, D., (2004). Ability of NIR spectroscopy to predict meat chemical composition and quality – a review. Czech Journal of Animal Science 49(11), 500-510.

Prevolnik, M., Čandek-Potokar, M., Škorjanc, D., (2010). Predicting pork water-holding capacity with NIR spectroscopy in relation to different reference methods. Journal of Food Engineering 98(3), 347-352.

Prieto, N., Andrés, S., Giráldez, F.J., Mantecón, A.R., Lavín, P., (2008). Ability of near infrared reflectance spectroscopy (NIRS) to estimate physical parameters of adult steers (oxen) and young cattle meat samples. Meat Science 79(4), 692-699.

Prieto, N., Roehe, R., Lavín, P., Batten, G., Andrés, S., (2009). Application of near infrared reflectance spectroscopy to predict meat and meat products quality: A review. Meat Science 83(2), 175-186.

Puolanne, E., Halonen, M., (2010). Theoretical aspects of water-holding in meat. Meat Science 86(1), 151-165.

Q-PorkChains, (2007-2011). Fundamentals of water holding capacity (WHC) of meat. Accessed: 07/05/2015. http://qpc.adm.slu.se/6_Fundamentals_of_WHC/page_30.htm.

Renou, J.P., Kopp, J., Gatellier, P., Monin, G., Kozak-Reiss, G., (1989). NMR relaxation of water protons in normal and malignant hyperthermia-susceptible pig muscle. Meat Science 26(2), 101-114.

Renou, J.P., Monin, G., Sellier, P., (1985). Nuclear magnetic resonance measurements on pork of various qualities. Meat Science 15(4), 225-233.

Rinnan, Å., Berg, F.v.d., Engelsen, S.B., (2009). Review of the most common pre-processing techniques for near-infrared spectra. TrAC Trends in Analytical Chemistry 28(10), 1201-1222.

Ripoll, G., Albertí, P., Panea, B., Olleta, J.L., Sañudo, C., (2008). Near-infrared reflectance spectroscopy for predicting chemical, instrumental and sensory quality of beef. Meat Science 80(3), 697-702.

Rosenvold, K., Andersen, H.J., (2003). Factors of significance for pork quality—a review. Meat Science 64(3), 219-237.

Savenije, B., Geesink, G.H., van der Palen, J.G.P., Hemke, G., (2006). Prediction of pork quality using visible/near-infrared reflectance spectroscopy. Meat Science 73, 181-184.

Schäfer, A., Rosenvold, K., Purslow, P.P., Andersen, H.J., Henckel, P., (2002). Physiological and structural events post mortem of importance for drip loss in pork. Meat Science 61(4), 355-366.

Sørland, G., Larsen, P., Lundby, F., Rudi, A., Guiheneuf, T., (2004). Determination of total fat and moisture content in meat using low field NMR. Meat Science 66, 543–550.

Straadt, I.K., Aaslyng, M.D., Bertram, H.C., (2011). Assessment of meat quality by NMR—an investigation of pork products originating from different breeds. Magnetic Resonance in Chemistry 49, S71-S78.

Straadt, I.K., Aaslyng, M.D., Bertram, H.C., (2014). An NMR-based metabolomics study of pork from different crossbreeds and relation to sensory perception. Meat Science 96(2, Part A), 719-728.

Straadt, I.K., Rasmussen, M., Andersen, H.J., Bertram, H.C., (2007). Aging-induced changes in microstructure and water distribution in fresh and cooked pork in relation to water-holding capacity and cooking loss – A combined confocal laser scanning microscopy (CLSM) and low-field nuclear magnetic resonance relaxation study. Meat Science 75(4), 687-695.

Swatland, H.J., Irving, T.C., Millman, B.M., (1989). Fluid distribution in pork, measured by x-ray diffraction, interference microscopy and centrifugation compared to paleness measured by fiber optics. Journal of Animal science 67(6), 1465-1470.

Taylor, A.A., Dant, S.J., (1971). Influence of carcass cooling rate on drip loss in pigmeat. International Journal of Food Science & Technology 6(2), 131-139.

Texas A&M AgriLife Extension Service, Conversion of Muscle to Meat. Accessed: 26/07/2013. http://meat.tamu.edu/ansc-307-honors/conversion-muscle-to-meat/.

Thybo, A.K., Karlsson, A.H., Bertram, H.C., Andersen, H.J., Szczypinski, P.M., Donstrup, S., (2004). Nuclear magnetic resonance (NMR) and magnetic resonance imaging (MRI) in texture measurement, in: Kilcast, D. (Ed.), *Texture in Food*. Woodhead Publishing, pp. 184-204.

Tornberg, E., Andersson, A., Göransson, Å., von Seth, G., (1993). Water and fat distribution in pork in relation to sensory properties, in: E. Puolanne., D. I. Demeyer, M. Ruusunen., Ellis, S. (Eds.), *Pork quality: genetic and metabolic factors*. Oxon: CAB International, pp. 239–258.

Trout, G.R., (1988). Techniques for measuring water-binding capacity in muscle foods—A review of methodology. Meat Science 23(4), 235-252.

Venturi, L., (2008). NMR study of meat as related to its structural organization. Food science, University of Bologna, PhD thesis.

Warner, R., (2014). Measurement of meat quality | measurements of water-holding capacity and color: objective and subjective, in: Devine, C., Dikeman, M. (Eds.), *Encyclopedia of Meat Sciences (Second Edition)*. Academic Press, Oxford, pp. 164-171.

Wold, S., Sjöström, M., Eriksson, L., (2001). PLS-regression: a basic tool of chemometrics. Chemometrics and Intelligent Laboratory Systems 58(2), 109-130.

Wu, Z., Bertram, H.C., Böcker, U., Ofstad, R., Kohler, A., (2007). myowater dynamics and protein secondary structural changes as affected by heating rate in three pork qualities: a combined FT-IR microspectroscopic and 1H NMR relaxometry study. Journal of Agricultural and Food Chemistry 55(10), 3990-3997.

Wählby, U., Skjöldebrand, C., (2001). NIR-measurements of moisture changes in foods. Journal of Food Engineering 47(4), 303-312.

Zarate, J.R., Zaritzky, N.E., (1985). Production of weep in packaged refrigerated beef. Journal of Food Science 50(1), 155-159.

Paper I

NEW INSIGHT INTO THE DYNAMICS OF WATER AND MACROMOLECULES IN MEAT DURING DRIP AS PROBED BY PROTON CPMG NMR

Eddy W. Hansen[1,*] & Han Zhu[2, 3]
[1]Department of Chemistry, University of Oslo, P.O. BOX 1033, Blindern, N-0315 Oslo, Norway
[2]Department of Chemistry, Biotechnology and Food Science, Norwegian University of Life Sciences, P.O. Box 5003, 1432- Ås, Norway
[3]Nortura SA, Lørenveien 37, Økern, 0585 Oslo, Norway

ABSTRACT

BACKGROUND: Three distinct proton spin-spin relaxation rate components in meat are known to be associated with three corresponding spatial domains possessing different molecular ratios of water and/or macromolecules (extra- and inter/intramyofibrillar). In this work we acquire the proton signal intensity and corresponding relaxation rate of the three components during a drip experiment with the objective to probe the irreversible migration of water and macromolecules between domains with drip time.
RESULTS: Each CPMG relaxation curve is decomposed into three relevant and distinct relaxation components (intensity and relaxation rate). A first-order kinetic model is adopted which enables the irreversible and slow "migration" of water and macromolecules between domains to be monitored. A detailing of the kinetic model applied is thoroughly discussed.
CONCLUSIONS: The amount of water and macromolecules within the respective domains in meat is monitored and quantified by in situ CPMG measurements during drip. The observed and irreversible change in proton intensity/relaxation rate during drip is rationalized by a slow migration of water molecules and macromolecules between the domains.
GENERAL SIGNIFICANCE: To shed new light on the water holding capacity in biological material by probing the slow migration properties of water/macromolecules between different domains during drip loss.

Keywords: *Water holding capacity; relaxation rates; kinetic model; relaxation sink; drip loss; macromolecules*

1. INTRODUCTION

Water Holding Capacity (WHC) is a general term referring to the ability of a defined sample to retain intrinsic or extrinsic fluids under specified conditions [1]. Understanding WHC is crucial for meat industry, which will affect the product amount, quality, recipe and future processing yields [2]. Current methods for WHC prediction use gravity, centrifugation, and other external or capillary forces, for example drip loss, filter paper method, centrifuge force method, cooking/heating loss, processing loss, thawing loss, Napole yield and technological yield [3, 4]. The EZ-DripLoss method using gravitational force is favored by many labs in meat industries due to the simple procedure, high sensitivity and reproducibility and cost effective equipment [5].

Drip (or weep or purge) is the red aqueous solution of proteins (sarcoplasmic proteins, glycolytic enzymes and myoglobin) that flows out of the cut surface of a carcass [6]. Drip loss results in the undesirable appearance of meat, weight loss as well as nutritive value loss and thus lowers the value of meat [6, 7]. Lean muscles contain about 75% of water [8, 9], and according to the data obtained from 2009 in Norway, a 1% increase in drip loss would result in 738 less tons of meat [10]. In addition, drip is an excellent culture medium for certain micro-organisms, whereby the shelf life of meat may be shortened due to safety reasons [7].

There is a lack of complete understanding of the formation of drip. Although EZ-DripLoss method is able to predict WHC of meat, it does not provide any information about the dynamics behind the water loss, and from what sort of structure the water is lost. The experimental time of EZ-DripLoss is typically 24 hours or more, but no dynamic measurements are reported during this period of time. Unlike conventional methods, NMR relaxometry is a potentially powerful tool to quantify the mobility and distribution of water between different domains during the conversion of muscle to meat, which – in turn - may explain how these changes are linked to meat quality [11, 12]. Renou and coworkers were the first to correlate longitudinal (T_1) and transverse (T_2) relaxation times to WHC [13, 14]. Studies

have shown that three groups of T_2s exist in meat, namely a fast (0-10 ms), an intermediate (35-50 ms) and a slow relaxing component (100-250 ms) [13]. Also, Bertram et al has demonstrated a relation between the final sarcomere length and drip loss [15] and reported on some correlation between T_{21} and sarcomere length, and between T_{21} and myofilament spacing [15]. Much work has focused on the mechanisms of post-mortem water mobility in meat [16-20]. Also, kinetic studies during processing, namely cooking [21, 22], salting [23], cooling [24], demulsification [25] and rehydration [26] have been reported. However, to the best of knowledge, there seems to be little – if any - information regarding the kinetics related to the slow migration of water and macromolecules between various domains during drip.

The overall goal of this work is to monitor the proton Carr-Purcel-Meiboom-Gill (CPMG) response with time to gain information on the irreversible and slow transport or migration of water and macromolecules out from the sample during drip. This process is characterized by a much slower rate compared to the exchange process of water molecules and exchangeable protons on a macromolecule within specific domains. A first order kinetic model will be applied to characterize the "migration" rates by model fitting experimental CPMG curves acquired at different times during drip. In particular, the drip experiment is performed *in situ*, by placing the sample (randomly selected porcine *longissimus dorsi* muscles) within the NMR magnet. When decomposing the CPMG relaxation response into a discrete and finite number of exponential functions, distinct "dynamic domains" are identified. Three domains are generally reported in the literature based on the magnitude of their spin-spin relaxation rate, a fast relaxation component (X = F), an intermediate relaxation component (X = I) and a slow relaxation component (X = S) respectively [27].

2. EXPERIMENTAL

2.1. Sampling

Pigs used in this study are young boars from Landrace and Duroc breed, tested at the Norsvin boar test station (Ilseng, Norway) as part of an on-going breeding program. The boars not selected for semen production, were slaughtered and had carcass weights of around 95 kg. The animals were slaughtered at Nortura Rushøgda (Ringsaker, Norway) by carbon dioxide stunning (90%). Exsanguination, scaling and splitting were finished within 30 min *post mortem*. After cleaning and evisceration, the carcasses were carried through a cooling tunnel (-22 °C, 8-10 m/s air velocity). Subsequently, the carcass were left at 15 °C for 5 min and chilled at 1-3 °C for 96 hours. The carcasses were then transported to a partial dissection line at Animalia (Oslo, Norway), and the porcine *longissimus dorsi* muscle was obtained. Cylindrical samples (8ϕ x 10 mm, ~0.459 g) were cored and suspended with the fiber direction parallel to the cylindrical axis in an NMR glass tubes. Enough space (17 mm) was reserved between the bottom of the NMR glass tube and the muscle (figure 1 a). A layer of parafilm was placed on the top of the muscle to avoid water evaporation.

2.2. Low Field NMR Relaxation Measurements

The experiments were performed on a Maran Ultra NMR instrument (Resonance Instruments, Witney, UK) operating at a magnetic field strength of 0.54 T, corresponding to a proton resonance frequency of 23 MHz. The NMR signal response was acquired and stored every hour during the drip experiment (45 hours) by applying a traditional CPMG pulse-sequence [28] with a fixed inter-pulse time τ = 24 μs, 10 K echoes and 8 transients if not otherwise stated in the text. The time between each transient was set to 3 s to ensure quantitative sampling (T_1 was determined to be less than 0.5 s). All measurements were performed at t = 25 ˚C and equilibrated at this temperature for 10 minutes before initiating any NMR experiment. Some CPMG experiments were also performed on the drip fluid (figure 1 b) by lifting the sample tube manually so that only the drip fluid was located within the transmitter/receiver coil.

The strong dipolar interaction between protons within the solid matrix results in a much shorter spin-spin relaxation time of the order of a few microseconds [20, 29]. Since an 180˚-τ-90˚-τ echo pulse sequence will not refocus such strong dipolar interactions (short T_2), the echo amplitude of the "solid" like protons is made invisible. Actually, by increasing the inter-pulse timing τ from 24 μs to 100 μs, no observable change in the extrapolated CPMG signal intensity was noticed. Hence, we decided to apply the shortest possible τ (= 24 μs) in order to a) restrict the observable NMR signal to mobile protons only [30] and b) avoid T_2 contribution from mobile protons diffusing in an (internal) gradient field. Parafilm was tested under the same experimental conditions, and did not contribute to the signal.

A small signal of less than 2% of the total signal intensity and having a much longer T_2 relaxation than the other components was observed in all CPMG curves. The origin of this signal is discussed later in this work. The spin-lattice relaxation data were obtained at the end of the experiment (t_d = 45 h) using a 180˚-τ-90˚ pulse sequence.

Origin 9.0 (OriginLab Corporation, MA, USA) and Microsoft Excel 2010 (Microsoft Corporation, WA, USA) were used for curve fitting.

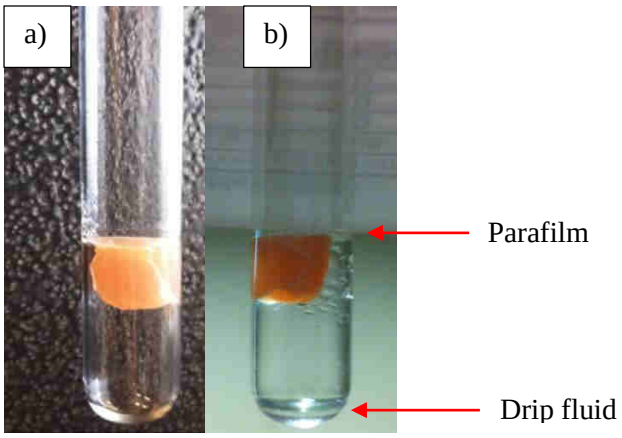

Figure 1. Sample setup during drip. a) at the start (t_d = 0h) and b) at the end (t_d = 45h) of the drip experiment where t_d represents drip time.

3. THEORETICAL OUTLINE

3.1. Migration – a Dynamic Model

In this section we present a simple dynamic model which describes the migration of water molecules W and macromolecules $\dot{M}$ from the inner to the outer part of a sample that is composed of two different spatial domains I and S. The molecules are only allowed to migrate irreversible from I to S and not vice versa, as illustrated in figure 2.

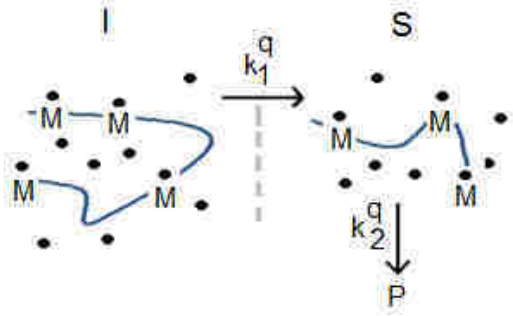

Figure 2. Schematic view of the distribution of water molecules (W: ●) and macromolecules $\dot{M}$ within domains I and S in which $\dot{M}$ contains functional groups possessing a proton E (●) that can exchange with water molecules. The dotted line (– –) is introduced to illustrate the spatial difference between domains I and S. The parameters k_1^q and k_2^q define the rate constants of migration of q (= W and E) between the domains. P represents the drip domain.

The total number of mobile protons N_T^X within domain X (= I or S) originate from two proton sources: 1) water molecules W and 2) exchangeable protons E located on some functional groups on $\dot{M}$. Since the hydrogen exchange between W and E is assumed to be much faster (order of ms^{-1}) than the slow and irreversible transport of water between domains (order of $hours^{-1}$), we will use the term "migration" for this latter dynamic process in order to make a clear distinction between the two different rate-processes. Hence, we may set up some dynamic equations describing the migration of water molecules W and exchangeable protons E between the domains.

3.2. Intensity versus Drip Time

At some time during the drip process, the number of water molecules N_W^X and the number of exchangeable protons N_E^X (located on macromolecules $\dot{M}$) in domain X will approach some constant values $N_{q,eq}^X$ (q = W or E). If assuming the time dependence of N_q^X to follow a first-order rate law during drip, a set of simple differential equations can be set up with reference to the reaction scheme shown in figure 2:

$$\frac{dN_q^I}{dt_d} = -k_1^q (N_q^I - N_{q,eq}^I) \tag{1a}$$

$$\frac{dN_q^S}{dt_d} = k_1^q (N_q^I - N_{q,eq}^I) - k_2^q (N_q^S - N_{q,eq}^S) \tag{1b}$$

$$\frac{dN_q^P}{dt_d} = k_2^q (N_q^S - N_{q,eq}^S) \tag{1c}$$

It should be remarked that if adding Eqs 1a – 1c we obtain the important result:

$$\frac{d}{dt_d}(N_q^I + N_q^S + N_q^P) = 0 \tag{1d}$$

Which implies that the total number of respectively E and W in the sample (including drip) at any time t_d during drip is conserved.

The above equations are derived under the assumption that the drip proceeds on a much slower time-scale (residence time of the order of hours) compared to the proton exchange between E and W within I and S (residence time of the order of milliseconds or seconds), respectively. It is explicitly assumed that q migrates out (P) via domain S and not directly from I. As a consequence, since the NMR signal intensity I_q^X is proportional to the number of nuclei N_q^X contributing to the NMR intensity, it follows from simple algebra that the solution to Eqs 1a – 1d can be expressed by I_q^X . After some simple but tedious algebra we find that;

$$\frac{I_q^I(t_d)}{I_q^I(0)} = 1 - \left[1 - \frac{I_q^I(45)}{I_q^I(0)}\right] \cdot \left[\frac{1 - Exp(-k_1^q t_d)}{1 - Exp(-45k_1^q)}\right] \tag{2a}$$

$$\begin{aligned}\frac{I_q^S(t_d)}{I_q^S(0)} &= 1 - \left[1 - \frac{I_q^S(45)}{I_q^S(0)}\right] \cdot \frac{1 - Exp(-k_2^q t_d)}{1 - Exp(-45k_2^q)} \\ &+ \frac{k_1^q}{k_2^q - k_1^q}\left[\frac{I_q^S(0)}{I_q^S(0)} - \frac{I_q^S(45)}{I_q^S(0)}\right]\left[\frac{1 - Exp(-k_2^q t_d)}{1 - Exp(-45k_2^q)} - \frac{1 - Exp(-k_1^q t_d)}{1 - Exp(-45k_1^q)}\right]\end{aligned} \tag{2b}$$

Consequently, it follows that the intensity I_q^P of the fluid dripping out of the sample can be expressed by:

$$I_q^P(t_d) = I_q^I(0) + I_q^S(0) - I_q^I(45) - I_q^S(45) \tag{2c}$$

Where $I_q^I(0), I_q^S(0), I_q^I(45)$ and $I_q^S(45)$ represent the proton signal intensities of q (E or W) in domains X (I, S or P) at the start (t_d = 0) and at the end (t_d = 45 hours) of the migration process, respectively. Moreover, it follows that the total proton signal intensity I_T^X within domain X (= I and S) at any time t_d can be expressed by:

$$I_T^X(t_d) = 2I_W^X(t_d) + I_E^X(t_d) \quad (2d)$$

3.3. Spin-Spin Relaxation versus Drip Time

In the following section the spin-spin relaxation rate of "free" water W within any domain X is represented by $R_{2,W}^0 (= 1/T_{2,W}^0)$ with $T_{2,W}^0$ being the spin-spin relaxation time. Likewise, the spin-spin relaxation rate of the exchangeable protons E located on some functional groups (for instance –COOH, –NH, –OH and –SH groups [31]) on M is denoted $R_{2,E}^0$, which is much faster than the relaxation rate of bulk water. Since various types of functional groups on M exist, a distribution of $R_{2,E}^0$ is expected. However, since it is not possible from the present NMR measurements to derive these relaxation distribution characteristics, we simply represent them by a single, average relaxation rate $\overline{R}_{2,E}^0$.

Hence, under the condition of fast exchange between E and W, a single, observable relaxation rate R_2^X for domain X can be assigned, according to:

$$(N_W^X + N_E^X)R_2^X = N_W^X \cdot R_{2,W}^0 + N_E^X \cdot \overline{R}_{2,E}^0 \Leftrightarrow N_E^X = \frac{R_2^X - R_{2W}^0}{\overline{R}_{2,E}^0 - R_2^X} N_W^X \quad (3)$$

where all symbols are previously defined. Eq 3 shows the important result that the number of exchangeable proton sites N_E^X (on M) can be calculated from the number of water molecules N_W^X by taking into account the relaxation. This relation becomes important in the model-fitting as it reduces the number of adjustable parameters.

In particular, spin-spin relaxation time measurements is required and essential in characterizing the fate of the exchangeable protons E during drip.

4. RESULTS AND DISCUSSION

4.1. CPMG Response Analysis

It has previously been reported that the proton CPMG response curve of meat/muscle can be well represented by a sum of three exponential functions [33]. Using the experimental set-up shown in figure 1, we found a "3-exponential" fit to the observed relaxation curve to give a slightly non-random error distribution, at least at longer drip times. For instance, a typical CPMG response curve observed in this work is reproduced in figure 3a and reveals a single exponential decay contribution, denoted D, for t $\geq$ 0.5 s which is characterized by a long T_2 (of the order of a second) and a small signal amplitude (~ 1 – 2 %). After subtracting I_D from the observed CPMG curve, a corrected CPMG curve is derived (figure 3b) which could be represented excellently by a sum of three exponential functions denoted F, I and S, respectively. The excellent quality is confirmed by the random distribution of the residual curve, as illustrated on figure 3c.

Although a model equation composed of a sum of four exponential functions may be expected to result in an ill-posed numerical problem, we found the above procedure to be very robust for all CPMG curves analyzed in the present work. Actually, after subtracting the fourth component (D) from the observed CMPG response function, the remaining 6 adjustable parameters - as obtained by a non-linear least-squares fit to a sum of three exponential functions - were found to be highly reproducible. One reason for this robustness is that the four relaxation rates R_{2i} are very different [34] and that the signal-to-noise (S/N) ratio is high (of the order of 200 or larger). For instance, the S/N-ratio of the CPMG curve shown in figure 3 a) was even larger (400). By arranging the relaxation rates in increasing order, each relaxation rate was found to be faster than the former by a factor of more than 3, i.e.: $R_2^D \approx 1\ s^{-1}$, $R_2^S \approx 9\ s^{-1}$, $R_2^I \approx$

25 s^{-1} and $R_2^F \approx 900$ s^{-1}, respectively, which is fortunate. A much smaller difference between the relaxation rates would reduce the reliability in resolving them.

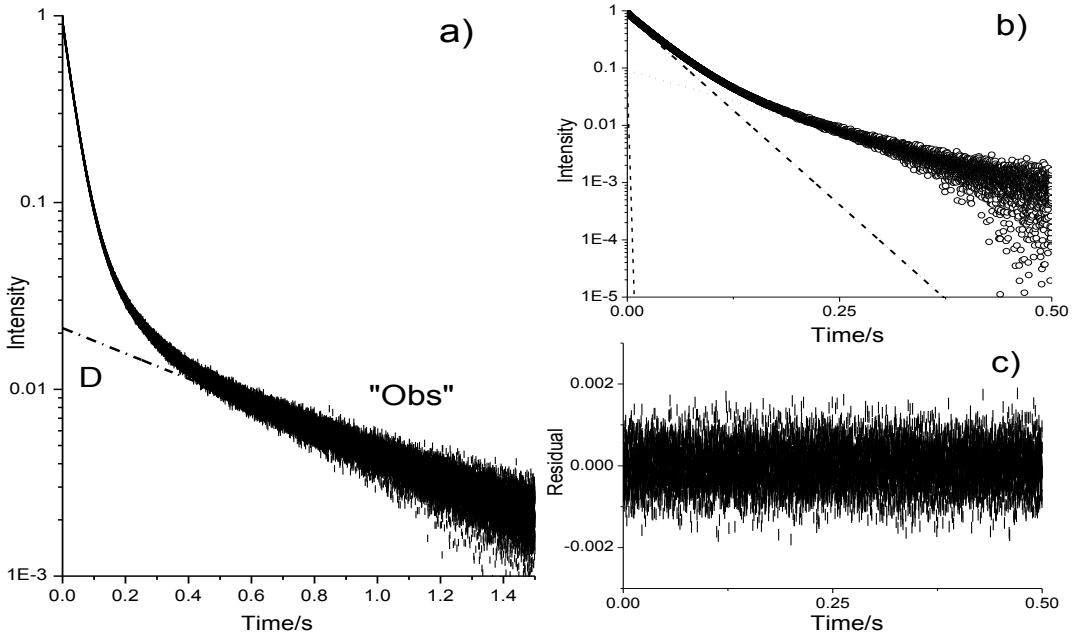

Figure 3. a) A typical CPMG response curve of the meat sample investigated in this work. The long-T_2 component D (- - -) is excellently fitted to a single exponential function for t > 0.5 s. b) Difference between observed relaxation curve and the long-T2 component D, denoted "Corrected", is fitted to a sum of three exponential functions F, I and S. c) Residual plot between the "corrected" CPMG curve and the model fitted curve (3-exponential function) in b). The data shown on figure a) are taken from a parallel experiment on an identical meat sample, using the same experimental parameters as presented in the experimental section, except for the repetition time which was set to 10 s and the number of scans which was fixed to 300.

Hence, Eq 4 is used as a model equation (or fitting function) throughout in this work in which the long-T_2 component (component D) was first fitted to a single exponential function for t > 0.5 s and then subtracted from the observed relaxation curve before a 3-exponential fit was applied. The goodness of the above model is illustrated on figure 4 in which the function;

$$I_T(t;t_d) = I_F(t_d)\exp\left[-R_2^F(t_d)t\right] + I_I(t_d)\exp\left[-R_2^I(t_d)t\right] + I_S(t_d)\exp\left[-R_2^S(t_d)t\right] + I_D(t_d)\exp\left[-R_2^D(t_d)t\right] \quad (4)$$

(with $R_2^F > R_2^I > R_2^S > R_2^D$) is plotted against time t for different drip times t_d = 3 hours, 9 hours, 21 hours and 45 hours, respectively. The intensity I_D (Eq 4) as a function of drip time will be presented in a later section in which its physical significance will be discussed more thoroughly.

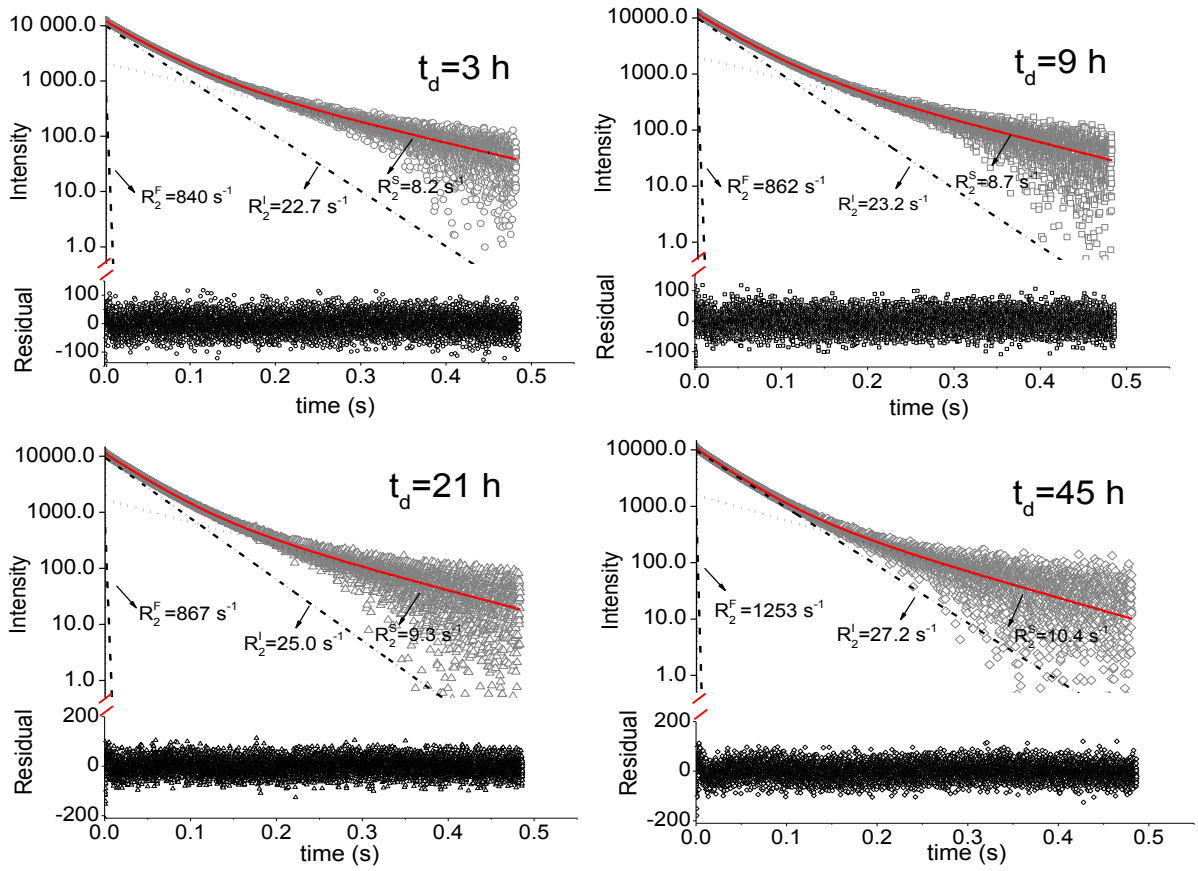

Figure 4. CPMG relaxation curves (obtained after subtracting the long - T_2 component (component D) from the observed CPMG curve) at drip times t_d = 3 h, 9 h, 21 h and 45 h. The three exponential components F, I and S are shown as dotted curves in each figure. The residual curves (the difference between observed and model calculated intensities) are shown below each figure. The red curves represent model fits to Eq 4. See text for further details.

The spin-spin relaxation rate of pure, distilled, and oxygen free water at room temperature is measured to be approximately 0.3 – 0.4 s^{-1} while bulk water saturated with air/oxygen reveals a somewhat larger relaxation rate (due to the interaction of water with paramagnetic oxygen) and amounts to between 0.6 – 1 s^{-1}. Since the shortest of the three proton relaxation rates in the present system is found to be larger than 8 s^{-1}, some additional interactions or dynamic processes must exist which dominate the relaxation of water and will be commented on in the next section. As can be further noticed from figure 4, all residual curves reveal small, random error distributions, suggesting the "4-exponential" relaxation model (Eq 4) to give an adequate representation of the relaxation behavior. Importantly, these random error distributions were observed in all model-fitted relaxation curves, throughout the drip experiment.

4.2. Spin-Lattice Relaxation

In contrast to CPMG, the Inversion Recovery measurements revealed only two distinct relaxation components; a short relaxation component possessing a T_1 = (77 $\pm$ 6) ms and a relative intensity of (4.5 $\pm$ 0.5)% and a second and much longer relaxation component of T_1 = (499 $\pm$ 2) ms (figure 5).

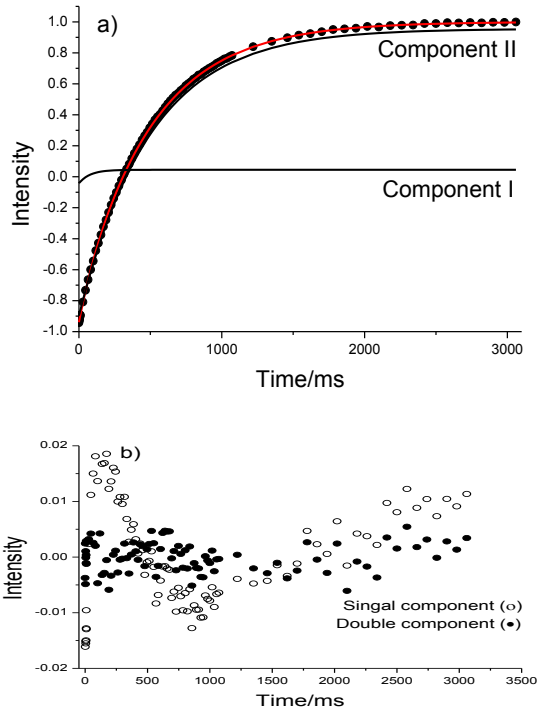

Figure 5. Inversion recovery NMR experiment acquired 45 hours after start of the drip experiment. Based on the residual curve analysis (bottom), two distinct relaxation components were identified.

Within experimental error, the intensity of the short-T_1 component equals the intensity of the short T_2-component of the *F*-domain, as derived from CPMG-measurements. Hence, we assign the short T_1-component to water molecules in domain *F* which do not exchange fast enough (on a T_2-time scale) with water molecules within domains *I* and *S*. In contrast, the much longer spin-lattice relaxation time component suggests that a fast exchange of water between domains *I* and *S* takes place on a time scale of second(s). Importantly, neither T_1- nor T_2 measurements give any direct information on the slow and irreversible transport process related to the migration of water, which occurs on a much longer time scale (residence time of minutes/hours) and will be discussed in the next section.

4.3. Redistribution of Water and Macromolecules during Drip

Based on the model-fitted CPMG response curves (figure 4; Eq 4) the relative proton signal intensity I_T^X (see Eq 2d) is plotted on figure 6 as a function of drip time t_d for X = F, I, S and D. Since the time between each CPMG pulse sequence is longer than approximately 3 times the spin-lattice relaxation time T_1, the proton signal intensity can be considered quantitative.

Importantly, within experimental error all intensities I_T^X and relaxation rates R_2^X are excellently fitted to second order polynomials (solid curves in Figure 6) and suggest that the exponential terms in equations 2a and 2d can be Taylor expanded to second order with respect to time. This is advantegous since it makes it possible to easily and reliably calculate the intensities $I_q^X(0)$ and $I_q^X(45)$ and relaxation rates $R_2^X(0)$ and $R_2^X(45)$ in domain X for both q = E and W from Eqs 2d and 3. However, this approach requires information about the relaxation rate $\overline{R}_{2,E}^0$ which represents some average relaxation rate of proton E on a functional group (on M) which exchanges fast with water molecules located in the close vicinity of E. To the best of knowledge, one early publication reported on $\overline{R}_{2,E}^0$ of $1.0 \cdot 10^{-3}$ s^{-1} which is – within experimental error - equal to R_2^F of $(0.9 \pm 0.1) \cdot 10^{-3}$ s^{-1}, as reported in this work [19]. We have therefore adopted

this latter value of $\overline{R}_{2,E}^{0}$ and applied a second order polynomial fit to all data in Figure 6. The results of the analysis are summarized in Table 1.

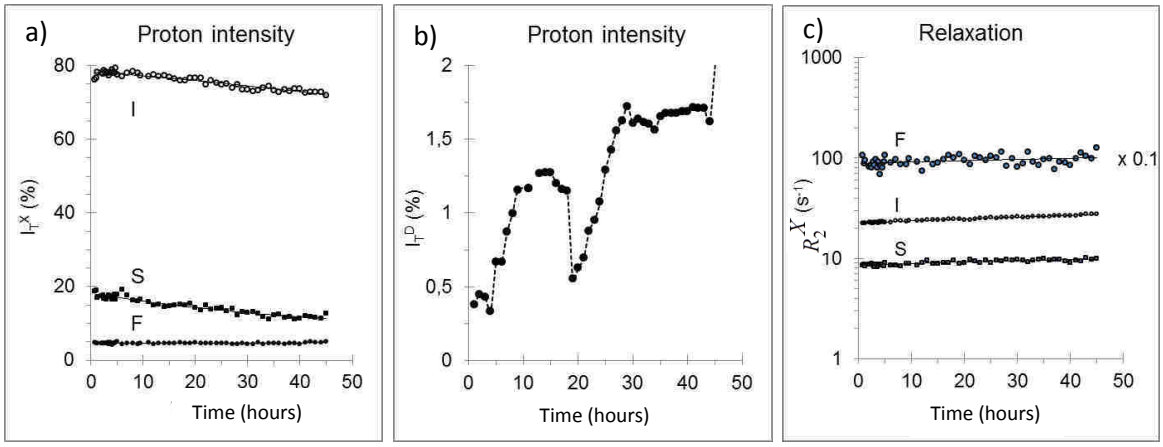

Figure 6. Normalized proton signal intensity of the four resolved components F, I, S (a) *and D* (b) *as a function of drip time. The initial sum of intensities of F, I, S and D was set to 100%. The corresponding spin-spin relaxation rates* R_2^X *as a function of drip time are plotted on figure c). All solid curves represent 2. order polynomial fits and are further discussed in the text.*

Within experimental error, no observable change in signal intensity or relaxation rate within domain F was noticed (figure 6 a). In contrast, the intensity I_T^D of the long-T_2 component D reveals a sort of oscillating behavior with drip time and will be commented on in a later section.

As can be inferred from the results presented in Table 1, the number of water molecules decreases by 8.5% (± 0.1%) in domain I and by 37% (±2%) in domain S during 45 hours of drip and truly shows the migration of water molecules from the respective domains. This is further supported by the increase in relaxation rate of 13.1% (± 0.3%) and 21.3% (± 0.3%) within the two respective domains. Also, the number of exchangeable protons in domain S decreases by approximately 25% (± 2%), suggesting that a significant number of macromolecules (probably smaller macromolecules) migrate into the drip solution. This argument is based on the assumption that exchangeable protons are associated to functional groups on the macromolecule.

Table 1. Relative intensities $I_q^X(0)$ *and* $I_q^X(45)$ *and corresponding relaxation rates* $R_{2q}^X(0)$ *and* $R_{2q}^X(45)$ *as calculated by second order polynomial fits to the data in Figure 6 by applying Eq 2d and 3.*

Parameter	*Value (%)*
$I_w^I(0)$	77.2 ± 0.7
$I_w^I(45)$	70.6 ± 0.7
$I_w^S(0)$	18.2 ± 0.6
$I_w^S(45)$	11.4 ± 0.6
$I_E^I(0)$	0.53 ± 0.01
$I_E^I(45)$	0.60 ± 0.01
$I_E^S(0)$	0.037 ± 0.002
$I_E^S(45)$	0.028 ± 0.002
$R_2^I(0)$	23.1 ± 0.2
$R_2^I(45)$	27.2 ± 0.2
$R_2^S(0)$	8.6 ± 0.2
$R_2^S(45)$	9.7 ± 0.2

From the present calculations we can estimate the fraction f of exchangeable protons (relative to the number of water molecules) within any domain which extends to f = 0.015 in domain I and f = 0.004 in domain S, respectively. From these numbers the relative ratio of macromolecules in domains I and S can be estimated to about 11. The corresponding ratio of water molecules within the same two domains is estimated to approximately 4, showing the density of macromolecules (macromolecule/water molecule) to be almost a factor of 3 higher in domain I than in domain S.

One observation which seems to violate the assumption regarding irreversibility of the dynamic reaction in scheme (Eq 1) is that the number of exchangeable protons in domain I increases with drip time by about 13% (after 45 hours of drip). We do not have a clear understanding of this result. However, we may speculate about it and we find two reasonable justifications:

1. Some small macromolecules (or acid protons) may diffuse from domain F and into domain I during drip. This net migration would not significantly affect the relaxation rate or proton signal intensity in domain F which is expected to possess a pool of macromolecules with a higher concentration of macromolecules compared to domains I and S. In contrast, a small amount of macromolecules migrating from F and into I may significantly affect the number of macromolecules in I. A potential migration of macromolecules and/or water from F is not implemented in the dynamic reaction model (scheme 1).
2. The accessibility of exchangeable protons on M may change during drip due to restructuring of the macromolecules - for instance by denaturation [13,36] and may affect the number N_E^X .

Finally, we address the question of molecular dynamics or migration, i.e., the rate of change of E and W during drip. This can simply be resolved by fitting Eqs 2a, 2b, 2d and 3 to the observed intensity/relaxation curves in Figure 6. All parameters, except the rate constants, are known (Table 1) and leave only four (4) parameters adjustable for model fitting. The model fitted relaxation curves and intensities are shown in Figure 6 and – not surprisingly – coincide with the 2.order polynomial fits, as mentioned previously. The rate constants are summarized in Table 2.

Table 2. Rate constants k_1^W , k_2^W , k_1^E and k_2^E as determined by a simultaneous fit of Eqs 2a, 2b, 2d and 3 to the data in Figure 6. All parameters except the rate constants were kept fixed (Table 1). The respective errors in the rate constants were estimated by Monte Carlo simulations in which the non-adjustable parameters (Table 1) were chosen randomly (from a normal distribution) before each model fit.

Rate constant	*Value*
k_1^W	$(1.7 \pm 0.8)\cdot10^{-6}$ s^{-1}
k_2^W	$(7.5 \pm 0.2)\cdot10^{-6}$ s^{-1}
k_1^E	$(3 \pm \quad)\cdot10^{-8}$ s^{-1}
k_2^E	$(1 \pm \quad)\cdot10^{-6}$ s^{-1}

The analysis demonstrates that neither k_1^E nor k_2^E could be reliably determined which is most probably caused by their rather small intensities of less than 2%.

In contrast, the rate constant for the migration of water from domain S was found to be approximately 4 – 5 times faster than the migration of water from domain I. This is not unexpected, as the migration of water from domain I is motionally more constraint, as it contains a larger concentration of macromolecules (macromolecules/water molecule) compared to domain S. As a consequence, the drip is strongly governed by migration of water from domain S while the migration from I probably comes into play at a later stage during drip. If assigning I and S to the inter/intra- and extramyofibrillar space, respectively [17] the reduced intensity at longer drip time may be explained by myofibrillar shrinkage and longitudinal contraction which "forces" free water from I and subsequently into S, and subsequently out into P, i.e., resulting in a net loss of water from both domains I and S. Such a shrinkage effect can be argued from the R_2^X -behavior with time, as it is well known that R_2^X is proportional to the surface-to-volume ratio (S/V) of domain X. For spherical or cylindrical geometries it thus follows that the inverse of the diameter or the inverse length of a cylinder becomes proportional to the water relaxation rate R_2^X . Hence, according to the relaxation data presented in figure 6 (right) the diameter/length of the domain (I and/or S) would decrease by 10 – 15% during 45 hours of drip resulting in a subsequent "collapse" (volume reduction) of the domain X as drip progresses. To the best of knowledge, this was first suggested by Bertram and colleagues [15].

4.4. "Drip" - curve

By applying Eq 4 the drip-loss can be calculated by subtracting the overall observed signal intensity $I_T(t_d)$ from the initial signal intensity $I_T(0)$ and is shown by open circles (o) on figure 7 a in which the solid curve was calculated by a simple second order polynomial fit. The difference between the observed and fitted drip curves is illustrated on figure 7 b by open circles (o).

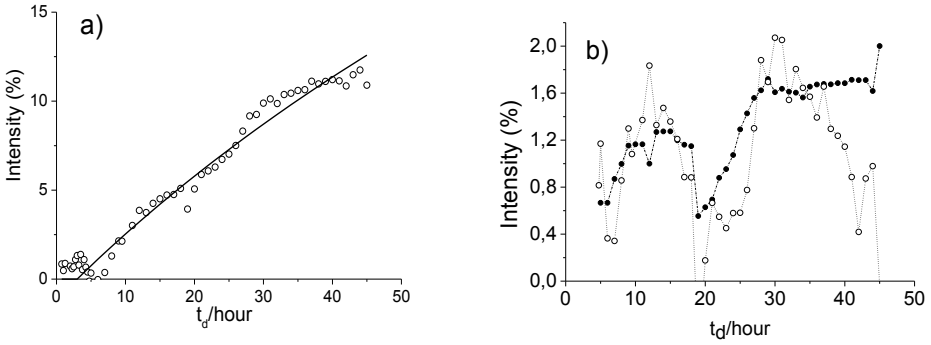

Figure 7. a) Observed drip curve (o) in meat as a function of drip time t_d. The solid curve (──) represents a simple 2.order polynomial fit. b) Difference between observed and model-fitted intensities from Figure a). The solid points (●) are reproduced from figure 6 (right).

As can be inferred from the data in Figure 7b, the "oscillating" behavior of the drip curve - as illustrated by the open circles (o) in Figure 7 a – resembles the behavior the corresponding oscillation behavior of the long-T_2 component D (●) and leads to the tentative conclusion that the overall drip-curve is composed of two compoments. One component which increases monotonically with time (main drip) and a second small-amplitude, oscillating component, denoted "residual drip" which is tentatively believed to build up on the outer surface of the sample. Probably, small water drops evaporated and condensed (or adhered) to the inner glass wall of the NMR tube and water confined at the sample surface. As time progresses, this water then drips (flows) out from the detector coil. However, the oscillating behavior continuous as long as the main drip component forms. Actually, we have seen this phenomenon on all drip experiments performed on our small sample NMR instrument. This topic is under further investigation in our laboratory and will be discussed elsewhere.

4.5. Spin-Spin Relaxation Time Characteristics of the Drip-Fluid

Although it is known that macromolecules (proteins) migrate out and into the drip solution with time [37] we will in this last section give support for this statement by spin-spin relaxation time measurements performed on the drip solution. According to Cooke et al. [38], the relaxation mechanisms in muscle fibers and protein solutions (here drip solution) are similar. Actually, to obtain a reliable fit of the observed relaxation curve of the drip fluid, it was necessary to adopt three individual relaxation components, as illustrated on the CPMG response curve of the drip fluid in figure 8 and by the results presented in Table 3, of which one component has an R_2 component comparable to bulk water. The other two components show much larger relaxation rates and are of the same order of magnitude as in the meat sample (see figure 4). The observation of three distinct components in the drip fluid suggests that the various proton species are not satisfying the fast exchange conditions.

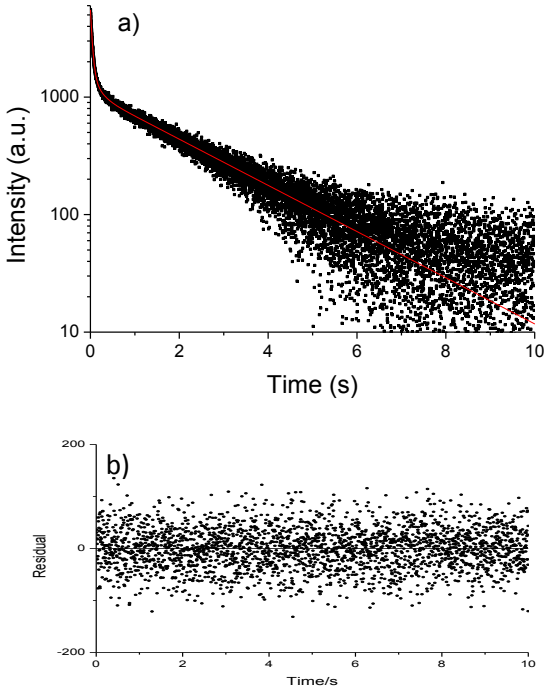

Figure 8. a) CPMG response of the drip fluid after 45 hours drip. b) Residual. The experimental parameters were the same as presented in the experimental section, except for the repetition time which was set to 15 s, τ = 0.5 ms and the number of transients N = 16.

Hence, the above relaxation time measurements simply support previous results that macromolecules migrate from the meat and into the drip solution. It is reasonable to expect that T_2 of the drip solution will change with drip time. However, this topic is not part of the present work and will not be discussed further.

Table 3. Spin-spin relaxation rate R_2 within the drip solution (after 45 hours of drip)

derived by a"3-exponential" fit to the observed relaxation response function in figure 8.

Component	R_2 (s^{-1})	Intensity (%)
1	23.7 ± 0.3	69.9 ± 0.8
2	6.2 ± 0.3	11.1 ± 0.1
3	0.452 ± 0.002	19.0 ± 0.1

6. SUMMARY AND CONCLUSION

In this work we have reported proton CPMG experiments performed on porcine *longissimus dorsi* muscle samples (8ϕ x 10 mm, ~0.459 g) during drip which enables three dynamic domains X (= F, I and S) to be identified and their proton signal intensity I_T^X and spin-spin relaxation rate R_2^X to be monitored as a function of time. A monotonic increase/decrease in R_2^X / I_X was noticed within all domains, except for the F-domain, which intensity and relaxation rate remained – within experimental error - constant during drip.

Meat/muscle is a rather heterogeneous and complex biological material containing macromolecules that are most probably described by a broad distribution of molar masses and possessing a corresponding distribution regarding the number of (water) adsorption sites per macromolecule.

It is further known that water molecules that interact with exchangeable protons on a macromolecule possess a faster spin-spin relaxation rate R_2 [38]. The existence of such relaxation sink sites are particularly important in biological materials and may significantly affect the relaxation rate.

It is thus necessary to make some model simplifications/assumptions in order to gain some relevant physical/chemical insight from the observed NMR intensity- and relaxation data. Hence, a simple first-order kinetic model was designed which solutions (Eqs 2 and 3) were fitted simultaneously to the observed NMR signal intensities/relaxation rates of domains I and S and enabled the rate constant for the migration of water between domains to be established.

A) The total number of protons within any domain X (= F, I and S) is expressed by the sum of exchangeable protons N_E^X on a macromolecule and free water molecules N_W^X. The exchange rate of these water molecules is a fast process (characterized by a short residence time of the order of a few ms) as compared to the irreversible transport or migration process , i.e. drip-loss, which is a slow process, characterized by long residence time of the order of hours).

B) The probability of water molecules W to exchange with exchangeable protons E on a macromolecule will depend on the population of both E and W, which may change during the migration process. Also, restructuring of the macromolecules may affect the number of E (for instance by denaturation [13,36]).

C) A contraction or shrinkage of a domain X may lead to an extra "push" of water molecules out of that domain and results in a relative enhancement of the fraction of adsorbed water molecules remaining. As a consequence, the spin-spin relaxation rate R_2 will increase (due to the fast exchange of free and bonded water molecules within the domain) and enables the S/V-ratio of the domain to be estimated.

Options A – B rationalize all the findings presented in this work, including the slow migration or drip of macromolecules.

Finally, we will emphasize that due to the rather small fraction of exchangeable protons (< 2% of the total proton intensity), it was not possible to obtain any reliable estimate of the migration rate of the macromolecules.

7. ACKNOWLEDGEMENTS

We want to thank the Research Council of Norway for financial support through the project "*On line determination of water retaining ability in pork muscle",* Project number *229192 and* the project INFORMED (*Increased Efficiency: Moving from Assumed Quality to Online Measurement and Process*, Nortura SA, Project no.: *210516*). Also, we are grateful for reviews from Prof. Bjørg Egelandsdal at Norwegian University of Life Sciences and director Per Berg at Nortura during the preparation of the manuscript.

8. REFERENCES

[1]. O.R. Fennema, J. Muscle. Foods. 1, 363-381 (1990)
[2]. A. Schäfer, K. Rosenvold, P.P. Purslow, H.J. Andersen, P. Henckel, Meat Sci. 61, 355–366 (2002)
[3]. C.J. Walukonis, M.T. Morgan, D.E. Gerrard, J.C. Forrest, A Technique for Predicting Water-Holding Capacity in Early Postmortem Muscle. (Purdue University 2002 swine research report, 2002), http://www.ansc.purdue.edu/swine/swineday/sday02/18.htm. Accessed 10 December 2013
[4]. M. Prevolnik, M. Čandek-Potokar, D. Škorjanc, J. Food Eng. 98, 347–352 (2010)
[5]. A.J. Rasmussen, M. Andersson, 42nd. International Congress of Meat Science and Technology, 1996
[6]. G. Offer, T. Cousins, J. Sci. Food. Agric. 58, 107-116 (1992)
[7]. M.J.D. Hertog-Meischke, R.J. Van Laack, F.J. Smulders, Vet Quart. 19, 175-181 (1997)
[8]. R.G. Kauffman, in Meat Science and Applications, ed. By Y.H. Hui, W.K. Nip, R. Rogers, (CRC Press: New York, 2001), p.1
[9]. K.L. Pearce, K. Rosenvold, H.J. Andersen, D.L. Hopkins, Meat Sci. 89, 111–124 (2011)
[10]. E. Gjerlaug-Enger, Genetic Analyses of Meat, Fat and Carcass Quality Traits Measured by Rapid Methods. Phd thesis, Norwegian University of Life Science, 2011.
[11]. H.C. Bertram, A.H. Karlsson, M. Rasmussen, O.D. Pedersen, S. Dønstrup, H.J. Andersen, J. Agr. Food. Chem. 49, 3092-3100 (2001)
[12]. E. Tornberg, M. Wahlgren, J. Brøndum, S.B. Engelsen, Food. Chem. 69, 407-418 (2000)
[13]. H.C. Bertram, H.J. Andersen, Ann. R. NMR. S. 53, 157–202(2004)
[14]. J.P. Renou, G. Monin, P. Sellier, Meat Sci. 15, 225-233 (1985)
[15]. H.C. Bertram, P.P Purslow, H.J. Andersen, J. Agr. Food. Chem. 50, 824–829 (2002)
[16]. P.S. Belton, K.J. Packer, Biochim. Biophys. Acta. 354, 305–314 (1974)
[17]. H.C. Bertram, A. Schäfer, K. Rosenvold, H.J. Andersen, Meat Sci. 66, 915–924 (2004)
[18]. R.T. Pearson, W. Derbyshire, J.M.V. Blanshard, Biochem. Bioph. Res. Co. 48, 873-879 (1972)
[19]. W.T. Sobol, I.G. Cameron, W.R. Inch, M.M. Pintar, Biophys. J. 50, 181-191 (1986)
[20]. C.F. Hazlewood, D.C. Chang, B.L. Nichols, D.E. Woessner, Biophys. J. 14, 583-606 (1974)
[21]. G. Favetto, J. Chirife, G.B. Bartholomai, J. Food. Technol. 16, 621-628 (1981)
[22]. A. Kondjoyan, A. Kohler, C.E. Realini, S. Portanguen, R. Kowalski, S. Clerjon, P. Gatellier, S. Chevolleau, J.M. Bonny, L. Debrauwer, Meat Sci. (2013) doi: 10.1016/j.meatsci.2013.07.032
[23]. M. Chabbouh, S.B.H. Ahmed, A. Farhat, A. Sahli, S. Bellagha, Food. Bioprocess. Tech. 5, 1882–1895 (2012)
[24]. G. Sartor, G.P. Johari, J. Phys. Chem, 100, 1045-1046 (1996)
[25]. B.E. Elizalde, A.M.R. Pilosof, L. Dimier, G.B. Bartholomai, J. Am. Oil. Chem. Soc. 64, 1454-1458 (1989)
[26]. I. Muñoz, N. Garcia-Gil, J. Arnau, P. Gou, Meat. J. Food. Eng. 110, 465–471 (2012)
[27]. E.E. Burnell, M.E. Clark, J.A. Hinke, N.R. Chapman, Biophys. J. 33, 1–26 (1981)
[28]. S. Meiboom, D. Gill, Rev. Sci. Instrum. 29, 688-691 (1958)
[29]. B.M. Fung, P.S. Puon, Biophys. J. 33, 27–37 (1981)
[30]. P.J. Lattanzio, K.W. Marshall, A.Z. Damyanovich, H. Peemoeller, Magnet. Reson. Med. 44, 840–851 (2000)
[31]. C.K. McDonnell, P. Allen, E. Duggan, J.M. Arimi, E. Casey, J. Duane, J.G. Lyng, Meat Sci. 95, 51–58 (2013)
[32]. J.R. Zimmerman, W.E. Brittin, T. J. Phys. Chem. 61, 1328-1333 (1957)
[33]. W.C. Cole, A.D. LeBlanc, S.G. Jhingran, Magnet. Reson. Med. 29, 19-24 (1993)
[34]. M. Nilsson, M. A. Connell, A. L. Davies and G. A. Morris. Anal. Chem. 78, 3040 – 3045 (2006)
[35]. M.J.A.D. Hertog-Meischke, F.J.M. Smulderst, J.G.V. Logtestijn, J. Sci. Food. Agr. 78, 522-526 (1998)
[36]. M.J.A.D. Hertog-Meischke, R.E. Klont, F.J.M. Smulders, J.G.V. Logtestijn, Meat. Sci. 47, 323-329 (1997)
[37]. A.W.J. Savage, P.D. Warriss, P.D. Jolley, Meat. Sci. 27, 289–303 (1990)
[38]. N. Bloembergen, E.M. Purcell, R.V. Pound, Phys. Rev. 73, 679-712 (1948)

Paper II

Journal of Food Engineering 175 (2016) 51–57

Contents lists available at ScienceDirect

Journal of Food Engineering

journal homepage: www.elsevier.com/locate/jfoodeng

Evaluating nuclear magnetic resonance (NMR) as a robust reference method for online spectroscopic measurement of water holding capacity (WHC)

Han Zhu [a, b, *], Marion O'Farrell [c], Gregory Bouquet [c], Kathrine Lunde [d], Bjørg Egelandsdal [a], Ole Alvseike [d], Per Berg [b], Eli Gjerlaug-Enger [e], Eddy W. Hansen [f]

[a] Norwegian University of Life Sciences, 1430 Ås, Norway
[b] Nortura SA, Lørenveien 37, 0585 Oslo, Norway
[c] SINTEF ICT, Forskningsveien 1, 0373 Oslo, Norway
[d] Animalia, Lørenveien 38, 0585 Oslo, Norway
[e] Norsvin, Furnesvegen 223, 2319 Hamar, Norway
[f] University of Oslo, Department of Chemistry, 0371 Oslo, Norway

ARTICLE INFO

Article history:
Received 11 September 2015
Received in revised form
6 November 2015
Accepted 6 December 2015
Available online 12 December 2015

Keywords:
Water holding capacity
NMR
Vis/NIR spectroscopy
X-ray transmission
EZ-DripLoss
Porcine *longissimus dorsi* muscles

ABSTRACT

The potential of using NMR as a reference method for WHC measurement in porcine *longissimus dorsi* was investigated. The accuracy of NMR when measuring small water changes was assessed in a model system and in muscles. Visible/near infrared (Vis/NIR) and X-ray were used as potential online spectroscopic methods to assess WHC on 40 muscles. Drip loss and spin–spin relaxation were also measured. Calibration models were built using partial least squares regression (PLSR) with Vis/NIR or X-ray spectra as input and NMR or drip loss values as output. The slowest spin–spin relaxation time (T_{22}) showed higher correlation with both Vis/NIR ($R^2_{CV} = 0.66$) and X-ray spectra ($R^2_{CV} = 0.76$) than EZ-DripLoss values, demonstrating NMR has potential as a reference method for WHC measurement. NMR was more robust against variation along the length of the muscle when compared to the EZ-DripLoss method.

1. Introduction

Water holding capacity is one of the most important traits for meat quality both in fresh meat and in processed products due to economic and sensory reasons. Online measurement of the WHC is still a dream for the meat industry despite the amount of research conducted in this area. WHC is affected by genetics, physiological factors, rearing conditions and factors with regards to slaughter and further processing (Den Hertog-Meischke et al., 1997).

The available methods for WHC determination (Trout, 1988) are mostly destructive and time consuming. Alternatives to conventional methods are fast spectroscopic methods that have the potential to be implemented online. Spectroscopic techniques have been investigated for assessing WHC in meat but there are unresolved issues with repeatability and accuracy (Brøndum et al., 2000; Elmasry et al., 2011; Prevolnik et al., 2009). Also, an unavoidable aspect of spectroscopic methods is their need to be calibrated against other methods. Assuming good experimental design when developing calibration models, the accuracy of spectroscopic techniques for measuring any quality parameters depend on three main factors: 1) the natural heterogeneity of all biological materials; 2) the distinctiveness and variation of the features in the measured spectra; and 3) the accuracy and repeatability of the reference method. The first and second are unavoidable due to sample characteristics and composition. Previous works have shown that when different reference methods of WHC were used for Vis/NIR spectroscopy, a significant variation in the coefficient of determination of calibration (R^2cal = 0.004–0.71) and prediction error of lost water (0.36–3.5%) appeared (Brøndum et al., 2000; Forrest et al., 2000;

Abbreviations: CPMG, Carr-Purcel-Meiboom-Gill; DFD, dark, firm and dry; NMR, nuclear magnetic resonance; PLSR, partial least squares regression; PSE, pale, softs and exudative; SG, Savizky-Golay; SNV, standard normal variate; Vis/NIR spectroscopy, Visible/near infrared spectroscopy; WHC, water holding capacity.

* Corresponding author. Norwegian University of Life Sciences, 1430 Ås, Norway.
E-mail address: zhuhanchien@gmail.com (H. Zhu).

http://dx.doi.org/10.1016/j.jfoodeng.2015.12.003
0260-8774/

Hoving-Bolink et al., 2005; Leroy et al., 2003; Pedersen et al., 2003; Prevolnik et al., 2010; Prieto et al., 2008; Savenije et al., 2006), probably related to variation in accuracy and repeatability of reference methods as well as differences in sample size.

Energy dispersive X-ray (or X-ray spectroscopy) and Vis/NIR spectroscopy were investigated as potential online spectroscopic methods. X-ray spectroscopy provides information of the intermolecular forces in water and meat microstructure (Diesbourg et al., 1988; Kosanetzky et al., 1987), i.e. the distance between myosin and actin fibers in the muscle, which is related to WHC (Hughes et al., 2014; Offer and Trinick, 1983). The volume of myofibrils can change up to threefold due to the changes in the interfilament spacing, which generates the driving force for drip losses and WHC variation (Offer and Trinick, 1983). Encouraging results have been obtained using lab-based X-ray diffraction measurements (due to scattering) showing post mortem changes in the pork myofilament lattice (Diesbourg et al., 1988; O'Farrell et al., 2014). Vis/NIR spectral changes occur due to pH reduction and subsequent denaturing of proteins affecting light scattering.

The EZ-DripLoss method has been preferred in many labs because it is simple, inexpensive, sensitive (Rasmussen and Andersson, 1996) and has produced relatively high heritability values in the Norwegian pig breeding program (Norsvin, Hamar, Norway, 2006-present). However, even as a reference method, the EZ-DripLoss method is slow ($t \geq 24$ h), labor intensive and highly dependent on the operator. The prediction of WHC using EZ-DripLoss as reference method does not provide any information about the dynamics behind the water loss, and from what sort of structural changes occurred. Hence, there is a need for a faster, accurate and robust reference method for WHC measurements. Although pork *longissimus dorsi* muscle, often used for EZ-DripLoss measurements, is visually homogeneous, inherent heterogeneities exist throughout the muscle, and they increase towards the cranial end (Christensen, 2003). The sampling procedure for EZ-DripLoss, as developed by the Danish Meat Research Institute, involves WHC measurements on two samples within the same slice to define a WHC value (Danish Meat Research Institute, 2010). The EZ-DripLoss value is known to depend on the position along the longissimus dorsi muscle. Christensen (2003) reported drip losses at three positions (A, B and C in Fig. 2, Christensen, 2003) using 11–15 slices of LD muscles from 34 animals. A, B and C indicate dorsal, superficial and ventral positions on LD muscle, and position A and C are the two normal sampling positions in routine EZ-DripLoss measurement. At position A the drip loss decreased linearly about 50% with slice number, while no change in drip loss with slice number was observed at position C. The heterogeneity of small meat samples may even increase when sample handling cannot be fully controlled since water distribution is sensitive to pressure. Standardization of manual or mechanical sample handling is crucial to minimize errors for most methods including NMR.

NMR proton relaxometry has been used for quantitative measurement of different components in meat (total fat and moisture content) (Sørland et al., 2004). It provides information on the physical (distribution, compartmentalization) and chemical (mobility, interactions with macromolecules) properties of the water (Bertram and Ersen, 2004). This means that NMR relaxometry could be used to quantify the mobility and distribution of water in different meat domains (Bertram et al., 2001; Tornberg et al., 2000) and has the potential to quantify WHC rapidly. To be more specific, WHC can be measured by relaxation time of water associated with pores in muscle of different size (Trout, 1988). Renou and Monin (1985) were among the first ones to show correlations between NMR relaxtometry (T_1 and the population of T_{21}) and WHC assessed by pH paper imbibition technique. Later on, an extensive number of studies have reported that meat of different WHC from Pale, Softs and Exudative (PSE) to Dark, Firm and Dry (DFD) can be distinguished by NMR transverse relaxtometry as reviewed by Pearce et al. (2011, Bertram et al., 2002b; Tornberg et al., 1993, Tornberg et al., 2000). Unlike bulk water, the Carr-Purcel-Meiboom-Gill (CPMG) relaxation curve of meat appears to be multi-exponential, i.e., characterized by a distribution function of spin–spin relaxation times, T_2s, resulting from microscopic meat heterogeneity (Renou et al., 1989). The slowest component (T_{22}, 100–250 ms, ~10% of signal intensity) corresponds to mobile water outside myofibrils (Bertram and Ersen, 2004; Tornberg et al., 1993). Tornberg et al. (1993) suggested that T_{22} corresponds to extracellular water, i.e. water that is most susceptible to dripping. Although T_{22} has been reported to relate to WHC as determined by Honikel bag method with correlation coefficients of 0.60–0.75 (prediction error was not reported) (Bertram et al., 2002a), T_{22} has not been investigated as a reference value for WHC.

The objective of this paper is to determine the suitability of NMR as a reference method for a faster, online spectroscopic method to evaluate WHC based on three studies. Since there is interest in the meat industry to know the total amount of moisture, immobilized and free water in the meat products (Q-PorkChains, 2007–2011), the ability of NMR to determine the parameters is investigated. The accuracy of NMR to measure small changes in water in meat was assessed. The measurement error of two spectroscopic methods, Vis/NIR spectroscopy and energy dispersive X-ray transmission in combination with two possible reference techniques, the EZ-DripLoss method and NMR are investigated. In addition, the possibility of using NMR as a reference method for WHC determination is discussed. The accuracy and repeatability of the NMR is evaluated.

2. Materials and methods

2.1. Animals and sampling

Without specification, the pigs used in studies 1 and 3 were young boars from Landrace and Duroc breed, tested at the Norsvin boar test station (Ilseng, Norway) as part of an on-going breeding program. The boars not selected for semen production, were slaughtered and had carcass weights of around 95 kg. The animals were stunned in an atmosphere with 90% carbon dioxide. The carcasses were left at 15 °C for 5 min and then chilled to 1–3 °C for 96 h before transporting to a partial dissection line at Animalia (Oslo, Norway), where the porcine *longissimus dorsi* muscle was removed.

In the second study, comparing EZ-DripLoss method, NMR and other spectroscopic techniques, 400 pigs of Landrace and Noroc (50% Duroc, 25% Landrace and 25% Yorkshire) were slaughtered (at Tønsberg, Norway) during 4 days. In order to obtain a wider range of WHC, forty pigs were selected based on their breed and pH measured 6 h postmortem (pH = 5.47–6.75). Left porcine *longissimus dorsi* loins were obtained 24 h postmortem and cut as shown in Fig. 1a) for the different measurement techniques.

2.2. NMR relaxation measurements

In the first study, transverse relaxation (T_2) was measured on a series of H_2O/D_2O mixtures (H_2O, vol% = 0, 2.5, 8, 12.5, 37.5, 50, 62.5, 75, 87.5, 100) using a Maran Ultra NMR instruments (Resonance Instruments, Witney, UK), operating at a magnetic field strength of 0.54 T, corresponding to a proton resonance frequency of 23 MHz. Sample volumes were 0.54 mL (height < 10 mm). Deionized water was purified in an ELGA-purelab system (Veolia Water, Paris, France). Deuterium water (99.9 atom% D) was purchased from Sigma–Aldrich (St. Louis, MO, USA). The NMR signal

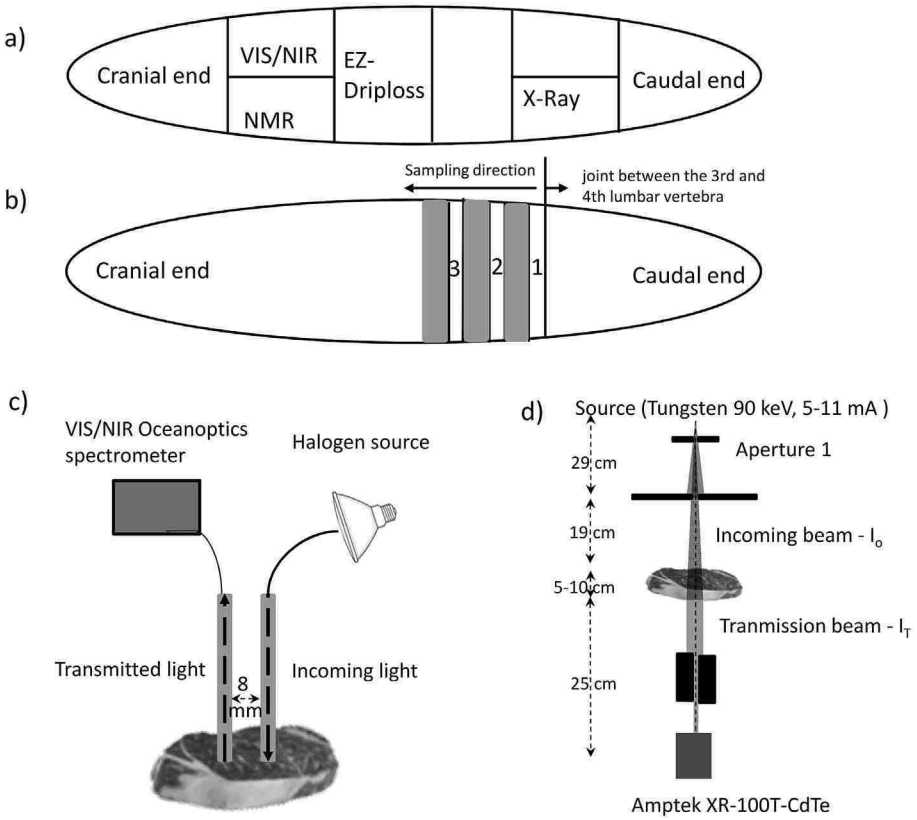

Fig. 1. a) Left porcine *longissimus dorsi* loin, divided for different techniques (approximately 250 g, ~7 × 7 × 5 cm for each technique) for WHC measurement. b) Left porcine *longissimus dorsi* loin for NMR measurement. Sampling started from the joint between the 3rd and 4th lumbar vertebra. The first 3 slices are shown, and gray area indicates slice that was discarded. The sample slice and discarded slice were 10 mm and 22 mm respectively. Set up of c) Vis/NIR and d) X-ray for WHC measurement.

response was recorded by applying a traditional CPMG pulse-sequence (Meiboom and Gill, 1958) with a fixed inter-pulse time $\tau = 1.0$ ms, 6 K echoes and 8 transients.

For studies 1 and 3, the same 20 meat samples were taken from the left *longissimus dorsi* muscle from one randomly selected animal, were measured by NMR. Sampling started from the joint between the 3rd and 4th lumbar vertebra, and slices of around 10 mm in thickness were cut (Fig. 1b). The remaining meat was covered with plastic and stored at 4 °C to avoid moisture loss while the slice was measured. Two cylindrical plugs (8ø × 10 mm, ~0.5 g) were cored using a sharp cork borer from each slice and marked as R or B, the dorsal or ventral part of the slice, respectively. Samples were gently inserted in closed Teflon sample holders (1 cm in length), thermostated at 25 °C for 10 min before CPMG measurements were performed. The NMR signals were recorded with $\tau = 150$ μs, 12 K echoes and 16 transients. The τ value for meat samples was set lower than for water in order to record lower T_2 values in meat. Between each slice, a slice of 2.2 cm was sliced off and discarded in case the drip loss process had started due to cutting. A total number of 10 slices were investigated with 2 plugs from each slice.

For study 2, three cylindrical samples (8ø × 10 mm, ~0.5 g) were cored for each loin (the position of the NMR-dedicated meat is shown on Fig. 1a and inserted into the bottom of the NMR glass tubes with the fiber direction parallel to the cylindrical axis. A layer of parafilm was placed on the top of each sample to avoid water evaporation. Spin–spin relaxation experiments were performed. The T_2 measurements were performed with a τ-value of 24 μs, 10 K echoes and 8 scans of repetition. The repetition time between two succeeding scans was set to 3 s. All samples were measured at 25 °C and equalized at this temperature for 10 min before NMR determinations. Parafilm tested under the same conditions, showed no signal contribution.

2.3. Drip loss measurements

Drip loss was measured using a standardized EZ-DripLoss method developed by the Danish Meat Research Institute, (2010; Rasmussen and Andersson, 1996). Two cylindrical samples (25ø × 25 mm) were cut from *longissimus dorsi* loin using a cork borer along the fiber direction for each animal. Each sample was placed in the specific containers (Danish Meat Research Institute, 2010), and stored at 4 °C for 24 h. The containers (empty and with meat sample) were weighed in the beginning, and drip and container were weighed at the end of the experiment. The drip loss percentage was calculated as the ratio between the drip weight and the initial meat weight.

2.4. Vis/NIR spectroscopy

UV/Vis/NIR spectra in the 350–1025 nm range were obtained using a USB2000 spectrometer (Ocean optics, Dunedin, FL). Interactance spectra were obtained using one optical fiber (400 μm) connected to a halogen source for illumination and another fiber (200 μm) connected to the spectrometer for detection. The distance between the illumination fiber and detection fiber was set to 8 mm (Fig. 1c) while the integration time was set to 40 ms. To increase the signal to noise ratio, an average of 10 consecutive spectra was used. For each sample, five spectra were recorded: a dark reference (source off); a white reference, and three spectra from different positions in the meat sample. The fibers were inserted ~1 cm into the meat slice at three randomly selected positions. The direction chosen was with the light traveling parallel to the myofibers. All

samples were measured at 25 °C and equalized at this temperature for 10 min before initiating measurements.

2.5. X-ray spectroscopy

Fig. 1d shows the experimental set-up used for X-ray transmission measurements. For each measurement, three spectra were recorded, the dark reference (source off), the white reference (source on and no meat) and the transmission measurement through the meat slice. Two measurements were recorded for each meat sample. The detector used was Amptek Cadmium Telluride (CdTe) diode detector (Amptek Inc., Bedford, MA). Further details of the X-ray set-up and components have been previously described (O'Farrell et al., 2014).

3. Data analysis

3.1. NMR spin–spin relaxation data

For study 1, the data from the H_2O/D_2O mixtures were fitted to a single exponential function model (Eq. (1a)).

$$I = I_2 * \exp(-t/T_2) \quad (1a)$$

where I represents the proton signal intensity and T_2 represents the resolved spin–spin relaxation time.

For study 2 and 3, the spin–spin relaxation curve was fitted to a 3-exponential function model (Eq. (1b)):

$$I = I_{20} * \exp(-t/T_{20}) + I_{21} * \exp(-t/T_{21}) + I_{22} * \exp(-t/T_{22}) \quad (1b)$$

where I represents the proton signal intensity, I_{20}, I_{21} and I_{22} represent the resolved proton signal intensity of the fast, intermediate and slow relaxing component. T_{20}, T_{21} and T_{22} are the spin–spin relaxation times of the three components respectively. In all three studies, Origin 8.6 (OriginLab Corp, Northampton, MA) was used for curve fitting.

3.2. Spectral correction

3.2.1. Vis/NIR spectra

The Vis/NIR spectra (460–950 nm) were corrected according to Eq. (2).

$$\text{Vis/NIR spectrum} = \frac{I_{Meat} - I_{Background}}{I_{Source} - I_{Background}} \quad (2)$$

I_{Meat} is the interactance spectrum of the meat, $I_{Background}$ is the spectrum when the source was turned off, and I_{Source} is the spectrum of source when the two fibers are inserted into glass beads (ø1 mm). Three measurements were taken for each of the 40 loins and the signal intensities were averaged before spectral correction.

3.2.2. X-ray spectra

The X-ray spectra were corrected as follows:

$$\text{X-ray Spectrum} = -\text{Log}\left(\frac{J_{Meat} - J_{Background}}{J_{Source} - J_{Background}}\right) \quad (3)$$

J_{Meat} is the spectrum of X-ray transmitted through the meat, J_{Source} is the spectrum without any meat in the path and $J_{Background}$ is the spectrum with the source off (dark reference). Two measurements were taken for each of the 40 loins, and the signal intensities were averaged before spectral correction.

3.2.3. Preprocessing and multivariate analysis of spectra

Spectra pre-processing was performed using Matlab version R2013b (The MathWorks Inc., Connecticut, USA). Savizky-Golay (SG) smoothing was applied on the Vis/NIR and X-ray spectra. After spectral correction and SG smoothing, further pre-processing methods including mean normalization and Standard normal variate (SNV) method (Rinnan et al., 2009) were also assessed. Calibration models were built separately when the processed spectra were used as input and NMR or EZ-DripLoss values were used as output in order to predict WHC using PLSR with full internal cross-validation (leave one out) using the Unscrambler (version X 10.3, CAMO Software AS, Oslo, Norway). Two calibration statistical parameters were used for model comparison including coefficient of determination of cross validation in calibration (R^2_{CV}) and standard error of cross validation in calibration (se_{CV}).

4. Results and discussion

4.1. Study 1: proton signal intensity and water content – a statistical evaluation

In proton NMR, the relaxation signal intensity is proportional to the number of protons in the system (Sørland et al., 2004). Fig. 2a shows the correlation (coefficient of determination, $R^2 = 0.9989$) between the relaxation signal intensity and the water mass in the

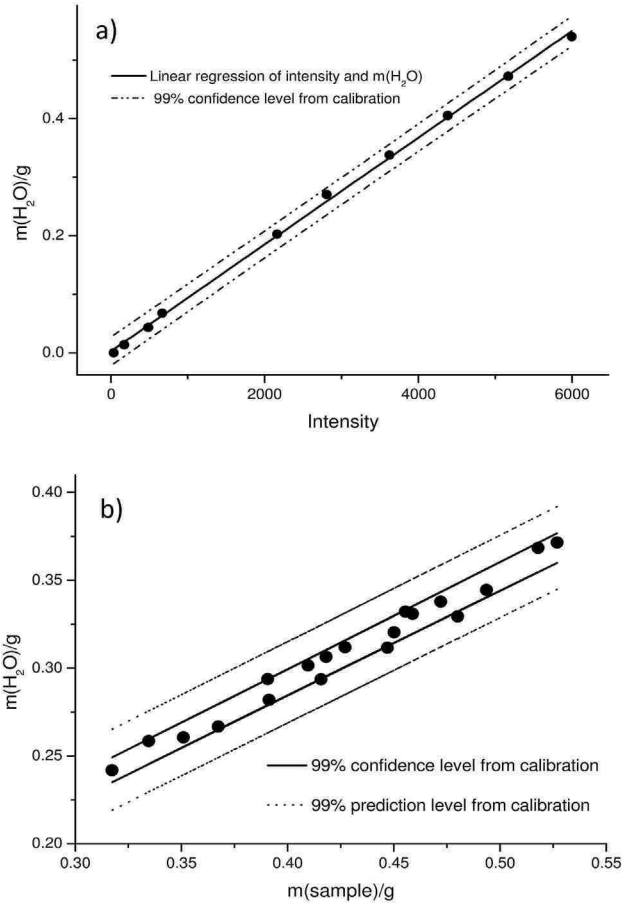

Fig. 2. a) Correlation between NMR signal intensity and water mass ($m(H_2O)$, fixed volume of 0.54 mL) based on a 99% prediction level, b) correlation between meat sample mass and water mass (calculated from the calibration curve in a) based on 20 meat samples. The straight lines represent 99% confidence (–) and prediction (···) intervals, respectively. One data point was removed (an outlier; not shown) from the statistical analysis.

system. The calculated 99% prediction level error was 2.6% representing the smallest error possible within the current NMR settings, shows that NMR accurately measures water mass in the sample. This number can be further decreased if a larger number of scans are used.

The measurement of proton in real meat samples using NMR is more complex. Meat samples contain more than one pool of protons including water, fat, protein and others (Hills, 1998). The correlation between NMR signal intensity and water mass in meat samples was slightly poorer ($R^2 = 0.9765$) than in the model system. Using the linear regression curve in Fig. 2a) as a calibration curve, the water mass in real meat samples can be estimated from the CPMG proton signal intensity, as illustrated in Fig. 2b). The root mean square of the error of linear regression in Fig. 2a) and b) are 0.0033 g (~0.54 g H_2O/D_2O mixtures) and 0.0139 g (~0.375 g H_2O in meat), respectively. Interestingly, the slope of the straight line in Fig. 2b) is relatively close to the water fraction in meat and reads 0.715 ± 0.014 (within a 99% confidence interval).

4.2. Study 2: correlation between spectroscopic techniques and reference methods for WHC measurement

In Study 2, two possible online spectroscopic methods including X-ray spectroscopy and Vis/NIR spectroscopy requiring absolute reference methods for industrial implementations were tested.

WHC was determined for 40 meat samples using two potential reference methods, NMR and EZ-DripLoss. Fig. 3 shows the Vis/NIR and X-ray spectra of samples characterized by the more extreme T_{22} times. The Vis/NIR spectra showed absorption (Fig. 3a, as indicated by the arrows) at around 578 nm due to myoglobin (Brøndum et al., 2000) and absorbance at 760 nm due to third overtone O–H stretching in water (Wu et al., 2013). The spectral characteristics that related to short and long T_{22} times, respectively, were over a large wavelength range agreeing with differences in light scattering due to protein aggregation. This again relates to differences in WHC. The spectra in Fig. 3a revealed that samples with long T_{22}, which are more likely to drip, possessed higher transmission. This is in agreement with PSE meat – which has high reflectance is correlated to low WHC, while DFD meat is normally associated with high WHC (Greaser, 2001; Monroy et al., 2010). The samples investigated in this work did not, however, belong to these extreme groups. Spectral differences detected within the visible range of wavelengths (<700 nm is these spectra) is mainly associated with sample color and not strictly relevant to WHC.

The X-ray spectrum is a result of both low-angle scattering and transmission. The scattering occurs due to the repeating structural units since muscle (myofilament thickness/spacing) has a long-range ordering of 10's of nanometers, which is absent in normal water whose ordering arises from a repeated inter-molecular distance of 4 Å (0.25 $Å^{-1}$). For example in the work of Harding and Kosanetzky (1987), X-ray scatter due to tendon has a peak at lower energy levels, which pure water doesn't have, since it has regular molecular arrangement with larger spacing of about 30 Å. In Fig. 3b it can be seen the spectra for $T_{22} < 0.08$ s is shifted towards higher energy levels (as indicated by the arrows in the figure), indicating a repeated pattern with shorter spacing. Since the most important region for water holding is the interfibrillar space, changes in the myofilament spacing are suggested. Microscopic data have shown that a longer T_{22} corresponds to a larger extra-fibrillar (fluid) space (Bertram et al., 2002b; Pearce et al., 2011).

All NMR relaxation curves presented in this work were fitted to a sum of three exponential functions, and thus characterized by three relaxation time constants (T_2s) and their corresponding intensities (I_2s). Several PLS models were designed using Vis/NIR or X-ray spectra as response parameters, and T_2s or I_2s as "design"

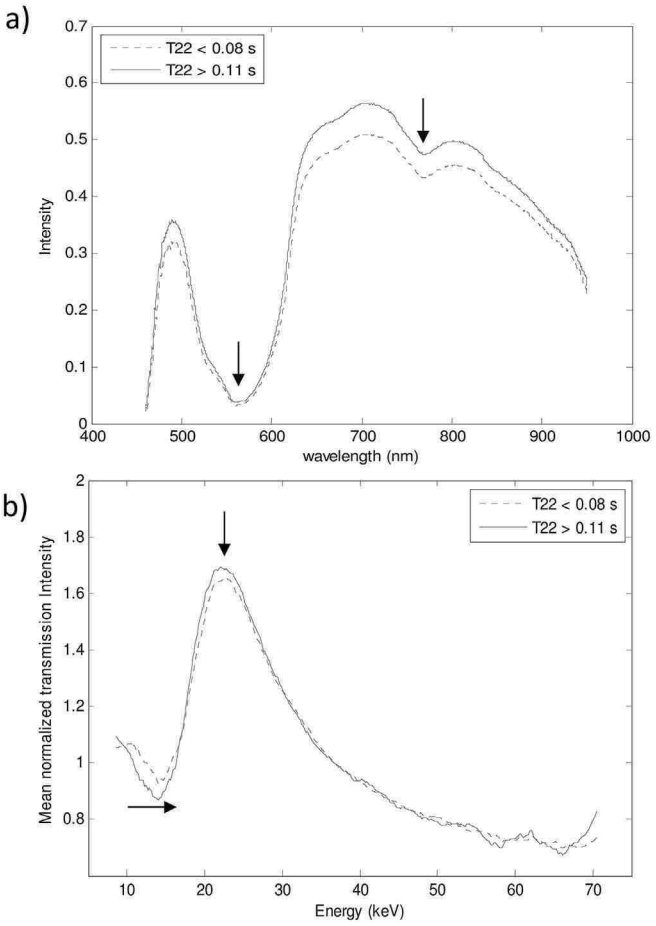

Fig. 3. a) Average of Vis/NIR transmission spectra and b) mean normalized average of X-ray spectra based on the short-(dotted line) and long- (solid line) T_{22} relaxation time.

variables, respectively. Table 1 gives a summary of the different PLS models, in which NMR and EZ-DripLoss were used as reference methods, respectively. In contrast to EZ-DripLoss, good correlations (R^2_{CV}) were found between Vis/NIR and NMR (T_{22}) and between X-ray and NMR (T_{22}). It should be mentioned that the standard error of cross validation of T_{22} and EZ-DripLoss are not directly comparable due to differences in units.

The poor correlation with EZ-DripLoss was not unexpected. There are only a few previous WHC prediction models aiming at correlating spectroscopic data and EZ-DripLoss (Forrest et al., 2000; Prevolnik et al., 2010). For instance, Forrest et al. (2000) reported a NIR study (900–1800 nm) on 99 porcine *longissimus dorsi* muscles (spectra acquired 30 min post exsanguination), and found a good correlation ($R = 0.84$) between NIR and EZ-DripLoss with a root mean square prediction error of 1.8%. Another study on 228 porcine *longissimus dorsi* muscles using Vis/NIR ($\lambda = 400–1100$ nm) and EZ-DripLoss reported an $R^2_{CV} = 0.62$ and $se_{CV} = 1\%$ (Prevolnik et al., 2010). Previous works have shown that when different WHC

Table 1
Statistical evaluation of potential reference methods for WHC measurement in meat using PLSR.

	T_{22}		EZ-DripLoss	
	R^2_{CV} [a]	se_{CV} [b]	R^2_{CV} [a]	se_{CV} [b]
X-ray	0.76	0.0047 s	0.3	1.667%
Vis/NIR	0.66	0.0055 s	0.04	1.933%

[a] Coefficient of determination of cross validation.
[b] Standard error of cross validation.

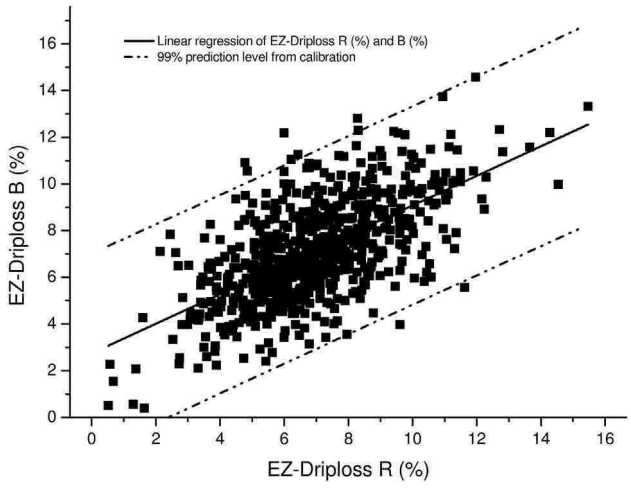

Fig. 4. Correlation between drip loss (%) measured on one slice near the dorsal end (R) and one slice near the ventral end (B) of 710 porcince *longissmus dorsi* muscles.

methods (i.e. Honikel bag method, tray drip loss, Barton-Gade method) were used as reference for Vis/NIR spectra, the correlation coefficients are not very robust (Brøndum et al., 2000; Forrest et al., 2000; Hoving-Bolink et al., 2005; Leroy et al., 2003; Prevolnik et al., 2010; Prieto et al., 2008; Savenije et al., 2006). The large variation in R^2cal indicates that the predictability of drip loss from current WHC measurement techniques lacks robustness and predictability. The reason for this is not clear.

The significant improvement in WHC predictability from relaxation time NMR data presented in this work (T_{22}) is encouraging, and suggests that NMR might be used as a reference method for WHC based on varying T_{22} values. Moreover, findings from this study suggest that energy dispersive X-ray, which has not critically been considered to be widely applicable to WHC measurements, should be further evaluated as a potential online spectroscopic technique for WHC.

4.3. Study 3: evaluation of experimental reference methods for WHC

EZ-DripLoss and NMR were evaluated as potential WHC reference methods. Fig. 4 shows the correlation ($R^2 = 0.395$) between the EZ-DripLoss from two presumed identical samples R and B (compares with position A and C in routine EZ-DripLoss measurements) (Christensen, 2003) from the same animal based on a total of 710 different animals slaughtered during 1 year (courtesy Norsvin, Hamar, Norway), with a root mean square error of linear regression 0.14%. The relative error was found to be around 1.7%.

CPMG NMR measurements at two different positions R and B within each slice of a total of 10 slices along a *longissimus dorsi* muscle (corresponding to position A and C in reference (Christensen, 2003)) were performed and their T_{22}'s determined by non-linear least squares fits (Eq. (1b)).

Since the proton signal intensity of the T_{22} component in meat is of the order of 10% of the total proton intensity it will certainly affect the error in the derived T_{22}. In principle we may consider the overall error σ_T in T_{22} to originate from two different and independent sources: 1) the error caused by the inherent signal-to-noise ratio in the NMR signal intensity, resulting in an error σ_{NMR} in T_{22} after application of Eqs. (1b) and (2)) the non-NMR error $\sigma_{non\text{-}NMR}$ originating from sample heterogeneity ($\sigma_{non\text{-}NMR(a)}$) and sample treatment ($\sigma_{non\text{-}NMR(b)}$, cutting and transferring of sample to the NMR probe etc.). Unfortunately, it is not possible to make a distinction between $\sigma_{non\text{-}NMR(a)}$ and $\sigma_{non\text{-}NMR(b)}$, so we simply write:

$$\sigma_T^2(T_{22}) = \sigma_{NMR}^2 + \sigma_{non-NMR(a)}^2 + \sigma_{non-NMR(b)}^2 + \varepsilon^2 \quad (4)$$

where ε represents random error (temperature, baseline correction etc.). σ_{NMR} was determined by simulation (Eq (1b)) using the known S/N-ratio of the signal intensity I, resulting in $\sigma_{NMR} \approx 1.2\%$.

Experimental T_{22} data as a function of slice number and position (R and B) on 20 different samples from the same loin are plotted in Fig. 5. In order to determine the longitudinal sample robustness, the average T_{22} in two successive slices i and $i+1$ at positions R and B was calculated. The results are shown as open squares (□) in Fig. 5. Based on these data the mean $\overline{T}_{22}$ at position R and B within all slices (except for slices 1, 8 and 9 (position R) and slices 1, 2 and 3 (position B)) was calculated, resulting in $\overline{T}_{22}(B) = (0.149 \pm 0.001)$ s and $\overline{T}_{22}(R) = (0.145 \pm 0.002)$ s. Importantly, these relative errors are slightly less than 1%, and are of the same order as the inherent NMR error σ_{NMR} ($\approx 1.2\%$).

Hence, we tentatively believe the large deviation (80–90%; Eq

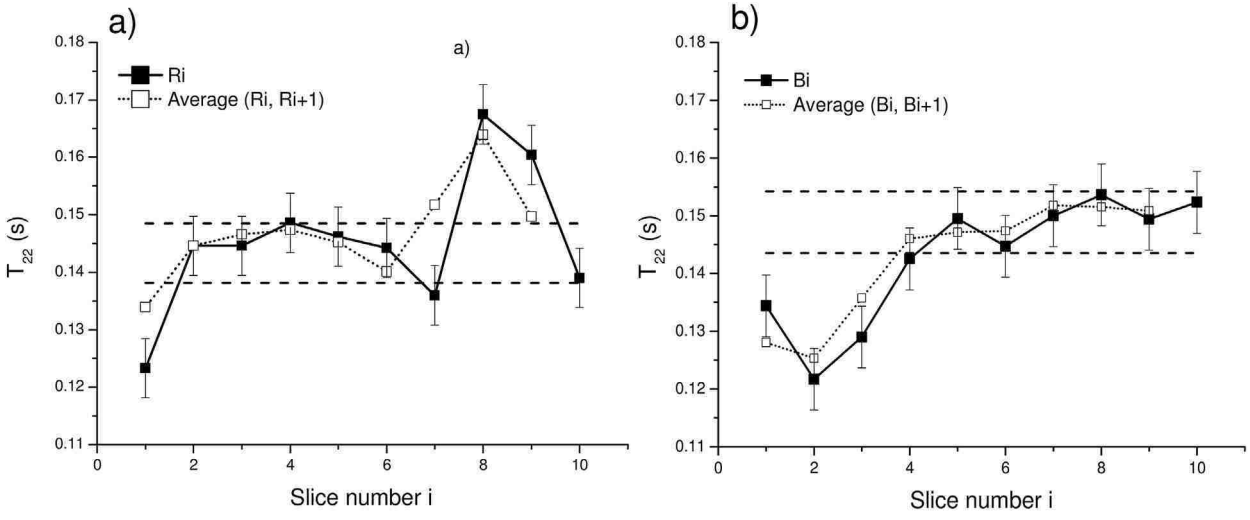

Fig. 5. Spin–spin relaxation time T_{22} (■), as derived from model fitting Eq. (1b) to the observed CPMG curves, against the slice number and the position R (a) and B (b) within a slice. The open squares (□) represent the average spin–spin relaxation time for two successive slices i and $i+1$ within R and B, respectively. The horizontal "band" (in dashed line) in each Figure represents a 99%-confidence interval ($\pm 3\sigma_{NMR}$) around the mean T_{22} (after excluding 3 outliers each). Also, the error bars are defined by $3\sigma_{NMR}$. See text for further details.

(4)) of the T_{22}s in slices 1, 8 and 9 (position R) and in slices 1, 2 and 3 (position B) to originate from non-NMR effects, i.e. sample heterogeneity and/or sample handling. It is worth noting that no significant difference in $\overline{T}_{22}$ between positions B and R was evidenced after removing the above "outliers".

Keeping in mind that T_{22} in 3 out of 10 slices was significantly different from$\overline{T}_{22}$, T_{22} measured on a randomly selected sample becomes less reliable as an estimator for$\overline{T}_{22}$. However, this reliability is improved by taking the mean T_{22} of two successive samples i and i + 1 we are still facing a problem of sample heterogeneity and/or sample handling. It will be important to identify the cause of the outliers if NMR should replace EZ-DripLoss.

It is expected that the effect of sample heterogeneity and sample-handling on T_{22} can be minimized by increasing sample size. In this respect, preliminary T_2 measurements (not shown) performed on much larger samples (~7 cm^3) at the same magnetic field strength suggested that heterogeneity and/or sample handling becomes of minor importance, if any. Work on this issue is in progress and will be reported elsewhere.

5. Conclusions

CPMG NMR was demonstrated as a potential reference method for measuring WHC. CPMG NMR is also a faster method than EZ-DripLoss method. The slowest relaxation time T_{22} shows a higher R-square with both Vis/NIR spectra and X-ray spectra compared with these spectra's correlation to EZ-DripLoss values. Energy dispersive X-ray gave lower prediction errors than Vis/NIR.

The longitudinal sample robustness along *longissimus dorsi* muscle was higher for T_{22} compared to EZ-DripLoss values. The results favor NMR as a reference method.

Acknowledgments

This investigation was funded by the Research Council of Norway through the project "On line determination of water retaining ability in pork muscle", Project number 229192 and the project INFORMED (Increased Efficiency: Moving from Assumed Quality to Online Measurement and Process, Nortura SA, Project no.: 210516). We would also like to thank André Christian Backer from Animalia (Oslo, Norway) for providing EZ-DripLoss data.

References

Bertram, H.C., Karlsson, A.H., Rasmussen, M., Pedersen, O.D., Donstrup, S., Andersen, H.J., 2001. Origin of multiexponential T(2) relaxation in muscle myowater. J. Agric. Food Chem. 49, 3092–3100.

Bertram, H.C., Dønstrup, S., Karlsson, A.H., Andersen, H.J., 2002a. Continuous distribution analysis of T2 relaxation in meat—an approach in the determination of water-holding capacity. Meat Sci. 60, 279–285.

Bertram, H.C., Rasmussen, M., Busk, H., Oksbjerg, N., Karlsson, A.H., Andersen, H.J., 2002b. changes in porcine muscle water characteristics during growth—an in vitro low-field NMR relaxation study. J. Magn. Reson. 157, 267–276.

Bertram, H.C., Ersen, H.J., 2004. Applications of NMR in meat science. Annu. Rep. NMR Spectrosc. 53, 157–202.

Brøndum, J., Munck, L., Henckel, P., Karlsson, A., Tornberg, E., Engelsen, S.B., 2000. Prediction of water-holding capacity and composition of porcine meat by comparative spectroscopy. Meat Sci. 55, 177–185.

Christensen, L.B., 2003. Drip loss sampling in porcine m. longissimus dorsi. Meat Sci. 63, 469–477.

Danish Meat Research Institute. Instruction Manual: EZ Driploss. URL (www.dti.dk/_root/media/58882_EZ_Driploss_instruction.pdf) (accessed 22.03.15.).

Den Hertog-Meischke, M.J., Van Laack, R.J., Smulders, F.J., 1997. The water-holding capacity of fresh meat. Vet. Quart. 19, 175–181.

Diesbourg, L., Swatland, H.J., Millman, B.M., 1988. X-ray diffraction measurements of postmortem changes in the myofilament lattice of pork. J. Anim. Sci. 1048–1054.

Elmasry, G., Barbin, D.F., Sun, D.W., Allen, P., 2011. Meat quality evaluation by hyperspectral imaging technique: an overview. Crit. Rev. Food Sci. Nutr. 52, 689–711.

Forrest, J.C., Morgan, M.T., Borggaard, C., Rasmussen, A.J., Jespersen, B.L., Andersen, J.R., 2000. Development of technology for the early post mortem prediction of water holding capacity and drip loss in fresh pork. Meat Sci. 55, 115–122.

Greaser, M.L., 2001. Postmortem muscle chemistry. In: Hui, Y.H., Nip, W.K., Rogers, R. (Eds.), Meat Science and Applications. CRC Press, Florida, USA, pp. 21–35.

Harding, G., Kosanetzky, J., 1987. Status and outlook of coherent-X-ray scatter imaging. J. Opt. Soc. Am. A 4, 933–944.

Hills, B., 1998. Molecular origins of relaxation contrast. In: Hills, B. (Ed.), Magnetic Resonance Imaging in Food Science. Wiley-VCH, Weinheim, Germany, pp. 267–300.

Hoving-Bolink, A.H., Vedder, H.W., Merks, J.W.M., De Klein, W.J.H., Reimert, H.G.M., Frankhuizen, R., van den Broek, W.H.A.M., Lambooij en, E., 2005. Perspective of NIRS measurements early post mortem for prediction of pork quality. Meat Sci. 69, 417–423.

Hughes, J.M., Oiseth, S.K., Purslow, P.P., Warner, R.D., 2014. A structural approach to understanding the interactions between colour, water-holding capacity and tenderness. Meat Sci. 98, 520–532.

Kosanetzky, J., Knoerr, B., Harding, G., Neitzel, U., 1987. X-ray diffraction measurements of some plastic materials and body tissues. Med. Phys. 14, 526–532.

Leroy, B., Dotreppe, O., Lecocq, H., Istasse, L., Clinquart, A., 2003. Prediction of technological and organoleptic properties of beef longissimus thoracis from near-infrared reflectance and transmission spectra. Meat Sci. 66, 45–54.

Meiboom, S., Gill, D., 1958. Modified spin-echo method for measuring nuclear relaxation times. Rev. Sci. Instrum. 29, 688–691.

Monroy, M., Prasher, S., Ngadi, M.O., Wang, N., Karimi, Y., 2010. Pork meat quality classification using visible/near-infrared spectroscopic data. Biosyst. Eng. 107, 271–276.

O'Farrell, M., Bouquet, G., Tschudi, J., Bakke, K.A.H., Egelandsal, B., Lunde, K., 2014. Measuring water holding capacity—a comparison between a miniature near infrared system and an energy dispersive X-ray scattering system. NIR news 25, 11–14.

Offer, G., Trinick, J., 1983. On the mechanism of water holding in meat: the swelling and shrinking of myofibrils. Meat Sci. 8, 245–281.

Pearce, K.L., Rosenvold, K., Andersen, H.J., Hopkins, D.L., 2011. Water distribution and mobility in meat during the conversion of muscle to meat and ageing and the impacts on fresh meat quality attributes — a review. Meat Sci. 89, 111–124.

Pedersen, D.K., Andersen, H.J., Engelsen, S.B., 2003. Early prediction of water-holding capacity in meat by multivariate vibrational spectroscopy. Meat Sci. 65, 581–592.

Prevolnik, M., Čandek-Potokar, M., Novič, M., Škorjanc, D., 2009. An attempt to predict pork drip loss from pH and colour measurements or near infrared spectra using artificial neural networks. Meat Sci. 83, 405–411.

Prevolnik, M., Čandek-Potokar, M., Škorjanc, D., 2010. Predicting pork water-holding capacity with NIR spectroscopy in relation to different reference methods. J. Food Eng. 98, 347–352.

Prieto, N., Andrés, S., Giráldez, F.J., Mantecón, A.R., Lavín, P., 2008. Ability of near infrared reflectance spectroscopy (NIRS) to estimate physical parameters of adult steers (oxen) and young cattle meat samples. Meat Sci. 79, 692–699.

Q-PorkChains. Fundamentals of Water Holding Capacity (WHC) of Meat. URL (http://qpc.adm.slu.se/6_Fundamentals_of_WHC/page_30.htm) (accessed 07.05.15.).

Rasmussen, A.J., Andersson, M., 1996. New method for determination of drip loss in pork muscles. In: Proc. 42nd International Congress of Meat Science and Technology. Lillehammer, Norway.

Renou, J.P., Kopp, J., Gatellier, P., Monin, G., Kozak-Reiss, G., 1989. NMR relaxation of water protons in normal and malignant hyperthermia-susceptible pig muscle. Meat Sci. 26, 101–114.

Renou, J.P., Monin, G., 1985. Nuclear magnetic resonance measurements on pork of various qualities. Meat Sci. 15, 225–233.

Rinnan, Å., Berg, F.V.D., Engelsen, S.B., 2009. Review of the most common pre-processing techniques for near-infrared spectra. Trends Anal. Chem. 28, 1201–1222.

Savenije, B., Geesink, G.H., van der Palen, J.G.P., Hemke, G., 2006. Prediction of pork quality using visible/near-infrared reflectance spectroscopy. Meat Sci. 73, 181–184.

Sørland, G.H., Larsen, P.M., Lundby, F., Rudi, A.P., Guiheneuf, T., 2004. Determination of total fat and moisture content in meat using low field NMR. Meat Sci. 66, 543–550.

Tornberg, E., Andersson, A., Göransson, Å., Von Seth, G., 1993. Water and fat distribution in pork in relation to sensory properties. In: Puolanne, E., Demeyer, D.I. (Eds.), Pork Quality: Genetic and Metabolic Factors, first ed. CABI, Wallingford, UK, pp. 239–258.

Tornberg, E., Wahlgren, M., Brøndum, J., Engelsen, S.B., 2000. Pre-rigor conditions in beef under varying temperature- and pH-falls studied with rigometer, NMR and NIR. Food Chem. 69, 407–418.

Trout, G.R., 1988. Techniques for measuring water-binding capacity in muscle foods—a review of methodology. Meat Sci. 23, 235–252.

Wu, D., Wang, S., Wang, N., Nie, P., He, Y., Sun, D.-W., Yao, J., 2013. Application of time series hyperspectral imaging (ts-hsi) for determining water distribution within beef and spectral kinetic analysis during dehydration. Food Bioprocess Tech. 6, 2943–2958.

Paper III

Discrete and continuous spin-spin relaxation rate distributions derived from CPMG NMR response curves ─ a comparative analysis exemplified by water in meat

Eddy W. Hansen[1,*] & Han Zhu[1 - 3]

[1]Department of Chemistry, University of Oslo, P.O. BOX 1033, Blindern, N-0315 Oslo, Norway

[2]Department of Chemistry, Biotechnology and Food Science, Norwegian University of Life Sciences, P.O. Box 5003, 1432- Ås, Norway

[3]Nortura SA, Lørenveien 37, Økern, 0585 Oslo, Norway

Abstract

The spin-spin relaxation rate distribution of water in a porcine *longissimus dorsi* muscle was derived from an inverse integral transformation of the proton CPMG (Carr-Purcell-Meiboom-Gill) NMR signal at each hour during a 49 hours drip period. This "continuous (C)" relaxation rate distribution was found to be excellently represented by an empirical peak function, characterized by three parameters: a peak width, an average relaxation rate and a skewness parameter, which enables the distribution to be quantitatively defined. Also, the same CPMG response were fitted to a sum of 3 single exponential decay functions, denoted a "discrete (D)" relaxation rate model. The analysis shows that when the fraction of the slow relaxation component f_2^C from the continuous model is close to 5%, which is a rather typical value, the mean relaxation rate $\overline{R}_{22}^D$ from the discrete model becomes larger than the corresponding relaxation rate $\overline{R}_{22}^C$ from the continuous model by nearly 25% and f_2^D becomes larger than f_2^C by more than 75%. Likewise, when f_2^C approaches 2.5%, $\overline{R}_{22}^D$ becomes larger than $\overline{R}_{22}^C$ by more than 75% and f_2^D becomes larger than f_2^C by more than a factor of 3 which are supported by model simulations. The relative quality and goodness of the two different relaxation rate models are discussed. Finally, the number of transients needed to obtain a preset error in relaxation rate and/or mole fraction was determined by model simulation.

Key words: NMR; meat muscle; discrete relaxation rate model; continuous relaxation rate model, simulation

[*] Corresponding author. University of Oslo, P.O. BOX 1033, Blindern, N-0315 Oslo, Norway.
E-mail address: e.w.hansen@kjemi.uio.no
Telephone: +47-22855692

1. Introduction

Water is the most abundant (~75 %) and important structural compound in skeletal muscle and allows substrate and enzymes to diffuse and to interact. Also water controls the rigidity, plasticity and gelatinization of the insoluble proteins (myofibrillar, cytoskeletal and connective tissue) [1]. Not only the total amount of water, but also its mobility is crucial for meat quality. Water organized within different structures in meat show different mobility. As shown on Fig 1, the muscle is divided into bundles of perimysium, in which each bundle is made up of muscle fibers encased in endomysium. It is generally agreed that three forms of water exist in muscle: bound, immobilized and free water [2]. Bound water is attracted to polar or ionic groups of macromolecules like proteins and is reported to make up less than a tenth of the total myowater. Moreover, it is characerized by a reduced mobility and changes only slightly in post-rigor muscle [4]. Immobilized water resides within muscle structure (e.g. water held in myofiber by cell membrane) and bounds only partially to proteins [3-6]. Free water moves unimpeded and is held by weak intermolecular forces between the liquid and the surrounding matrix, e.g. between myofibers in the inter-fascicular space (interfascicular) or between the muscle bundles in the extra-fascicular space (extrafascicular) [7]. Water holding capacity (WHC) describes how post-rigor muscle binds water under specified conditions, and hence influences the quality and palatability of meat [8]. There is still a lack of complete understanding of WHC, however monitoring the water distribution and its mobility with time might offer additional explanation of the mechanisms of drip loss [9]. In this respect, NMR proton relaxometry has the ability to probe the mobility and distribution of water in different meat domains [9, 10] and has been suggested as a fast reference method to quantify WHC [11]. Importantly, if NMR is to be applied as a reference method for WHC, an accurate method to characterize the T_2 distribution must be chosen, especially regarding the long T_2 component (T_{22}).

All biological systems exhibit heterogeneity on certain length scales, thus a distribution of relaxation times is expected [12]. Many efforts have been put into the elucidation of spin-spin relaxation of water in tissue/muscle since the early 1970s [13]. Two different approaches of data fitting have been considered regarding T_2 relaxation of tissue/muscle water, a discrete- and a continuous model. The discrete model fits the CPMG response curve to a sum of exponential decaying functions (2 or 3, and was favored by most authors when first studying T_2 relaxation in muscle/meat [14-18]. Due to sample heterogeneities caused by distribution of pore shapes, pore sizes and surface relaxation sites, a three-component relaxation may only represent an approximation [12, 19]. To the best of knowledge, Lillford et al. were among the first to suggest that a continuous relaxation model gives a better characterization of the water relaxation in complex heterogeneous samples, such as muscle/meat [20]. Later, Kroeker and Henkelman [21] applied a continuous relaxation distribution model to describe the T_2 relaxation in mice leg tissue and identified two well separated distributions between 0 to 0.2 s.

Regarding relaxation in meat science, both models have been widely used, and the continuous model has been preferred in recent studies [18, 19, 22-32]. However, there are very few works comparing the two methods directly [12, 19]. Menon and Allen [12] applied nonlinear least squares techniques to spin-spin relaxation data on layered red blood cell ghosts as model sample. Both the nonlinear least squares technique and the nonnegative least square model gave an adequate fit from a goodness of fit point of view, but they failed to reveal the true distribution of relaxation times [12]. In another work, Bertram et al. measured T_2 relaxation on 74 porcine *longissimus dorsi* muscles, and found that the correlation between WHC (determined using Honikel bag method) and T_2 relaxation data was higher using the continuous model ($r = -0.85$) than the discrete model ($r = -0.77$, 2-exponential function) [19].

In this work, we present experimental and simulated CPMG data of water in meat with the objective to make a direct comparison between water relaxation rates and their corresponding mole fractions, as obtained by the discrete and the continuous relaxation model, respectively. The quality and the goodness of both models will be discussed.

2. Material and methods

2.1. Meat sample

Porcine *longissimus dorsi* muscle is among the most studied muscles regarding WHC, and was selected as the study material due to its lean (intramuscular fat content ~ 1%) and homogeneous appearance. Boars used in this study were young boars from Landrace and Duroc breed, tested as part of an on-going breeding program (Norsvin, Ilseng, Norway). The boars (~ 95 kg) were slaughtered at Nortura Rushøgda (Ringsaker, Norway) by carbon dioxide stunning (90%). Exsanguination, scaling and splitting were finished within 30 min post mortem. The carcasses were carried through a cooling tunnel (-22 °C, 8-10 m/s air velocity) after cleaning and evisceration, and were left at 15 °C for 5 min and chilled at 1-3 °C for 96 hours. The carcasses were then transported to a partial dissection line at Animalia (Oslo, Norway), and *longissimus dorsi* muscles were prepared. One *longissimus dorsi* muscle was randomly selected, from which one cylindrical plug (8 ϕ x 10 mm, ~0.5 g) was cored gently using a sharp cork borer. The sample was suspended with the fiber direction parallel to the cylindrical axis in an NMR glass tube. A gap of 17 mm was reserved between the muscle and the bottom of the NMR glass tube, for the drip fluid to flow/drip down to the bottom. A layer of parafilm was placed on top of the muscle to avoid water evaporation. The parafilm was found to not contribute to the NMR signal.

2.2. NMR measurements

The meat sample was placed within the homogeneous part of rf-coil of a 23 MHz Maran Ultra NMR instrument (Resonance Instruments, Witney, UK). The CPMG signal response was acquired using a 90˚ rf-pulse of 2.0 µs with 16K echoes and a time distance 2τ = 0.1 ms between successive 180˚ rf-pulses. The sample was stabilized at 25 ˚C for 10 min before measuring and the temperature was kept constant at 25 ˚C during the whole experiment, without changing the sample position. A CPMG relaxation response was acquired every hour for 49 hours.

2.3. Theoretical outline

The CPMG signal response was analyzed by two different approaches:

2.3.1 Continuous relaxation model (C)

A distributed exponential fitting on each acquired CPMG response, as characterized by an inherent signal-to-noise ratio equal to 350, was performed by the built-in Maran Ultra integral transform algorithm (RI Win-DXP software release version 1.2.3, Resonance Instruments, Witney, UK) to obtain a continuous $\log(T_2)$-relaxation time distribution $dI/d\log(T_2)$. The 16K data points (0.1 ms to 1600 ms) were pruned logarithmically to 256 points prior to analysis. The weight parameter λ was determined by an implemented noise estimation algorithm, resulting in $\lambda = 0.026$, a value which ensured a minimum broadening of the resulting line shape and avoided spurious peaks. Additional information regarding the numerical procedure is outlined in a paper published by Bertram et al. [19]. The $dI/d\log(T_2)$-distribution was

subsequently transformed into a spin-spin relaxation rate distribution $F(R_2)$ using the transformation (see Appendix 1 for further details):

$$F(R_2) = \frac{dI}{dR_2} = \frac{dI}{d(LogT_2)} \cdot \frac{d(LogT_2)}{dR_2} = -\frac{T_2}{\ln 10} \cdot \frac{dI}{d(LogT_2)} \qquad \text{with } R_2 = 1/T_2 \qquad (1)$$

The reason for using R_2 rather than T_2 is that it became possible to design an analytical equation in closed form which Laplace transform was calculated to yield an excellent approximation to the observed CPMG response function. This is of great advantage when performing model simulations, as the results become more reliable, robust and consistent since the numerical ill-posed problem of finding the Inverse Laplace transform is circumvented. This will become clearer later in section 4.1.

In principle, it is commonly accepted in meat science that the R_2-distribution of water in meat can be represented by a linear combination of three distinct and normalized relaxation distributions $F_0(R_2)$, $F_1(R_2)$ and $F_2(R_2)$:

$$\int_0^\infty F_i(R_2)dR_2 = 1 \qquad (2a)$$

which are associated with the fast-, the intermediate- and the slow relaxation components, respectively [33].
Hence, the overall relaxation distribution takes the form:

$$F(R_2) = \sum_{i=0}^{2} I_i^C F_i(R_2) \qquad (2b)$$

where I_i^C represents the signal intensity and $\overline{R}_{2i}^C$ represents the "mean" relaxation rate of component "i", i.e.:

$$\overline{R}_{2i}^C = \int_0^\infty R_2 F_i(R_2)dR_2 \Big/ \int_0^\infty F_i(R_2)dR_2 \qquad (2c)$$

The three relaxation distribution components reflect the bound-, immobilized- and free water, respectively. Alternatively, we may introduce the mole fraction f_i^C of (water) protons in domain "i", as defined by:

$$f_i^C = \frac{\int_0^\infty F_i(R_2)dR_2}{\int_0^\infty F(R_2)dR_2} = \frac{I_i}{\sum_{i=0}^{2} I_i} \qquad (2b)$$

where $\overline{R}_{20}^C > \overline{R}_{21}^C > \overline{R}_{22}^C$.

2.3.2. Discrete relaxation model (D)

The discrete relaxation rate model D is defined by a sum of three simple exponential functions:

$$I_{CPMG}(t) = \sum_{i=0}^{2} I_i^D \cdot \exp\left[-\overline{R}_{2i}^D t\right] \quad (3)$$

Where I_i^D and $\overline{R}_{2i}^D$ represent the signal intensity and the mean relaxation rate of component i, respectively. These parameters are obtained by fitting Eq 3 to the CPMG signal response using Origin 9.0 (OriginLab Corporation, MA, USA) and will be discussed in the next section.

3. Results and discussion

3.1. Continuous relaxation model (C)

The overall relaxation rate distribution $F(R_2)$ was obtained by an inverse integral transformation of the CPMG responses $I_{CPMG}(t)$, as commented on in section 2.3.1, and is plotted in Fig 2. Not surprisingly, the error is small and randomly distributed along the R_2-axis (not shown) as expected due to the inherent constraints involved in the integral transform technique. The signal intensity I_0^C of the fast relaxing component $F_0(R_2)$ with R_2 > 300 s^{-1} was – within experimental error – found to be constant and independent on (drip) time. The results displayed in Fig 2 show that all three relaxation rate distributions are skewed and hence asymmetric.

3.2 Discrete relaxation model (D)

Excellent fits of Eq 3 to the observed CPMG responses in Fig 2 were achieved on all 49 relaxation curves, as illustrated by three examples of CPMG curves acquired at 5, 25 and 45 hours on drip, respectively (Fig 3). The residuals were small and randomly distributed except for a slight effect of non-randomness in the early part of the CPMG curve. This is not too surprising as the initial part includes the fast relaxation component, which surely deviates from a pure exponential decay as its inverse Laplace transform $F_0(R_2)$ is represented by a rather complex shape, as noticed in Fig 2a. The discrete model analysis (Eq 3) also revealed a constant intensity I_0^D of the fast relaxing component. Hence, both models revealed a constant amount of strongly bound water which was independent on drip time, although the discrete model predicts a somewhat larger amount compared to the continuous model, by about 23($\pm$8) %. The fast relaxing component is claimed not to contribute to drip loss (WHC) [34] and is consistent with the results presented in Fig. 4d, although an exchange of water molecules between domains can't be ignored. Of more concern, however, is their difference in relaxation rate with time (Fig. 4a), which affects the physical interpretation of the relaxation data. That is, the continuous model predicts an increasing molecular motional constraint of the bound water whereas the discrete model does not reveal any such change with time.

Corresponding differences in signal intensity and relaxation rate versus time between the two other components, as obtained by the two different models are displayed in Figs 4b/e and 4c/f and clearly confirm the inconsistency between the two relaxation models. In particular, the fast relaxing component $F_0(R_2)$ reveals a more complex distribution shape as compared to the two slower relaxing components $F_1(R_2)$ and $F_2(R_2)$.

Plotting f_i^D / f_i^C and $\bar{R}_{2i}^D / \bar{R}_{2i}^C$ against f_2^C (for i = 1 and 2) eliminates the time parameter, as shown in Fig 5. The important and general conclusion to be drawn from Fig 5 is that both ratios f_i^D / f_i^C and $\bar{R}_{2i}^D / \bar{R}_{2i}^C$ increase with decreasing f_2^C, and reflect the inconsistency between the two model approaches C and D. Also, different ratios of f_i^D / f_i^C and $\bar{R}_{2i}^D / \bar{R}_{2i}^C$ appears for the same f_2^C which - at first glance – seems remarkable. However, as will be seen in the next section these observations can be rationalized from model calculations on simplified "two-component"-systems.

4. Simulation and modelling

4.1 Relaxation distribution and corresponding CPMG response functions

The analytical representation (or formula) of the relaxation rate distribution $F_i(R_2)$ for i equal 1 or 2 is – *a priori* – unknown. However, by trial and error we found a simple and normalized three parameter function (Eq 4) to provide an excellent representation of all the relaxation rate distribution components $F_i(R_2)$ displayed in Fig 2 (using a non-linear least squares fit technique).

$$F(R_2) = \frac{K^2\Delta^2 + \pi^2}{\pi\Delta\left[1+\exp(-K\Delta)\right]} Sin(\pi \frac{R_2 - R_{2a}}{\Delta}) \cdot Exp\left[-K(R_2 - R_{2a})\right] \qquad (4)$$

with:

$$\Delta = R_{2b} - R_{2a} \ (R_{2a} \le R_2 \le R_{2b}) \text{ and } \int_0^\infty F(R_2)dR_2 = \int_{R_{2a}}^{R_{2b}} F(R_2)dR_2 = 1.$$

The three parameters K, R_{2a} and Δ represent adjustable parameters which uniquely define the relaxation rate distribution $F(R_2)$. Note, the function attains the value 0 for $R_2 < R_{2a}$ and for $R_2 > R_{2b}$.

The model-fitting of Eq 4 to the observed relaxation distributions are illustrated in Fig 6 for three different relaxation distributions acquired at 1, 25 and 49 hours of drip (Fig 2). Actually, the first (5 hours drip) and final (49 hours drip) distributions represent extreme relaxation behaviors while the relaxation rate distribution derived after 25 hours of drip represents some "intermediate" relaxation behavior. Furtermore, the distribution function (Eq 4) was successfully tested on approximately 100 different relaxation distributions of water in meat, acquired previously in this lab.

Hence, any relaxation distribution component $F_i(R_2)$ with i = 1 or 2 (Fig 2) is uniquely represented by Eq 4, which comprises three independent parameters: *K*, R_{2a} and Δ. The distribution parameters obtained for the three distributions are summarized in Table 1.

Table 1. Relaxation distribution parameters K, R_{2a} and Δ of $F_1(R_2)$ and $F_2(R_2)$, as derived by fitting Eq 4 to the "observed" distributions presented in Fig 6. The alternative distribution

characteristics: mean relaxation rate $\overline{R}_2^C$ (Eq 6a), distribution width *w* (Eq 7) and skewness *s* (Eq 8a) are shown, as well.

$F(R_2)$-parameters	Time on drip experiment		
	1 h	25 h	49 h
$K_1//K_2$ (s)	0.457//0.075	0.352//0.0643	0.316//0.0585
$R_{2a1}//R_{2a2}$ (s^{-1})	3.85//6.88	3.84//6.52	3.81//7.19
$\Delta_1//\Delta_2$ (s^{-1})	3.03//30.3	2.69//33.3	3.37//52.5
f_2^C (%)	4.0	3.4	5.1
$\overline{R}_{21}^C//\overline{R}_{22}^C$ (s^{-1})	5.17//23.7	5.07//27.7	5.33//38.8
$w_1//w_2$ (s^{-1})	1.83//16.3	1.71//18.2	2.12//25.4
$s_1//s_2$	0.129//0.296	0.065//0.269	0.081//0.462

Of particular importance, the CPMG signal response R(t) is nothing but the Laplace Transform (LT) of Eq 4, hence:

$$\begin{aligned} R(t) &= I_1^C \int_0^\infty F_1(R_2)\cdot\exp(-R_2 t)dR_2 + I_2^C \int_0^\infty F_2(R_2)\cdot\exp(-R_2 t)dR_2 \\ &= I_1^C \int_{R_{2a1}}^{R_{2b1}} F_1(R_2)\cdot\exp(-R_2 t)dR_2 + I_2^C \int_{R_{2a2}}^{R_{2b2}} F_2(R_2)\cdot\exp(-R_2 t)dR_2 \end{aligned} \quad (5a)$$

in which each integral term in Eq 5a takes the form:

$$\begin{aligned} &\int_{R_{2ai}}^{R_{2bi}} F_i(R_2)\cdot\exp(-R_2 t)dR_2 \\ &= \frac{K_i^2\Delta_i^2+\pi^2}{(K_i+t)^2\Delta_i^2+\pi^2}\cdot\frac{\exp[-(\Delta_i+R_{2ai})\cdot(K_i+t)]+\exp[-R_{2ai}(K_i+t)]}{\exp[-(\Delta_i+R_{2ai})\cdot K_i]+\exp[-R_{2ai}\cdot K_i]} \end{aligned} \quad (5b)$$

Thus, knowing the two sets of distribution characteristics K_i, R_{2ai} and Δ_i (i = 1 and 2), the exact CPMG response function R(t) of a two-component system can be expressed analytically in closed form (Eqs 5a and 5b) and enables the numerically ill-posed ILT operation to be by-passed and facilitates a more reliable, robust and effective way of comparing the continuous (C) and the discrete (D) model approaches by simulation. This will be discussed in the next section.

4.2 Two-component simulation

Since the $F_0(R_2)$-distribution is rather complex (Fig 2), its LT cannot be represented by a simple analytical formula. However, we may still obtain relevant information about the three-component system by performing two-component simulations. If denoting the two component system by the index II and the three-component system by the index III we can show that the mole fraction $(f_2^C)_{III} \approx 0.094(f_2^C)_{II}$, $(f_1^C/f_1^D)_{III} \approx (f_1^C/f_1^D)_{II}$ and $(f_2^D/f_2^C)_{III} \approx (f_2^D/f_2^C)_{II}$. This is elaborated on in Appendix II. Importantly, this approach is further justified by the fact that the relaxation distribution $F_0(R_2)$ is well separated by the distributions $F_1(R_2)$ and $F_1(R_2)$ as reflected by their very different mean relaxation rates: $\overline{R}_{20}^C >> \overline{R}_{21}^C > \overline{R}_{22}^C$.

Hence by presetting the mole fraction f_2^C (and $f_2^C = 1 - f_1^C$) and the parameters K_i, R_{2ai} and Δ_i (i = 1 and 2) not only the overall relaxation rate distribution (Eqs 2b and 4) is specified, but also the CPMG response function *R(t)* of the two-component system is uniquely defined (Eqs 5a and 5b). A short procedure for how to generate a synthetic CPMG response $R_{SYN}(t)$ is summarized below:

- Choose K_i, R_{2ai} and Δ_i (with i = 1 and 2), which uniquely define the relaxation distributions $F_1(R_2)$ and $F_2(R_2)$ via Eq 5b.
- Select a value f_2^C
- Calculate the mean relaxation rates $\overline{R}_{21}^C$ and $\overline{R}_{22}^C$ from Eq 2c.
- Calculate $I_{CPMG}(t)$ by combing Eqs 5a and 5b, i.e.:

$$I_{CPMG}(t) = (1 - f_2^C)\frac{K_1^2\Delta_1^2 + \pi^2}{(K_1 + t)^2\Delta_1^2 + \pi^2} \cdot \frac{\exp[-(\Delta_1 + R_{2a1}) \cdot (K_1 + t)] + \exp[-R_{2a1}(K_1 + t)]}{\exp[-(R_{2a1} + \Delta_1) \cdot K_i] + \exp[-R_{2a1} \cdot K_1]}$$

$$+ f_2^C \frac{K_2^2\Delta_2^2 + \pi^2}{(K_2 + t)^2\Delta_2^2 + \pi^2} \cdot \frac{\exp[-(\Delta_2 + R_{2a2}) \cdot (K_2 + t)] + \exp[-R_{2a2}(K_2 + t)]}{\exp[-(R_{2a2} + \Delta_2) \cdot K_2] + \exp[-R_{2a2} \cdot K_2]}$$

- Generate a synthetic CPMG response $I_{SYN}(t)$ by adding random-noise ε(t) to $I_{CPMG}(t)$:

$$I_{SYN}(t) = I_{CPMG}(t) + \varepsilon(t)$$

- Fit equation: $I_{CPMG}(t) = (1 - f_2^D) \cdot \exp\left[-\overline{R}_{21}^D t\right] + f_2^D \cdot \exp\left[-\overline{R}_{22}^D t\right]$ to the synthetically generated response data $I_{SYN}(t)$ to determine f_2^D, $\overline{R}_{21}^D$ and $\overline{R}_{22}^D$
- Plot f_i^D / f_i^C and $\overline{R}_{2i}^D / \overline{R}_{2i}^C$ against f_2^C and repeat the procedure if necessary.

The results of the simulation outlined above are summarized by the continuous curves in Fig 5 and confirm the general trend that the difference in intensities and mean relaxation rates, as obtained by the two models C and D, increase with decreasing f_2^C. In particular, rather different biophysical interpretations of the two data sets (C and D) may appear regarding the change in water distribution and their corresponding molecular dynamic characteristics with time which are of significance in understanding the WHC. Bertram et al. [19] has suggested that such a difference exist, by correlating T_2 relaxation time constants and their intensities (calculated by continuous or discrete model) to WHC reference values (determined using Honikel bag method). Importantly, the data presented in Fig 5 reconfirmed such a significant difference. For instance, for f_2^C ~ 5%, which is a rather typical value, $\overline{R}_{22}^D$ becomes larger than $\overline{R}_{22}^C$ by nearly 25% and f_2^D becomes larger than f_2^C by more than 75%. Likewise, when f_2^C approaches 2.5%, $\overline{R}_{22}^D$ becomes larger than $\overline{R}_{22}^C$ by more than 75% and f_2^D becomes larger than f_2^C by more than a factor of 3.

In principle, the three parameters *K*, R_{2a} and Δ (or alternatively: the mean relaxation rate $\overline{R}_2^C$ (Eq 6a), the distribution width *w* (Eq 7) and the skewness *s* (Eq 8a)) together with f_2^C should be varied systematically in order to fully evaluate the relative impact of these parameters on $\overline{R}_{21}^D$, $\overline{R}_{22}^D$ and the mole fraction f_2^D (and f_1^D). Such a detailing is, however, outside the scope of the present work. Nevertheless, as discussed above, some information on this important topic was obtained by generating synthetic CPMG responses from the three "extreme" sets of relaxation parameters (Table 1) and varying only the mole fraction f_2^C followed by fitting the discrete two-component relaxation model to these synthetically generated CPMG data (Fig 5).

4.3. Interlude - alternative distribution characteristics

Since K, R_{2a} and Δ in Eq 4 are not very informative distribution parameters, we prefer to replace these parameters by the mean relaxation rate $\overline{R}_2^C$ (Eq 2c), the full width *w* at half maximum height (FWHM), and the skewness factor *s*. By some simple but tedious algebra the mean spin-spin relaxation time $\overline{R}_2^C$ of the distribution can be derived and reads:

$$\overline{R}_2^C = \int_{R_{2a}}^{R_{2b}} R_2 F(R_2) dR_2 \Big/ \int_{R_{2a}}^{R_{2b}} F(R_2) dR_2 = R_{2a} + \Delta \cdot \left[\frac{1}{1+\exp(\alpha)} + \frac{2\alpha}{\alpha^2 + \pi^2} \right] \tag{6a}$$

Where α = K· Δ. Likewise, the relaxation rate R_{2m} defining the relaxation rate at the maximum signal height $F(R_{2m})$ can be easily derived:

$$R_{2m} = R_{2a} + \frac{\Delta}{\pi} A\tan\left[\frac{\pi}{\alpha}\right] \tag{6b}$$

Also, the full width at half maximum height *w* or FWHM can be calculated by solving Eq 6c numerically.

$$F(R_2) = \frac{1}{2} F(R_{2m}) \tag{6c}$$

which results in;

$$w = \Delta \left[\frac{a}{1 + b \cdot \alpha^2} + \frac{c}{1 + d \cdot \alpha} \right] \tag{7}$$

The results are illustrated in Fig 7 showing that *w* (□) can be well approximated by an empirical formula depending solely on K and Δ, with α = K· Δ and *a* = 0.2966, *b* = 0.1194, *c* = 0.3768 and *d* = $2.956 \cdot 10^{-2}$. The maximum relative error in *w* (Eq 7) was found to be less than 2%.

Likewise, the skewness parameter of the distribution function F, as defined by the skewness *s* reads:

$$s = \frac{\sum_{i=1}^{N} (F_i - \overline{F})^3 / N}{\left[\sum_{i=1}^{N} (F_i - \overline{F}) / (N-1) \right]^{3/2}} \tag{8a}$$

where $\overline{F}$ represents the mean value of all F_i's, as calculated from Eq 8b (a modified and simplified version of Eq 4) with i = 1 K data points and equally spaced relaxation rates u_i and 40 randomly chosen pairs of (Δ, α)-points.

$$F_i = \frac{\alpha^2 + \pi^2}{\pi \cdot \Delta[1 + \exp(-\alpha)]} Sin(\pi \cdot u_i) \cdot \exp[-\alpha u_i] \quad (8b)$$

The results are illustrated in Fig 7 where the skewness s (■) is well approximated by an empirical formula of the form:

$$s = \frac{1}{a\alpha^{-q} + b\alpha^{-r}} \quad (8c)$$

With α = K· Δ and a = 12.48, q = 2.018, b = 1.499 and r = 0.486 and the maximum relative error in s becomes less than 3.0%, showing that the skewness can be reliably estimated from the parameter α alone.

4.4. Error analysis

In the final section we will address the question regarding the relative error in the derived ratios $\overline{R}_{22}^{D} / \overline{R}_{22}^{C}$, $\overline{R}_{21}^{D} / \overline{R}_{21}^{C}$ and f_2^D / f_2^C. In particular, how to improve the data quality by minimizing the relative error in derived NMR parameters (by increasing the number of transients). The signal-to-noise ratio (S/N) of the CPMG response on current NMR instrument is 350 with N_1 = 64 transients. By changing the number of transient from N_1 to N_2, the S/N-ratio would change to $350\sqrt{N_2/N_1}$. Hence, we modified the random error, or noise term ε in section 4.2 accordingly, before generating synthetic CPMG data. We then selected a set of distribution parameters K, R_{2a} and Δ (which were identical to those found at 25 hours of drip: Table 1), which represent a rather typical or "average" set of parameters.

By performing a series of Monte Carlo simulations we enabled to estimate the standard error in $\overline{R}_{21}^{D} / \overline{R}_{21}^{C}$, $\overline{R}_{22}^{D} / \overline{R}_{22}^{C}$ and f_2^D / f_2^C as a function of f_2^C for three different sets of transients: 16, 64 and 256 respectively. The results are summarized in Fig 8 and show that the relative standard errors $\sigma(f_2^D / f_2^C)$, $\sigma(\overline{R}_{21}^{D} / \overline{R}_{21}^{C})$ and $\sigma(\overline{R}_{22}^{D} / \overline{R}_{22}^{C})$ all follow a master curve of the form:

$$\sigma\left(\frac{f_2^D}{f_2^C}\right) = k\frac{1}{\sqrt{N}}\left(\frac{1}{f_2^C}\right)^{0.78},\ \sigma\left(\frac{\overline{R}_{21}^{D}}{\overline{R}_{21}^{C}}\right) = k'\frac{1}{\sqrt{N}}\left(\frac{1}{f_2^C}\right)^{0.18} \text{ and } \sigma\left(\frac{\overline{R}_{22}^{D}}{\overline{R}_{22}^{C}}\right) = k''\frac{1}{\sqrt{N}}\left(\frac{1}{f_2^C}\right)^{0.95}$$

where k, k' and k" are constants. The standard error in all three parameters decreases with the square-root of the number of transients N, which is not unexpected. However, the same standard error is strongly dependent on the fraction f_2^C of the slower relaxation rate and decreases with increasing f_2^C. Interestingly, the present simulation study shows that the standard error in the above parameters can be preset by adjusting the number of transients (for fixed f_2^C).

5. Conclusions

Since meat is a truly heterogeneous material composed of a distribution of both pore shapes, pore sizes and surface relaxation sites of different types (and strengths), it is reasonable to

353 expect the spin-spin relaxation rate of the confined water to be described by a broad range of
354 relaxation times (the continuous model), as confirmed by the study presented in this work and
355 in numerous other publications. Generally, two or three distinct and individual water
356 relaxation distributions can be assigned for any meat sample.

357 Moreover, a generalized, empirical peak function was designed which fitted excellently to the
358 relaxation rate distributions derived by an inverse integral transformation of the experimental
359 CPMG response curve (on a porcine *longissmus dorsi* muscle) acquired in this work. In
360 particular, this approach enables a more quantitative assessment of the relaxation distribution
361 to be made, which involves three independent parameters: mean relaxation rate, full width at
362 half height (FWHM) and the skewness (or asymmetry) of the distribution.

363 The same CPMG response curves could equally well be represented by a sum of three single
364 exponential decay-functions (the discrete model), characterized by the same number of
365 distinct relaxation components as found by the inverse integral transform. However, a
366 comparison between the relaxation rates and their corresponding mole fraction derived from
367 the two different models revealed significant differences. For instance, when the mount f_2^C of
368 the slower relaxation component $\overline{R}_2^C$ decreased from about 10 to 2.5%, the intensity ratio
369 (f_2^D / f_2^C) increased from 1.25 to about 3 and the relaxation rate ratio $\overline{R}_{22}^D / \overline{R}_{22}^C$ increased
370 from 1.1 to about 1.6. Only the relaxation rate ratio $\overline{R}_{21}^D / \overline{R}_{21}^C$ was found to increase only
371 slightly from 1.0 to about 1.1 and was supported by model calculations from synthetic CPMG
372 response data. As a consequence, the two different relaxation models may result in
373 significantly different biophysical and biochemical interpretations of the NMR data, a result
374 which is of utmost importance. By simulation it was demonstrated that also the shape (width
375 and skewness) of the continuous relaxation distribution may have a substantial impact on the
376 NMR properties of the three relaxation components, Finally, the relative error in $\overline{R}_{2i}$ and f_i
377 was found to depend strongly on the signal-to-noise (S/N) ratio of the CPMG response data.
378 Based on simulated or synthetic CPMG response data, the number of transients needed to
379 obtain a preset error in $\overline{R}_{2i}$ and f_i was determined and is discussed.

380 **Acknowledgement**

381 We want to thank the Research Council of Norway for financial support through the project
382 “On line determination of water retaining ability in pork muscle”, project number 229192.

383

384 **Appendix I**

385 The procedure applied to calculate the R_2-distribution dI/dR_2 from the $\log T_2$-distribution
386 $dI/d\log T_2$ is as follows:

387 We first calculate two “support” parameters T and N as defined by:

$$T = \int R_2 \frac{dI}{dR_2} dR_2 = \int R_2 \frac{dI}{d\log T_2} \frac{d\log T_2}{dR_2} dR_2$$

388 $$= \int (1/T_2) \frac{dI}{d\log T_2} d\log T_2 \qquad \text{A1.1}$$

$$\approx \Delta(\log T_2) \sum \frac{1}{T_{2i}} \left(\frac{dI}{d\log T2}\right)_i$$

and:

$$N = \int \frac{dI}{dR_2} dR_2 = \int \frac{dI}{d\log T_2} \frac{d\log T_2}{dR_2} dR_2$$
$$= \int \frac{dI}{d\log T_2} d\log T_2 \qquad \text{A1.2}$$
$$\approx \Delta(\log T_2) \sum (dI / d\log T_2)_i$$

Hence:

$$< R_2 >= \overline{R}_2 = \frac{\int R_2 \cdot (dI / dR_2) dR_2}{\int (dI / dR_2) dR_2} = \frac{T}{N} \qquad \text{A1.3}$$

and:

$$F(R_2) = \frac{dI}{dR_2} = \frac{dI}{d\log T_2} \frac{d\log T_2}{dR_2} = -\frac{1}{\ln 10} \frac{dI}{d\log T_2} \frac{d\ln T_2}{dR_2} =$$
$$= -\frac{1}{\ln 10} \frac{dI}{d\log T_2} \frac{d\ln R_2}{dR_2} = -\frac{1}{R_2 \cdot \ln 10} \frac{dI}{d\log T_2} \qquad \text{A1.4}$$
$$= -\frac{T_2}{\ln 10} \frac{dI}{d\log T_2}$$

Appendix II

The relation between intensities of a two-component (II) system and a three-component (III) system.

We start with writing down the mole-fraction of a two-component system (II):

$$(f_i^X)_{II} = \frac{I_i^X}{I_1^X + I_2^X} = \frac{I_i^X}{I_1^X + I_2^X} \cdot \frac{1 + I_0^X / (I_1^X + I_2^X)}{1 + I_0^X / (I_1^X + I_2^X)}$$
$$= \frac{I_i^X}{I_1^X + I_2^X + I_0^X} \cdot \left[1 + \frac{I_0^X}{I_1^X + I_2^X} \right] = (f_i^X)_{III} \left[1 + \frac{I_0^X}{I_1^X + I_2^X} \right] \qquad \text{A2.1}$$

where X = C (continuous model) or D (discrete model). Since the total intensity $I_T = I_1^X + I_2^X + I_0^X$, the above equation can be rearranged to read:

$$(f_i^X)_{II} = (f_i^X)_{III} \left[1 + \frac{I_0^X}{I_T - I_0^X} \right] \qquad \text{A2.2}$$

For a normalized signal intensity (I_T = 1) we have observed that both I_0^C and I_0^D are constants and equal to $I_0^C = 0.062 \pm 0.003$ and $I_0^D = 0.074 \pm 0.009$, respectively. Inserting these numbers into the above equations we obtain:

409 $(f_2^C)_{II} = 1.06 \cdot (f_2^C)_{III}$ (A2.3)

410 and:

411 $(f_i^D / f_i^C)_{II} = 1.012 \cdot (f_i^D / f_i^C)_{III} \approx (f_i^D / f_i^C)_{III}$ A2.3

412

413 **References**

414 1. J.M. Hughes, S.K. Oiseth, P.P. Purslow, R.D. Warner, Meat Sci 98, 520 (2014)
415 2. B.M. Abdullah, J.D. Cullen, O. Korostynska, A. Mason, A.I. Al-Shamma'a, in
416 Sensing Technology: Current Status and Future Trends I, ed. By A. Mason, S.C.
417 Mukhopadhyay, K.P. Jayasundera, N. Bhattacharyya (Springer International
418 Publishing, 2014), p. 117
419 3. M. Aubin, R.E. Prud'Homme, M. Pézolet, J.-P. Caillé, BBA-Gen Subjects, 631, 90
420 (1980)
421 4. E. Huff-Lonergan, S.M. Lonergan, Meat Sci, 71, 194 (2005)
422 5. E. Huff-Lonergan, Water-Holding Capacity of Fresh Meat. 2002, Fact sheet (04669),
423 National Pork Board: Des Moines, IA.
424 6. W.D. Powrie, M.A. Tung, in Water Relations of Foods, ed. By R.B. Duckworth
425 (Academic Press, 1975), p. 249
426 7. K.L. Pearce, K. Rosenvold, H.J. Andersen, D.L. Hopkins, Meat Sci, 89, 111 (2011)
427 8. B.C. Kim, R.G. Kauffman, J.M. Norman, S.T. Joo, Meat Sci 39, 363 (1995)
428 9. H.C. Bertram, H.J. Andersen, A.H. Karlsson, Meat Sci 57, 125 (2001)
429 10. E. Tornberg, M. Wahlgren, J. Brøndum, S.B. Engelsen, Food Chem 69, 407 (2000)
430 11. H. Zhu, M. O'Farrell, G. Bouquet, K. Lunde, B. Egelandsdal, O. Alvseike, P. Berg, E.
431 Gjerlaug-Enger, E.W. Hansen, J Food Eng 175, 51 (2016)
432 12. R.S. Menon, P.S. Allen, Magn Reson Med, 20, 214 (1991)
433 13. E. Tornberg, in International Congress of Meat Sci and Technology. 2001. Kraków,
434 Poland: Meat and Fat Research Institute.
435 14. P.S. Belton, R.R. Jackson, K.J. Packer, BBA , 286, 16 (1972)
436 15. P.S. Belton, K.J. Packer, BBA, 354, 305 (1974)
437 16. E.E. Burnell, M.E. Clark, J.A. Hinke, N.R. Chapman, Biophys. J. 33, 1 (1981)
438 17. C.F. Hazlewood, D.C. Chang, B.L. Nichols, D.E. Woessner, Biophys. J. 14, 583
439 (1974)
440 18. J.P. Renou, G. Monin, P. Sellier, Meat Sci 15, 225 (1985)
441 19. H.C. Bertram, S. Dønstrup, A.H. Karlsson, H.J. Andersen, Meat Sci 60, 279 (2002)
442 20. P.J. Lillford, A.H. Clark, D.V. Jones, in Water in Polymers, ed. By S.P. Rowland
443 (American Chemical Society, Washington, D.C. 1980), p. 177
444 21. R.M. Kroeker, R. M. Henkelman, J Magn Reson (1969), 69, 218 (1986)
445 22. H.C. Bertram, A.H. Karlsson, M. Rasmussen, O.D. Pedersen, S. Donstrup, H.J.
446 Andersen, J Agric Food Chem, 49, 3092 (2001)
447 23. H.C. Bertram, P.P. Purslow, H.J. Andersen, J Agric Food Chem, 50, 824 (2002)
448 24. H.C. Bertram, A.K. Whittaker, H.J. Andersen, A.H. Karlsson, J Agric Food Chem, 51,
449 4072 (2003)
450 25. C. Li, D. Liu, G. Zhou, X. Xu, J. Qi, P. Shi, T. Xia, Meat Sci, 92, 79 (2012)
451 26. C.K. McDonnell, P. Allen, E. Duggan, J.M. Arimi, E. Casey, G. Duane, J.G. Lyng,
452 Meat Sci, 95, 51 (2013)
453 27. E. Micklander, H.C. Bertram, H. Marnø, L.S. Bak, H.J. Andersen, S. B. Engelsen, L.
454 Nørgaard, LWT - Food Sci Technol 38, 437 (2005)

28. E. Micklander, B. Peshlov, P.P. Purslow, S.B. Engelsen, Trends Food Sci Tech 13, 341 (2002)
29. J.P. Renou, J. Kopp, P. Gatellier, G. Monin, G. Kozak-Reiss, Meat Sci, 26, 101 (1989)
30. G. Sørland, P. Larsen, F. Lundby, A. Rudi, T. Guiheneuf, Meat Sci, 66, 543 (2004)
31. I.K. Straadt, M.D. Aaslyng, H.C. Bertram, Magn Reson Chem, 49, S71 (2011)
32. I.K. Straadt, M. Rasmussen, H.J. Andersen, H.C. Bertram, Meat Sci, 75, 687 (2007)
33. H.C. Bertram, H.J. Andersen, Annu Rep NMR Spectro, 53, 157 (2004)
34. E.W. Hansen, H. Zhu, IJRRAS, 23, 207 (2015).

Figure captions

Figure 1. Schematic representation of the skeletal muscle organization.

Figure 2. a) Observed CPMG response curve and b) relaxation rate distribution $F(R_2)$ of water in meat as a function of drip time. The relaxation rate distribution was derived by an inverse integral transformation of the observed CPMG response curve using the "built-in" software package on the Maran NMR instrument to derive the dI/dlogT_2-distributon. By applying Eq 1, the R_2-distribution $F(R_2) = dI/dR_2$ was obtained (see Appendix I). The intensity of the fast R_2-distribution component $F_0(R_2)$ with $R_2 > 300$ s^{-1} was multiplied by a factor of 100 for clarity. The figures are shown in a color scale from the start of experiment (blue) towards the end of the experiment (red).

Figure 3. CPMG relaxation curves acquired after drip times 5 hours (a-b), 25 hours (d-e) and 45 hours (g-h), respectively. Original data are shown in black squares (□), circles (○) and triangles (Δ) on each plot. The red curves represent model fits to Eq 3. Relaxation curves are presented both on a linear scale (top) and a logarithmic scale (middle). The residual plots (the difference between observed and model calculated intensities) are shown in the bottom part (c – i).

Figure 4. Intensity I_i^X and mean relaxation rate $\overline{R}_{2i}^X$ (i = 0, 1 and 2) in meat as a function of drip time as derived from two different model approaches, the continuous model (X = C: □) and the discrete model (X = D: ■). See text for further details.

Figure 5. Experimental (■) and model calculated (dotted curved lines) ratios f_i^D / f_i^C and $\overline{R}_{2i}^D / \overline{R}_{2i}^C$ against f_2^C for i = 1 and 2. The superscripts "C" and "D" represent the continuous and discrete model approaches, respectively. The continuous curves were obtained by model calculations (see section 4.2).

Figure 6. The "Observed" (dots) two-component relaxation rate distribution $F(R_2)$ (= $\sum_{i=1}^{2} F_{2i}^C$) as obtained by an integral transformation of the CPMG response curve R(t) of water in meat at three different times (1 hour (●), 25 hours (○) and 49 hours (□)) during drip. The solid curves were calculated by non-linear least squares fits of Eq 4. An extended view of the slow relaxation component R_{22}^C (see Figure 2b) is plotted in Figure 4b.

Figure 7. Full width w at half maximum height (FWHM) and the skewness s of the normalized distribution function (Eq 4) as a function of α (= K· Δ).

Figure 8. Standard error in the ratios $\overline{R}_{22}^D / \overline{R}_{22}^C$, $\overline{R}_{21}^D / \overline{R}_{21}^C$ and f_2^D / f_2^C as a function of f_2^C for three different number of transients N (= 16, 64 and 256) respectively, as determined by simulation (sections 4.2 – 4.4) .

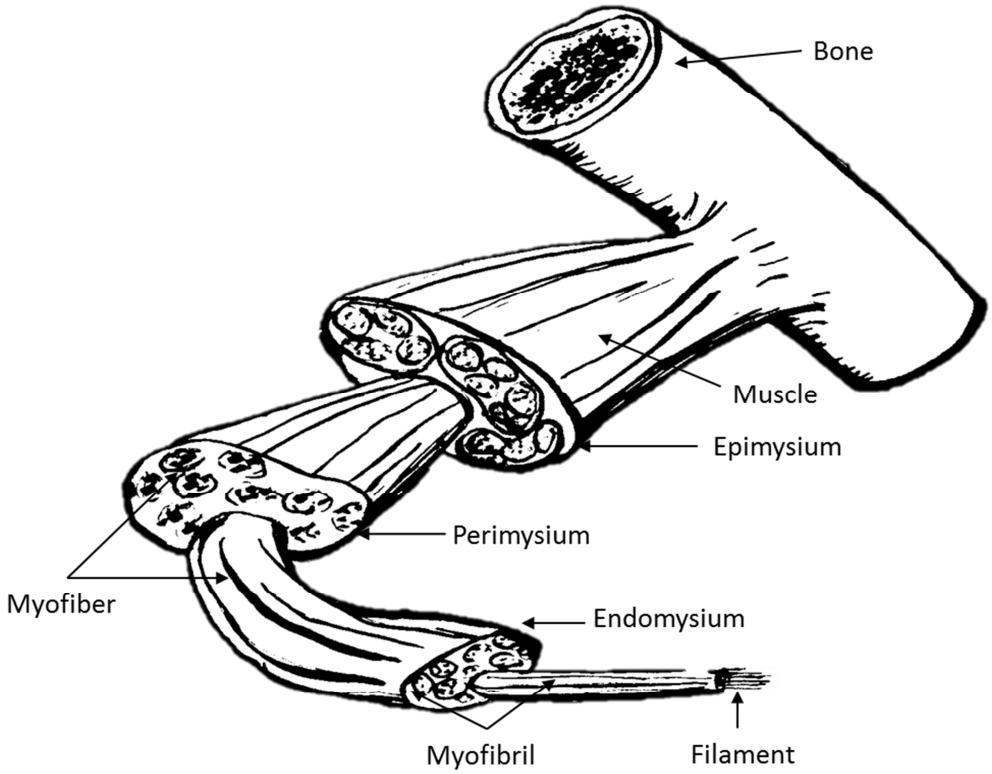

501

502 Figure 1

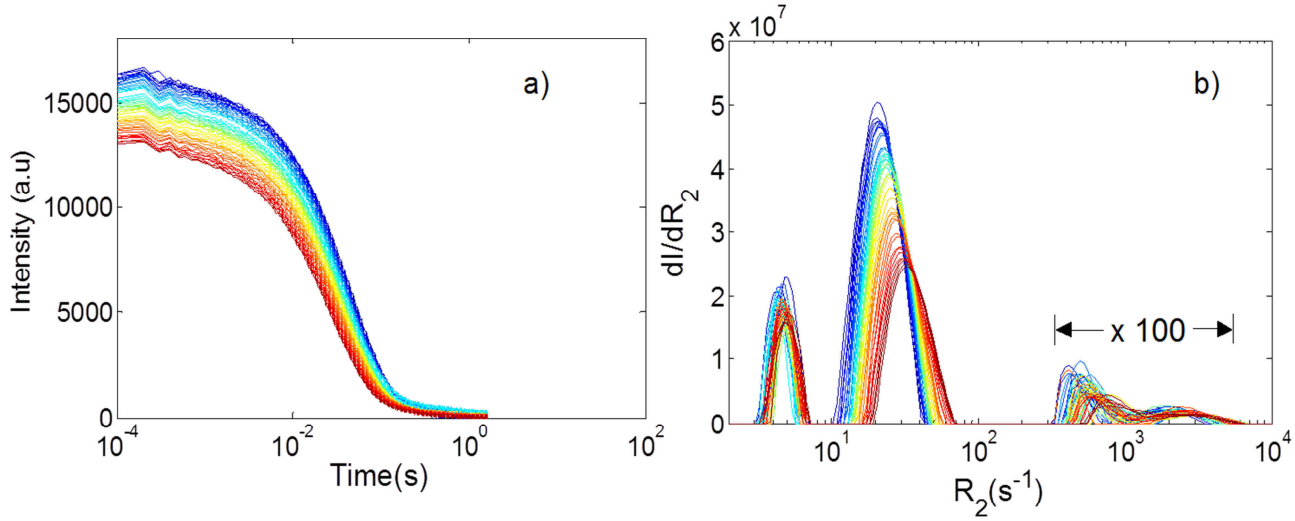

503

504 Figure 2

505

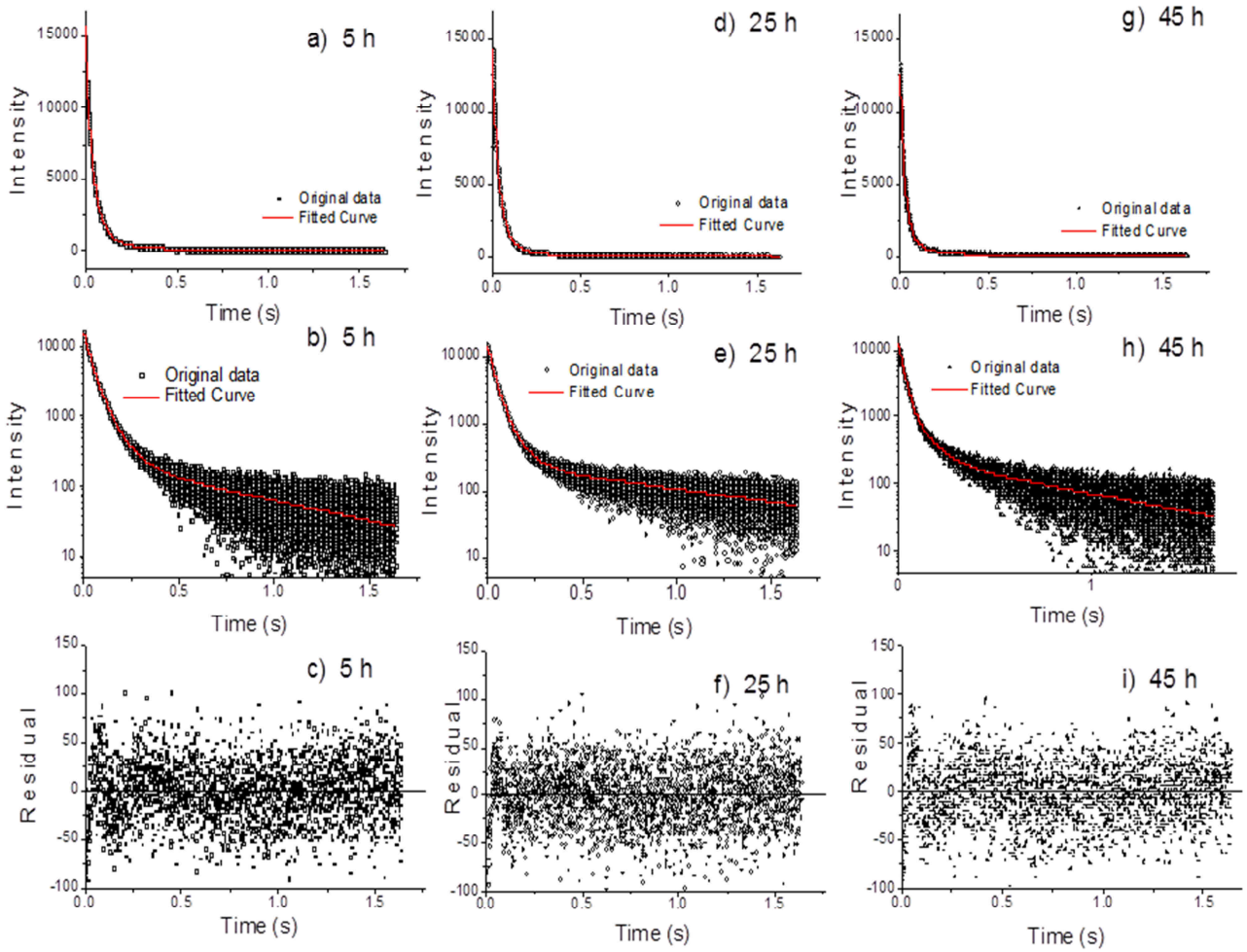

506
507 Figure 3

508

509

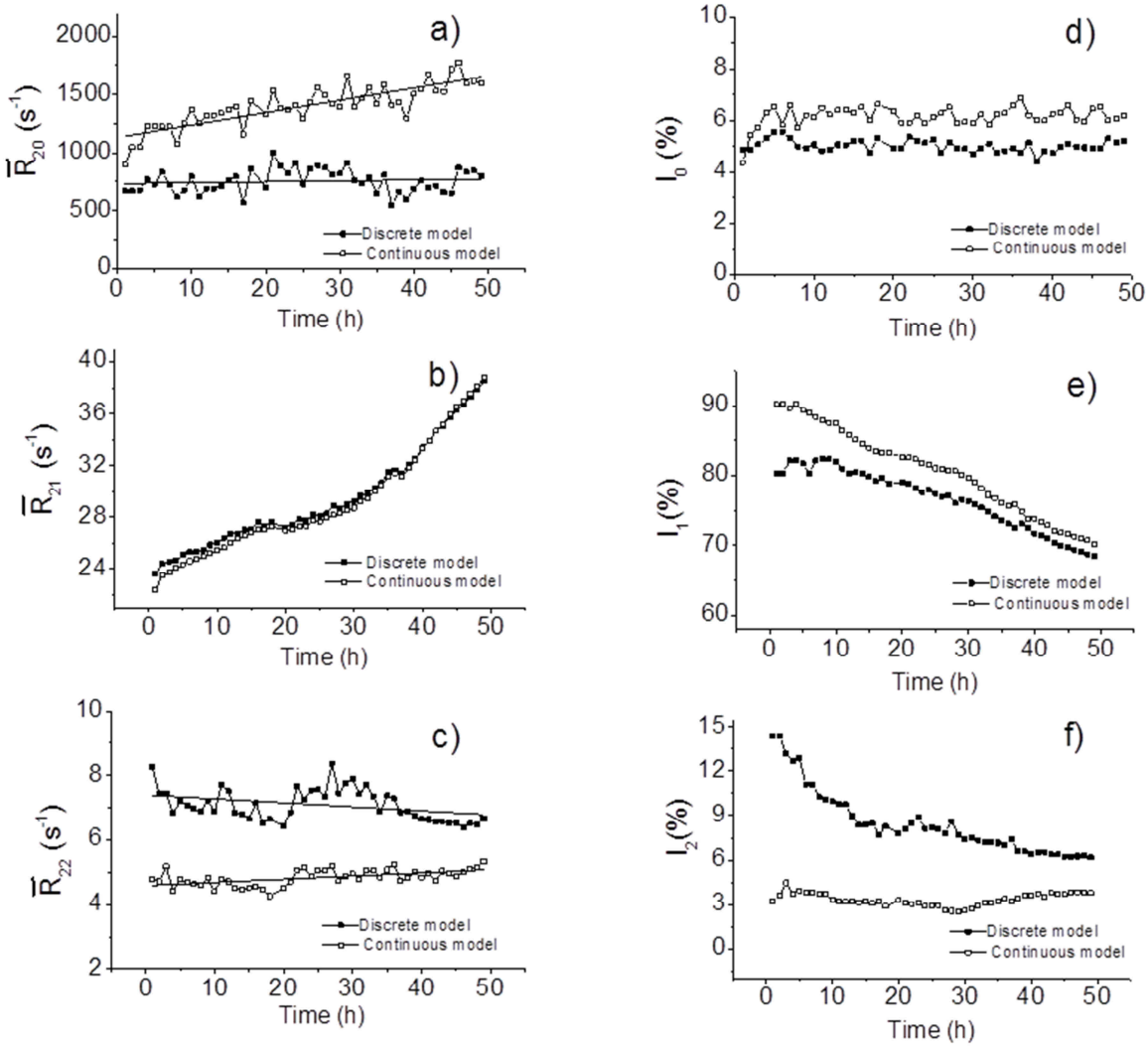
a)
$\bar{R}_{20}$ (s^{-1})
Time (h)
Discrete model
Continuous model
b)
$\bar{R}_{21}$ (s^{-1})
Time (h)
Discrete model
Continuous model
c)
$\bar{R}_{22}$ (s^{-1})
Time (h)
Discrete model
Continuous model
d)
I_0 (%)
Time (h)
Discrete model
Continuous model
e)
I_1 (%)
Time (h)
Discrete model
Continuous model
f)
I_2 (%)
Time (h)
Discrete model
Continuous model

Figure 4

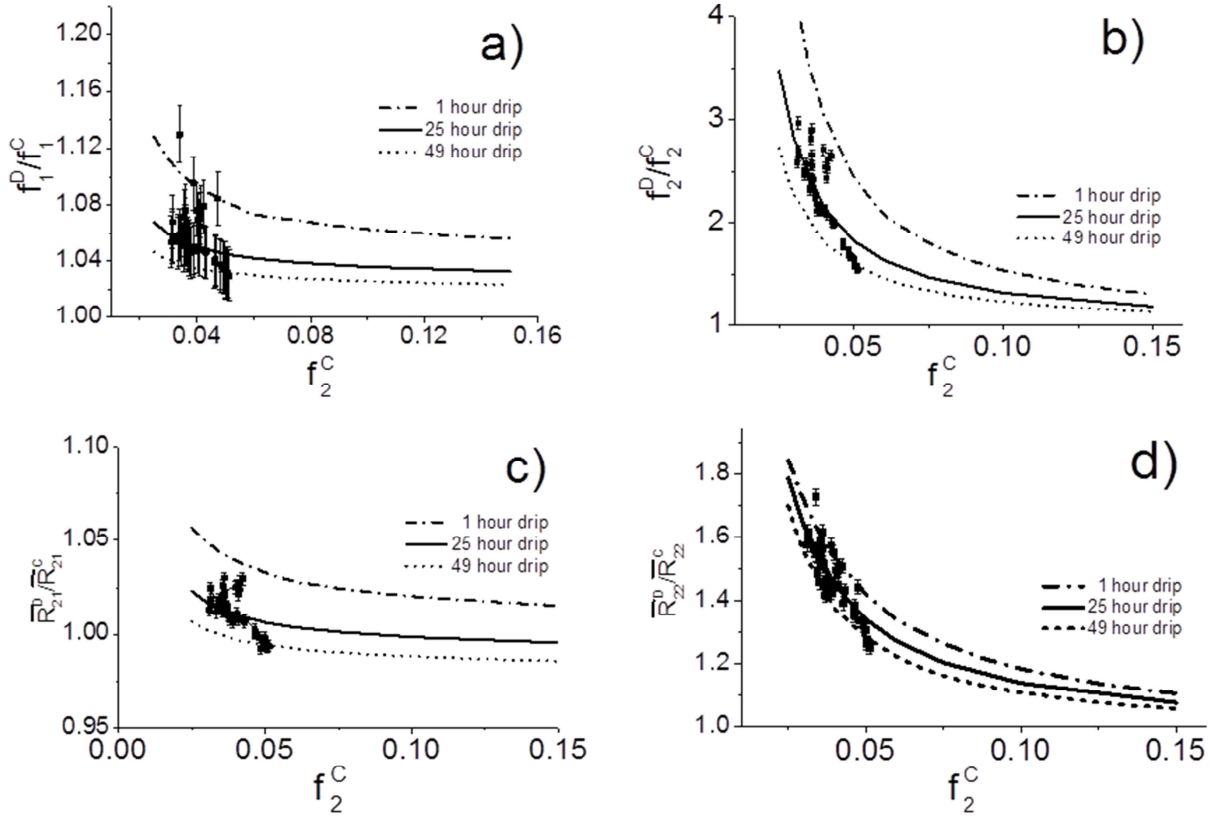

515

516 Figure 5

517

518

519

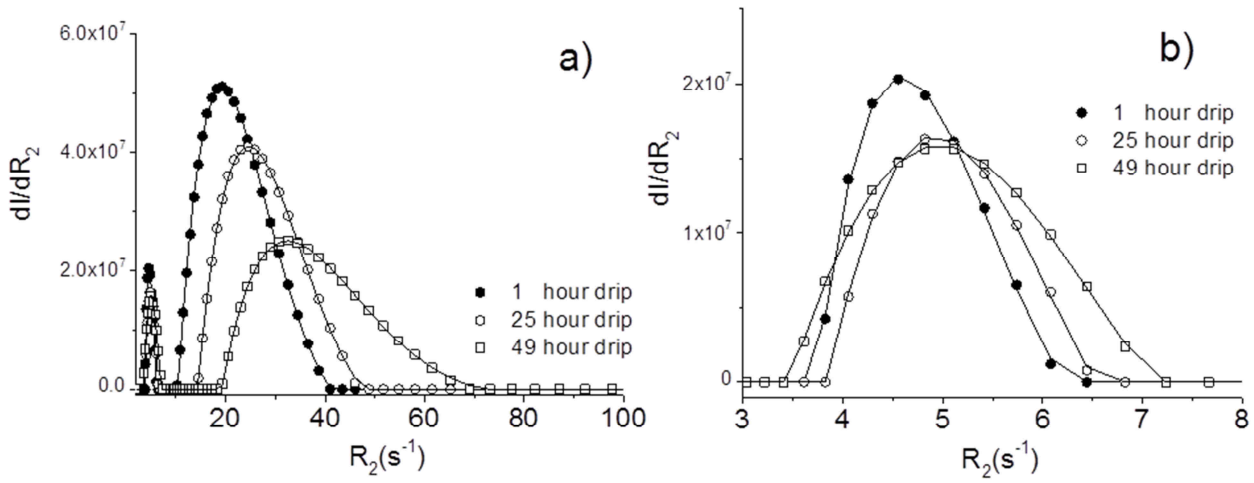

520
521 Figure 6

522

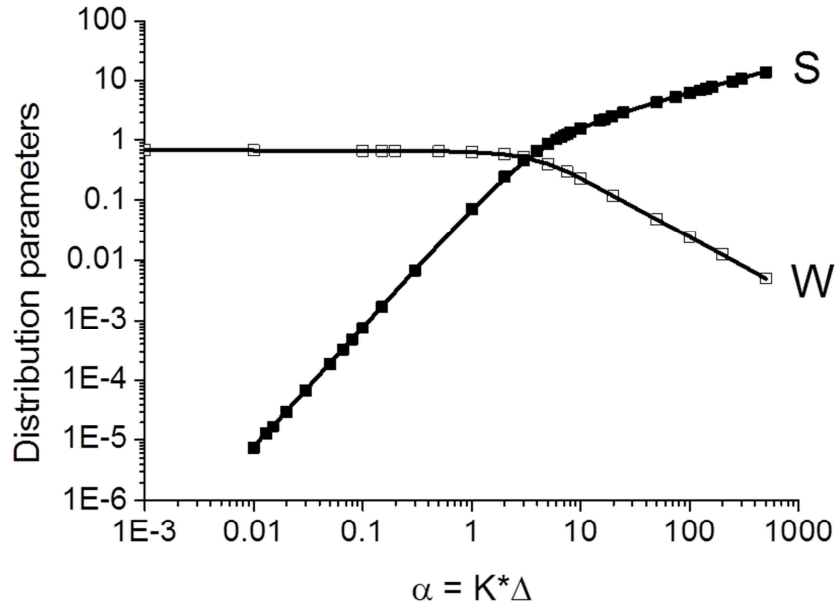

523
524 Figure 7
525

526
527

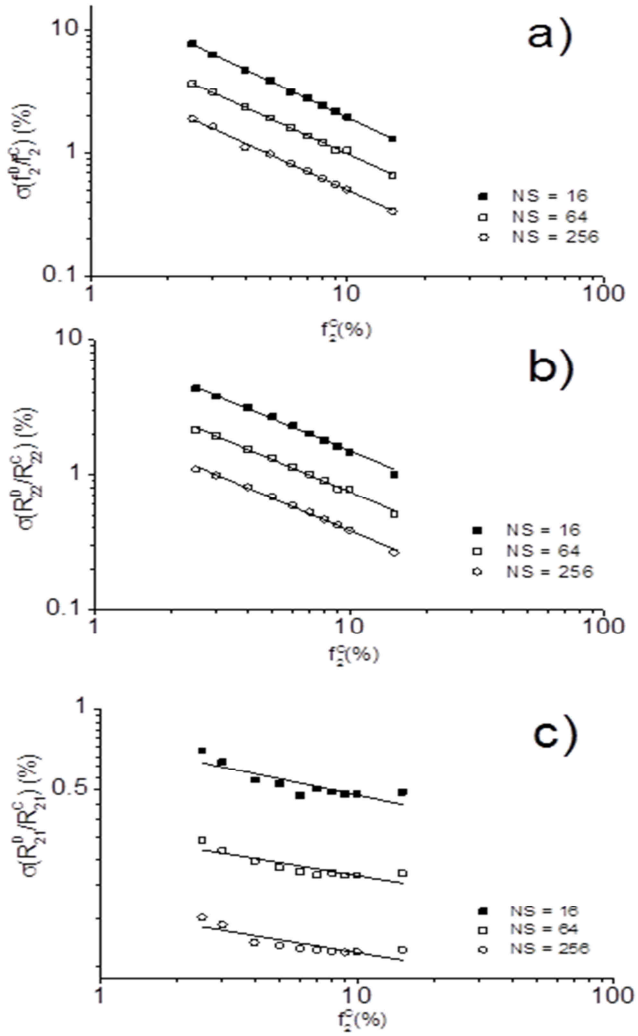

528
529
530 Figure 8

Paper IV

The potential for predicting purge in packaged meat using low field NMR

Han Zhu[1,2*], Eddy Walther Hansen[3], Marion O`Farrell[4], Petter Vejle Andersen[5], Per Berg[2], Bjørg Egelandsdal[1]

[1] Norwegian University of Life Sciences, 1430 Ås, Norway,

[2] Nortura SA, Lørenveien 37, 0585 Oslo, Norway,

[3] University of Oslo, Department of Chemistry, Postboks 1033 Blindern, 0315 Oslo, Norway,

[4] SINTEF ICT, Forskningsveien 1, 0373 Oslo, Norway,

[5] Nofima, Osloveien 1, 1430 Ås, Norway.

Abbreviations

CPMG, Carr-Purcel-Meiboom-Gill; LD, *longissimus dorsi*; *p.m.*, post mortem; PSE, Pale Soft Exudative; WHC, water holding capacity

[*] Corresponding author: Tel.: +4722844426

E-mail address: zhuhanchien@gmail.com

Abstract

The ability of NMR to predict purge from pork (*longissimus dorsi*) after vacuum-packed storage for 9 days was investigated. T_2 relaxation was measured at 24 h post mortem (*p.m.*) and again after 9 days chilled and vacuum-packed storage. Pearson correlation analysis showed that purge at day 9 correlated well ($p<0.05$) with several parameters at or before 24 h *p.m.* However, NMR measurements from day 1 *p.m.* were limited in predicting day-9 purge ($|r| = 0.37$-0.52). The root mean square error of linear regression (RMSD) was 1.31% (range: 1.15-7.69% purge) for purge using the relaxation time of intra-myofibrillar water (T_{21}) measured on day 1 *p.m.* ($r = -0.46$), corresponding to ±2.6% (2 x RMSD) prediction error of purge with 95% probability. This indicated that for purge production, the distribution and mobility of water in meat on day 1 *p.m.* may be of little relevance. Further tests were conducted to investigate this poor predictability, where NMR measurements of water mobility and distribution made on the same meat sample (taken at 96 h *p.m.*) during a 9-day storage period. By analyzing the T_{21} and T_{22} domains every day, during the 9 days of storage, it was revealed that during the first 5-day of storage, water (63%) moved from intra-myofibrillar space to extra-myofibrillar space. However, this movement did not result in detectable drip. A major liquid loss followed after 5 days. On days 8 and 9 an uptake of water occurred, causing water to return to the intra-myofibrillar space. The complexity of the water movement between domains during storage is investigated to further understand the poor prediction and to determine if it is possible to improve robustness of the prediction of day-9 purge using NMR.

Key words: Purge; Water holding capacity; NMR; Storage; Porcine *longissimus dorsi* muscles; Meat structure

1. Introduction

The drip loss of meat during chilled storage depends on the amount of water that is available and the ease with which the water can exit the muscle structural network (Warner, 2014). The drip loss of meat is influenced by four major structural factors: 1) the degree of myofibrils shrinkage during rigor and myofibrillar interfilamentous spacing; 2) the permeability of the cell membrane to water; 3) the degree of cytoskeletal protein degradation and 4) the development of drip channels and extracellular space (Hughes, Oiseth, Purslow, & Warner, 2014). Water holding capacity (WHC) is very often measured as drip loss; i.e. the weight loss percentage of a meat sample after a defined period of chilled storage (24 or 48 h) in specifically designed holder (Christensen, 2003) or in a plastic bag (Honikel, 1998), where the meat has no physical contact with drip. Purge, in this paper, refers to the weight loss from meat during storage, where the meat is in contact with the fluid. Purge is the accumulation of a red aqueous solution of proteins in packaged, refrigerated meat and relates to what would be visible to a consumer. Drip loss and purge are important variables relating to profitability and quality of meat products and are highly relevant to both meat industry and consumers. However, these two variables have been reported to be controlled by different processes. Drip loss shows the WHC of meat at certain time post mortem; whereas purge is likely to be the accumulative effect of changes in WHC during storage. Several experiments have recorded a change in drip loss from 24 h *p.m.* up to 14 days p. m. (Joo, Kauffman, van Laack, Lee, & Kim, 1999; Kristensen & Purslow, 2001; Moeseke & Smet, 1999; Straadt, Rasmussen, Andersen, & Bertram, 2007) using different methods (48 h Honikel bag method or 24 h centrifugation). In general, the measured drip loss (%) peaked at around 48 h post mortem and subsequently decreased. The daily drip loss post mortem seems to be animal/sample dependent. For instance, in the work of Kristensen and Purslow (2001), the average centrifugation loss of 6 muscles reached its maximum on day 7 *p.m.*, whereas the average centrifugation loss of 4 other muscles in the same work reached its maximum on day 3 *p.m.*

There exist two explanations regarding the decrease in rate of drip loss (increase in WHC) in meat that is stored in contact with its own drip:
1). The reduction in drip loss with sampling time post mortem is a result of "leaking out", i.e. the meat with poor WHC (i.e. pale soft exudative meat, PSE) will lose relatively more water early postmortem (Joo et al., 1999; Moeseke & Smet, 1999). This leaves limited water available for dripping in later stages. Meat with a normal WHC has relatively more water to lose in later stages and this water serves as a "drip reservoir" that will eventually produce similar amount of drip as meat with poorer WHC (Joo et al., 1999).

2). Degradation of cytoskeleton proteins can result in an increase of WHC later post mortem (Huff-Lonergan & Lonergan, 2005; Kristensen & Purslow, 2001; Melody et al., 2004; Straadt et al., 2007). Cytoskeleton proteins (represented by vinculin, desmin and talin) gradually degrade during 10-day *p.m.* storage period (Kristensen & Purslow, 2001). The inter-myofibrillar linkages and costameric connections are removed, and myofibril shrinkage becomes energetically less favorable. The flow of water into the extracellular space ceases, and previously expelled water can to some degree reverse, and support swelling of the myofibrils. The intramyofibrillar structure has been shown to be more homogeneous after 14 days of storage using a confocal laser scanning microscopy, which supported this hypothesis (Straadt et al., 2007).

There have been very few articles investigating the prediction of purge using data obtained early post mortem (Bidner et al., 2004; Calkins, Holthaus, Johnson, Eskridge, & Berg, 2005; Huff-Lonergan & Lonergan, 2005). As summarized by Huff-Lonergan & Lonergan (2005),

one study have studied using the desmin degradation on day 1 *p.m.* to predict purge loss over 7 days using stepwise regression models. It was found that desmin degradation accounted for only 24.1% variation of purge. Similarly, another study also showed poor prediction of purge using several measurements (21 % variation explained), which aimed at predicting 21-day purge in vacuum packaged whole pork loins using models based on variables measured early *p.m.* (including season, fat depth, muscle depth, hot carcass weight, color, pH and electrical impedance) (Calkins et al., 2005). It seems, therefore, that purge is challenging to predict due to the complexity of purge production process. Zarate and Zaritzky (1985) studied the effect of storage conditions on purge production in the package along storage time (until 22-day storage) in packaged refrigerated beef (cut at 48h *p.m.*). Two temperatures (0 and 4 ˚C) and two films (low density polyethylene and EVA/SARAN/EVA coextruded film) were studied and compared. During the first 24-hour storage (induction period), the purge (%) increased nonlinearly, and then the increase followed a reduced but constant rate. Similar results have been reported by Moeseke and Smet (1999) that the dripping rate decreased after 48 h post mortem. In addition, purge percentage was found to be linearly correlated to the equivalent area/unit volume ratio of the sample (Zarate & Zaritzky, 1985). Their work also suggested that the water that turned into purge during storage was located extracellularly and extramyofibrillarly, and the purge was mainly produced by gravitational force since the purge (%) rate is constant after induction time (Zarate & Zaritzky, 1985). They also refuted that diffusion is to explain the purge production, since a decreasing rate should be expected (Zarate & Zaritzky, 1985).

Since WHC increases with storage time, the WHC difference between meat with high or low initial WHC might decrease significantly towards later storage period, as shown in the study using meat with four different quality groups (Joo et al., 1999). However, the results showed that the meat with initial lower WHC (i.e. PSE) still had lower WHC on day 6 *p.m.* than meat that had a higher initial WHC. It is then reasonable to suggest that the accumulated purge of meat having an initial low WHC might be relatively high. This change in drip loss rate with time might make purge prediction difficult and demand methods with high and relevant analytical precision.

NMR is a powerful tool to study water mobility and distribution, and has been used extensively in studying meat structure and WHC. However, to the best of our knowledge, no studies have addressed the possibility of using NMR to measure purge. In this paper, we explored the ability of low field NMR and other measurements/variables obtained at or before 24 h *p.m.* to predict purge from pork muscle after vacuum-packed storage for 9 days. The 9-day storage period was chosen because it is the average storage time used for fresh meat cuts before displayed in retail stores according to Norwegian meat industry. The correlation between purge and variables obtained on samples after 9-day storage was also studied in order to: 1) determine the predictability of purge on day 9 from NMR measurements on day 1; 2) understand the purge production mechanism during the same number of days.

To support 1) and 2) the measurement error of the NMR instrumentation also needed to be verified to determine if NMR can measure a difference in water content between 80 % and 75 % water.

2. Materials and methods

2.1. Animals and sampling

In order to obtain meat samples with reasonable WHC variation, 18 pigs were selected from 2 different slaughterhouses (Tønsberg and Oslo, Norway) based on their meat percentage/ back

fat thickness during three weeks. The chilling rate affects drip loss and this can vary due to the meat percentage/ back fat thickness. The animals were, therefore, selected to give variation in fat thickness and two different chilling methods were carried out in the two slaughter houses. The pigs used had carcass weights between 56.1 to 100.1 kg. Breeds used were LYDD (25 % Landrace, 25 % Yorkshire and 50 % Duroc) and LYLL (25 % Yorkshire and 75 % Landrace). The pigs were stunned in an atmosphere with 90% carbon dioxide and slaughtered. At Tønsberg slaughterhouse, the carcasses were cooled for 30 min in the shock-cooler/freezer and then chilled down to 7 ˚C for 18 hours. At Oslo slaughter house, the carcasses were cooled for 18-20 h to below 7 ˚C, in a cooling room at 0-1˚C. The left porcine *longissimus dorsi* (LD) muscles were removed. Connective tissue and fat were carefully trimmed around the muscle.

The LD muscle from each animal was divided into two sections based on location (denoted L1 and L2, Figure 1a) with some space discarded between L1 and L2 (shown in grey, Figure 1a). The samples were treated as separate samples since a difference of WHC (as drip) has been reported between cranial and caudal ends (Taylor & Dant, 1971). For each location (L1 or L2), the muscle was divided as shown in Figure 1b on day 1 *p.m.*

The meat sample in the study of storage time effect (section 3.3) was randomly selected from one LD muscle of a young boar of Landrace and Duroc breed. The loin was cut at 96 h *p.m.*

2.2. Purge measurement

On day 1 p. m., a chop of 12 cm in thickness (for L1 and L2 each) towards cranial end was divided, weighed (M_0, of 348.21-860.55 g) and vacuum packed using a Intevac vacuum packing machine with internal programming level 6 (Bissendorf, Germany) in a plastic bag (shown as purge in Figure 1b). The vacuum packed muscles were stored at 4 ˚C until day-9 post mortem; surface dried with tissue paper and weighed again (M). Purge (%) was calculated as the weight loss in percentage of the initial muscle weight (Purge (%) = 100 x (M_0-M)/ M_0). Purge values varied between 1.15% and 7.69 % (Table 1).

2.3. pH and color measurements

The muscle pH was measured at different times post mortem (45 min, 5 h, 24 h and day-9). The pH at 45 min and 5 h *p.m.* was measured by placing a Knick Portamess 752 electrode (Berlin, Germany) approximately in the middle of the loin. The pH at 24 h and day-9 *p.m.* was measured on the sample using Beckman Φ31 pH Meter (Brea, USA). The sample used for purge measurement on day-9 post mortem was divided according to Figure 1c. Color parameter including L*, a* and b* were determined using a Konica Minolta Chroma meter CR-400 (Tokyo, Japan) after 1 hour blooming. Three measurements were taken for each slice. Relevant statistics for pH at different time post mortem and color values are shown in Table 1.

Table 1. Ranges, means and standard deviations of chemical-physical parameters of porcine *longissimus dorsi* samples.

	Range	Mean	Standard Deviation
pH 45 min (n=18)	6.09-6.73	6.46	0.16
pH 5 h (n=12)	5.61-6.09	5.90	0.15
pH D1 (day 1)	5.26-5.63	5.43	0.10
pH D9 (day 9)	5.30-5.47	5.39	0.04
Purge (%, day 9)	1.15-7.69	3.71	1.46
L* (day 9)	52.41-61.12	56.92	2.10
a* (day 9)	6.32-11.20	8.30	1.37
b* (day 9)	4.80-8.32	6.10	0.73

Note: the number of samples (n) was 36 unless otherwise stated

2.4. NMR measurement

Transverse relaxation (T_2) was measured on meat samples both day-1 (Figure 1b) and day-9 (Figure 1c) *p.m.* using a Maran Ultra NMR instrument (Resonance Instruments, Witney, UK), operating at a magnetic field strength of 0.54 T, corresponding to a proton resonance frequency of 23 MHz. The NMR signals were recorded by applying a traditional Carr-Purcel-Meiboom-Gill (CPMG) pulse sequence (Meiboom & Gill, 1958) with τ = 150 µs, 12 K echoes and 16 transients. Three cylindrical samples (16ø x 22 mm, ~2.80 g) were cored using a sharp cork borer for each location (L1 and L2), and samples were gently inserted in closed Teflon sample holders (2.2 cm in length), and placed within the homogeneous part of the rf-coil. The samples were thermostated at 25 ˚C for 10 min before CPMG measurements were performed.

The influence of storage time on a single meat sample (section 3.3) was also studied using another Maran Ultra NMR instrument (Resonance Instruments, Witney, UK) of the same magnetic field strength, but different sample size (~ 8ϕ x 10 mm, ~0.59 g). The meat sample was suspended in the NMR tube with the fiber direction parallel to the cylindrical axis. Enough space (17 mm) was reserved between the bottom of the NMR glass tube and the muscle. A layer of parafilm was placed on the top of the muscle to avoid water evaporation. The CPMG signal response was acquired and stored every day during a 9-day storage period, performed at T = 6 °C and equilibrated at this temperature for 10 minutes before initiating any experiment. Samples were stored at 4 °C when not subjected to measurements. The NMR measurement was performed with a τ = 50 µs, 32 K echoes and 32 transients. The parafilm was found to not contribute to the NMR signal. After 9 days of storage, one CPMG experiment was performed on the drip fluid by lifting the sample tube manually (only the drip fluid was within the transmitter/receiver coil).

2.5. Data analysis

Distributed exponential fitting analysis was performed on the obtained T_2 relaxation data. A continuous T_2 relaxation time distribution $dI/d\log(T_2)$ was first derived from the CPMG signal response using Maran Ultra algorithm (RI Win-DXP software release version 1.2.3, Resonance Instruments, Witney, UK), which was described by Bertram et al. (Hanne Christine Bertram, Dønstrup, Karlsson, & Andersen, 2002). I is the signal intensity of the NMR relaxation curve. Then a relaxation rate distribution $F(R_2)$ was obtained using the following transformation:

$$F(R_2) = \frac{dI}{dR_2} = \frac{dI}{d(LogT_2)} \cdot \frac{d(LogT_2)}{dR_2} = -\frac{T_2}{\ln 10} \cdot \frac{dI}{d(LogT_2)} \quad \text{with } R_2 = 1/T_2 \quad (1)$$

Three peaks were observed for all samples reflect the bound-, immobilized- and free water respectively. The overall relaxation distribution takes the form:

$$F(R_2) = \sum_{i=0}^{2} I_i F_i(R_2) \quad (2)$$

where I_i represents the signal intensity and $\overline{R}_{2i}$ represents the "mean" relaxation rate of component "i", i.e.:

$$\overline{R}_{2i} = \int_0^\infty R_2 F_i(R_2) dR_2 \Big/ \int_0^\infty F_i(R_2) dR_2 \quad (3)$$

where i = 0, 1 or 2, and $\overline{R}_{20} > \overline{R}_{21} > \overline{R}_{22}$. Using a distribution function written in Microsoft Excel 2010 (Microsoft Corporation, WA, USA), the derived relaxation rate distributions were closely fitted. Only the domains with the longer relaxation times (T_{21} and T_{22}) changed during storage (Hansen & Zhu, 2015), and were further discussed. The relaxation times T_{21} and T_{22} correspond to intra-myofibrillar water and extra-myofibrillar water respectively. The integrated areas of relaxation populations were normalized by sample mass (A_{21} and A_{22}), corresponding to T_{21} and T_{22}.

Correlation coefficients between variables ($P < 0.05$) were calculated using OriginPro 2016 (OriginLab Corporation, MA, USA).

3. Results and Discussion

3.1. Univariate Correlation Analysis

The Pearson correlation coefficients (r) for the measured variables can be seen in Table 2. Purge (%) was found to be more correlated to the following parameters: pH D1 (-0.46), pH D9 (-0.33), a* (-0.38), b* (-0.42), T_{21}-D1 (-0.46), T_{22}-D1 (-0.37), A_{21}-D1 (-0.43), A_{22}-D1 (0.52) and T_{21}-D9 (-0.70). Correlations between ultimate pH (pH D1) and purge in vacuum packages (7-day) have been reported with a similar correlation (r = -0.49) to the current study (Bidner et al., 2004). For color measurements, significant correlations were found between L* and b*, as well as a* and b* at $p<0.05$ (Table 2). Significant positive correlations regarding same color parameters (L* and b*, a* and b*) have been reported for beef *longissimus thoracis* muscle by Leroy et al. (Leroy et al., 2003). Interestingly, among all the color parameters, only a* (measuring redness to greenness) correlated better with the NMR parameters. This may indirectly be due to pH variation (Table 1). Another interesting observation was the decrease in pH *p.m.* when an increase was expected due to amino acid degradation.

Table 2 Pearson correlation coefficients (r) between measured variables.

	pH 5 h	pH D1 (day 1)	pH D9 (day 9)	Purge (%)	L*	a*	b*	T_{21}-D1 (s)	T_{22}-D1 (s)	A_{21}-D1	A_{22}-D1	T_{21}-D9 (s)	T_{22}-D9 (s)	A_{21}-D9	A_{22}-D9
pH 45 min	**0.64**	-0.07	-0.30	-0.29	0.09	-0.11	0.20	-0.26	-0.04	0.13	-0.20	0.02	-0.25	-0.12	0.12
pH 5 h		0.29	0.27	-0.32	-0.22	-0.01	0.19	-0.15	0.05	0.19	**-0.47**	0.39	0.06	-0.06	-0.03
pH D1 (day 1)			**0.52**	**-0.46**	-0.02	**0.59**	0.26	**0.51**	0.32	**0.33**	**-0.52**	**0.63**	**0.40**	-0.13	0.13
pH D9 (day 9)				**-0.33**	-0.28	0.30	-0.06	**0.40**	**0.36**	0.31	**-0.43**	**0.54**	**0.54**	-0.07	0.10
Purge (%)					-0.22	**-0.38**	**-0.42**	**-0.46**	**-0.37**	**-0.43**	**0.52**	**-0.70**	-0.29	0.03	-0.28
L*						0.01	**0.41**	0.04	0.21	-0.04	-0.03	-0.01	-0.16	0.13	0.06
a*							**0.49**	**0.51**	**0.39**	**0.44**	**-0.46**	**0.54**	**0.46**	-0.02	0.16
b*								0.14	0.15	0.21	-0.26	0.24	0.11	0.03	0.12
T_{21}-D1 (s)									**0.60**	**0.52**	**-0.50**	**0.65**	**0.62**	0.12	-0.10
T_{22}-D1 (s)										**0.73**	**-0.72**	**0.52**	**0.58**	0.18	-0.10
A_{21}-D1											**-0.84**	**0.43**	**0.54**	0.03	-0.17
A_{22}-D1												**-0.59**	**-0.61**	-0.06	0.15
T_{21}-D9 (s)													**0.56**	0.24	0.13
T_{22}-D9 (s)														**0.41**	**-0.49**
A_{21}-D9															**-0.54**

Notes: T_{21}-D1 and T_{22}-D1 are relaxation time constants measured on day 1 *p.m.* A_{21}-D1 and A_{22}-D1 are areas of each domain normalized by sample mass, measured on day 1 *p.m.* T_{21}-D9 and T_{22}-D9 are relaxation time constants measured on day 9 *p.m.* A_{21}-D9 and A_{22}-D9 are areas of each domain normalized by sample mass, measured on day 9 *p.m.*

$P < 0.05$, all the significant correlation coefficients are marked in bold.

The longest spin-spin relaxation time (T_{22}) corresponds to water that resides outside the myofibrillar protein network, which is most susceptible to dripping (H. C. Bertram, Purslow, & Andersen, 2002). T_{22} has been investigated as a reference value for WHC (at 24 h *p.m.*) in a previous study, which was based on drip loss (Zhu et al., 2016), but T_{22} did not show a good prediction ability towards purge after storage. The correlation coefficient between T_{22} measured on day-1 *p.m.* and purge was -0.37 (Table 2) and therefore nominally lower than the correlation given for T_{21} above (r = -0.46, RMSD = 1.31%, of 1.15-7.69% purge). In principle this indicated that purge can be predicted as ±2.6% (2 x RMSD) with 95% probability. The normalized area of the two domains, A_{21}-D1 (r = -0.43, RMSD = 1.33%, of 1.15-7.69% purge) and A_{22}-D1 (r = 0.52, RMSD = 1.27%, of 1.15-7.69% purge) also correlated to purge, which indicates that both domains are relevant regarding purge production. The measurement error in purge using the current method is unfortunately unknown. However, error of purge loss on beef steaks (~0.23 kg) was estimated to be 3-4 % (Elam, Brooks, Morgan, & Ray, 2002). The error in water mass (g) predicted by NMR total intensity measured on 20 meat samples from 1 loin was 0.019 g (~ 2.150 g H_2O in meat sample of mass 2.87 g, r = 0.9945), assuming 75 % of water in the meat samples (data not shown). This indicates that NMR has the ability to discriminate meat samples that has water content difference of 1.77%, with 95% probability. This actually suggests that the purge can be predicted but that the major reason for the lack in predictability of NMR variables is due to the low reproducibility of NMR on heterogeneous samples like meat. This could be improved using the average of several samples or increasing the size of the samples.

The shorter spin-spin relaxation time (T_{21}) corresponds to intra-myofibrillar water. T_{21} could not alone predict purge (Table 2) with high accuracy. Multivariate models, using different variables in Table 2, were also investigated, but no improvement in correlation was obtained. One explanation as to why it is difficult to predict purge from early post mortem measurements is that there is a sum of events related to water mobility that occur during the storage period (Moeseke & Smet, 1999), which results in changes in the drip rates with storage time (i.e. 1-9 days). To explore these further, T_2 characteristics from day 1 and day 9 were compared.

3.2. T_2 characteristics on day 1 and day 9 *p.m.*

As shown in Figure 2, both T_{21} and T_{22} decrease after 9-day storage (slope <1, $p<0.05$). The change in T_2 relaxation times reflects the change in mobility of water molecules, shorter T_2 indicated water that has lower mobility and *vice versa*. The decrease in T_{21} and T_{22} indicates a decrease in both intra-myofibrillar and extra-myofibrillar water mobility. Straadt et al. (2007) also observed a decrease in T_{21} after 7-day storage, as well as a change in width of the T_{21} distribution. The T_{21} width in their studies decreased at day 7 (and day 14) compared to day 1 *p.m.*, indicated a more homogeneous characteristics of intra-myofibrillar water, presumably due to swelling (Straadt et al., 2007). Similarly, a decrease in T_{21} width (calculated as full width at half maximum height) has been observed in the current study when comparing day 1 and day 9 post mortem (data not shown). T_{22} has been shown to reflect the width of gaps between meat fiber bundles, and to correlate positively with drip loss measured at short time intervals (Tornberg, Andersson, Göransson, & von Seth, 1993). Thus the observed decrease in T_{22} after 9-day storage indicates a decrease in drip loss or, in other words, an increase in WHC. The range of T_{22} among samples decreased after 9 days of storage, which indicated that the spread in WHC of meat samples has decreased. Our results are in accordance with the findings of Joo et al. who has also reported a reduced spread in WHC after storage (Joo et al., 1999). The area of T_{21} and T_{22} was normalized by sample mass, and the difference was calculated between day 1 and day 9. There was an average increase of T_{21} area by 2.4%, and

an average decrease of T_{22} area by 36.1% observed on day 9 compared to day 1 p. m. The relative small change in T_{21} area is somewhat expected, since the water representing the T_{21} domain (intra-myofibrillar water) is about 85% of total water in the meat, a big absolute change might appear to be small when it is shown on the relative scale. The decrease in T_{22} domain is most likely a result of fluid dripping out. Drip formation mechanism early post mortem has been discussed by Bertram et al. (2004). NMR characteristics were measured on porcine *longissimus dorsi* muscle continuously for 24 hours. They suggested that during early post mortem, muscle cells swell within 2-3 h *p.m.* (increase in T_{21}), and then expel water into extra-myofibrillar space (increase in T_{22} area) which reflect potential drip loss. Unlike early p. m., structural changes during storage for a longer period is different. As explained by Kristensen and Purslow (2001), within 24 h storage, water flows from intra- to extracellular water compartment due to pressure. After several days of storage, the shrinkage of myofibrils is halted due to slow degradation of cytoskeletal connections, and extracellular water is able to flow into myofibrils. The increase in the area of T_{21} domain (intra-myofibrillar water) support inflow of water at longer storage times (9-day storage). During the 9-day storage, the meat was vacuum packed, and the meat surface was in contact with the drip fluid at all times. It is thus suggested that the uptake of extra-myofibrillar water became possible not only from T_{22} water domain, but also from drip fluid if in contact with the meat. To verify this hypothesis, an experiment was designed and results presented in section 3.3.

3.3. T_2 characteristics during storage

In order to study the effect of storage time on continuous purge production and verify that the area change of myofibrillar water was partly due to the inflow of water from the extracellular space, a meat sample was inserted into an NMR tube and measured every day during storage at 4 ˚C for 9 days. The relaxation distribution of the meat sample during storage is shown in Figure 3. Since enough space was reserved between meat sample and the bottom of the NMR tube, drip fluid could flow freely to the bottom of the NMR tube and did not interact with the meat after it had dripped. The sample ends were not fixed which enabled natural muscle contraction.

Figure 4. a and b show the decrease in T_2 during 9 days of storage , which is in accordance with the observation mentioned in section 3.2, indicating more restricted mobility of water in both domains. The decrease in T_{21} followed a constant rate until day 7, after which T_{21} remained constant. A noticeable decrease in T_{22} took place between day 1 and day 2. The area of each domain was also plotted along storage time (Δ in Figure 4 a-b). The accumulated decrease in the area of T_{21} and T_{22} domains was considered to be drip and was plotted against storage time in Figure 4 c. The change of area of the two domains indicating water movement along storage time can be divided into three phases (shown as 1-3 in Figure 4), and will be addressed accordingly.

The first phase was the exchange between intra- and extra-myofibrillar water, took place from day 1 to day 5. The area of the T_{21} domain decreased while the area of the T_{22} domain increased from day 1 to day 5 (Δ in Figure 4 a-b). The increase in the area of the T_{22} domain accounted for 63% of decrease in area of T_{21} domain on the day 5 of storage. The area changed in both domains and indicated that water movement within the first 5 days of storage was mainly water exchange between domains. This is illustrated by a slow decrease in the total area loss (Figure 4 c), i.e. slow drip loss. This observation is not consistent with the findings of Zarate and Zaritzky (1985), who reported a high purge production rate during the first 24 h storage, followed by a lower and then constant rate after 5 days. The difference can be explained by the difference in sample history and sample preparation. The sample in this

study was cut at 96 h *p.m.*, while in Zarate and Zaritzky (1985), the samples were cut at 48 h *p.m.* The initial fast purge loss may have been released in current experiment right after cutting. The experimental setup by Zarate and Zaritzky (1985) was meat wrapped in plastic film, which enabled the inflow of water from purge fluid, while in the setup in this study; the meat sample was separated from purge fluid. The second phase was the extra-myofibrillar water being releases as drip (day 5-7). In this phase, both T_{21} and T_{22} area decreased continuously (Figure 4 a-b). Significant purge occurred during this phase, indicated by the decrease in the total area (Figure 4 c). The third phase was water flowing back (inflow) from extra-myofibrillar domain to intra-myofibrillar domain. The decrease in total area loss slowly decreased on day 8 and day 9. There was an obvious increase in T_{21} area on day 8-9 of storage (Δ in Figure 4 a). A similar NMR study, with the same experimental setup regarding in situ drip-loss in an NMR tube (45 hours) was conducted on a *longissimus dorsi* (Hansen & Zhu, 2015). In this case a dynamic model was suggested where the gross migration of macromolecules and water molecules is irreversible. The dynamic model occurs in the following sequence: water flows from the intermediate relaxation domain (intra-myofibrillar) to the slow relaxation domain (extra-myofibrillar), and then moves out as drip. The results can be applied to early storage time, when inflow of water from extra-myofibrillar is not yet enabled due to existence of shrinking pressure. In the present study, the increase in T_{21} area (day 8) suggested an inflow of liquid from T_{22} domain directly, presumed due to the degradation of cytoskeletal structure and thereby inflow of extra-myofibrillar water. This liquid inflow then might account for the nominal area difference between early and later postmortem in T_{21} domain reported in section 3.2. The relaxation distribution of the drip fluid in the bottom of the NMR tube was also analyzed at the end of the experiment. There was mainly one domain present with a relaxation time of 0.216 s, which resembles T_{22} in meat. Thus it is reasonable to suggest that the some intake of water from drip fluid into myofibril water compartment is possible.

It is, therefore, suggested that purge at a later time storage (i.e. 9 days) might be better predicted after a few days of storage (i.e. 5 days) using NMR, or when the water transport is mainly flowing out rather than exchanging between domains. In this later phase, the water will flow out as drip from both domains, and the NMR signal will not be disturbed by water exchanging between domains. This topic is under further investigation.

4. Conclusions

A number of quality parameters measured early postmortem appeared to correlate well with purge measured on day 9 *p.m.* T_{21} measured on day 1 *p.m.* correlated negatively to purge (r = -0.46, RMSD = 1.31% with a purge range of 1.15-7.69%). Area of both T_{21} (r = -0.43, RMSD = 1.33%, of 1.15-7.69% purge) and T_{22} domains (r = 0.52, RMSD = 1.27%, of 1.15-7.69% purge) correlated to purge, i.e. both domains contributed to purge. However, the prediction ability was limited, showing that water mobility and distribution on day 1 *p.m.* might be of little value with regards to purge production.

Further analysis on a meat sample (taken at 96 h *p.m.*) was measured daily using NMR to monitor the changes in water mobility and distribution in both T_{21} and T_{22} domains for 9 days. The results indicated complex water movement during storage, which might serve an explanation for the poor prediction of purge in the package from early p. m. data. The water movement can be divided into three phases. During the first phase (day 1-5), water movement was mainly due to a shrinking pressure, from intra-myofibrillar water space to the free water domain. Significant purging of this free water occurred during the second phase (day 5-7). In

the last phase (day 7-9), the increase in T_{21} area indicated an inflow of water to the intra-myofibrillar water domain, due to degradation of cytoskeletal structure. At the end of the storage period, the mobility (indicated by T_2 values) of intra-myofibrillar water and free water decreased, and the spread in WHC among meat samples decreased.

In conclusion, it is believed that the complexity of water mobility and distribution during storage requires to be taken into account if robust predictions of 9-day purge are to be achieved. Initial investigation reveals that robustness may be increased by being more selective about when measurements are taken during storage, especially if the meat is in contact with its own drip water.

Conflict of interest

The authors declare no conflict of interest.

Acknowledgements

We want to thank the Research Council of Norway for financial support through the project "On line determination of water retaining ability in pork muscle" (project number 229192), also Norwegian Levy on Agricultural Products and the Agricultural Agreement Research Fund of Norway for financial support through the project "H_2O Monitor - Monitoring water holding capacity mechanisms of meat", project number 233910.

References

Bertram, H. C., Dønstrup, S., Karlsson, A. H., & Andersen, H. J. (2002). Continuous distribution analysis of T_2 relaxation in meat—an approach in the determination of water-holding capacity. *Meat Science, 60*(3), 279-285.

Bertram, H. C., Purslow, P. P., & Andersen, H. J. (2002). Relationship between meat structure, water mobility, and distribution: a low-field nuclear magnetic resonance study. *Journal of Agricultural and Food Chemistry, 50*(4), 824-829.

Bertram, H. C., Schäfer, A., Rosenvold, K., & Andersen, H. J. (2004). Physical changes of significance for early post mortem water distribution in porcine M. longissimus. *Meat Science, 66*(4), 915-924.

Bidner, B. S., Ellis, M., Brewer, M. S., Campion, D., Wilson, E. R., & McKeith, F. K. (2004). Effect of ultimate pH on the quality characteristics of pork. *Journal of Muscle Foods, 15*(2), 139-154.

Calkins, C. R., Holthaus, T. W., Johnson, R. C., Eskridge, K. M., & Berg, E. P. (2005). Rapid Methods to Predict Lean Quality Attributes in Pork (A. S. Department, Trans.) *Nebraska Swine Reports* (pp. 36-39): University of Nebraska - Lincoln.

Christensen, L. B. (2003). Drip loss sampling in porcine m. longissimus dorsi. *Meat Science, 63*(4), 469–477.

Elam, A. T., Brooks, J. C., Morgan, J. B., & Ray, F. K. (2002). Yield and Fabrication Time for Value Added Beef from the Chuck and Round. Retrieved from http://www.ansi.okstate.edu/research/research-reports-1/2002/2002-4%20Elam%20Research%20Report.pdf

Hansen, E. W., & Zhu, H. (2015). New insight into the dynamics of water and macromolecules in meat during drip as probed by proton CPMG NMR. *International Journal of Research and Reviews in Applied Sciences, 23*(3), 207-220.

Honikel, K. O. (1998). Reference methods for the assessment of physical characteristics of meat. *Meat Science, 49*(4), 447-457.

Huff-Lonergan, E., & Lonergan, S. M. (2005). Mechanisms of water-holding capacity of meat: The role of postmortem biochemical and structural changes. *Meat Science, 71*(1), 194-204.

Hughes, J. M., Oiseth, S. K., Purslow, P. P., & Warner, R. D. (2014). A structural approach to understanding the interactions between colour, water-holding capacity and tenderness. *Meat Science, 98*(3), 520-532.

Joo, S. T., Kauffman, R. G., van Laack, R. L. J. M., Lee, S., & Kim, B. C. (1999). Variations in Rate of Water Loss as Related to Different Types of Post-rigor Porcine Musculature During Storage. *Journal of Food Science, 64*(5), 865-868.

Kristensen, L., & Purslow, P. P. (2001). The effect of ageing on the water-holding capacity of pork: role of cytoskeletal proteins. *Meat Science, 58*(1), 17-23.

Leroy, B., Lambotte, S., Dotreppe, O., Lecocq, H., Istasse, L., & Clinquart, A. (2003). Prediction of technological and organoleptic properties of beef Longissimus thoracis from near-infrared reflectance and transmission spectra. *Meat Science, 66*(1), 45–54.

Meiboom, S., & Gill, D. (1958). Modified Spin-Echo Method for Measuring Nuclear Relaxation Times. *Review of Scientific Instruments, 29*(8), 688-691.

Melody, J. L., Lonergan, S. M., Rowe, L. J., Huiatt, T. W., Mayes, M. S., & Huff-Lonergan, E. (2004). Early postmortem biochemical factors influence tenderness and water-holding capacity of three porcine muscles1. *Journal of Animal Science, 82*(4).

Moeseke, W. V., & Smet, S. D. (1999). Effect of time of deboning and sample size on drip loss of pork. *Meat Science, 52*, 151–156.

Straadt, I. K., Rasmussen, M., Andersen, H. J., & Bertram, H. C. (2007). Aging-induced changes in microstructure and water distribution in fresh and cooked pork in relation to water-holding capacity and cooking loss – A combined confocal laser scanning microscopy (CLSM) and low-field nuclear magnetic resonance relaxation study. *Meat Science, 75*(4), 687-695.

Taylor, A. A., & Dant, S. J. (1971). Influence of carcass cooling rate on drip loss in pigmeat. *International Journal of Food Science & Technology, 6*(2), 131-139.

Tornberg, E., Andersson, A., Göransson, Å., & von Seth, G. (1993). Water and fat distribution in pork in relation to sensory properties. In E. Puolanne., D. I. Demeyer, M. Ruusunen. & S. Ellis (Eds.), *Pork quality: genetic and metabolic factors* (pp. 239–258). Helsinki: Oxon: CAB International.

Warner, R. (2014). Measurement of meat quality | Measurements of Water-holding Capacity and Color: Objective and Subjective A2 - Dikeman, Michael. In C. Devine (Ed.), *Encyclopedia of Meat Sciences (Second Edition)* (pp. 164-171). Oxford: Academic Press.

Zarate, J. R., & Zaritzky, N. E. (1985). Production of Weep in Packaged Refrigerated Beef. *Journal of Food Science, 50*(1), 155-159.

Zhu, H., O'Farrell, M., Bouquet, G., Lunde, K., Egelandsdal, B., Alvseike, O., Berg, P., Gjerlaug-Enger, E., Hansen, E. W. (2016). Evaluating nuclear magnetic resonance (NMR) as a robust reference method for online spectroscopic measurement of water holding capacity (WHC). *Journal of Food Engineering, 175*, 51-57.

Highlights

1. A number of quality parameters measured early postmortem appeared to correlate well with purge from pork meat (longissimus dorsi) after vacuum-packed storage for 9 days.

2. NMR measurements from day 1 *p.m.* were limited in predicting day-9 purge, indicating that for purge production, the distribution and mobility of water in meat on day 1 post mortem may be of little relevance.

3. The complex water movement between domains during storage might explain the poor prediction using NMR.

Graphical abstract

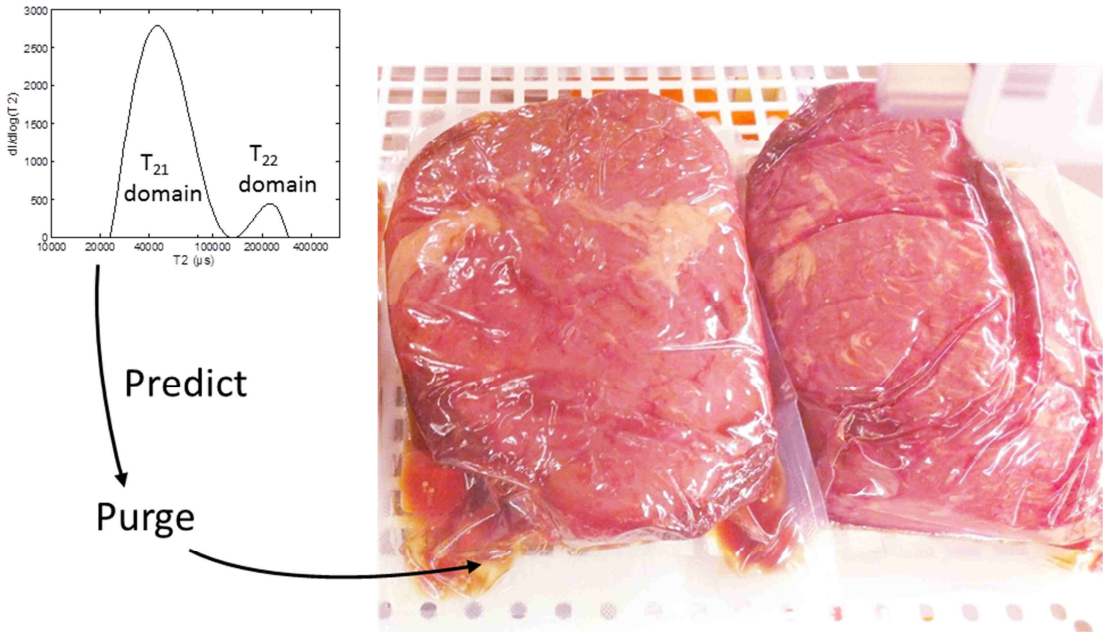

Figure captions

Figure 1. a) The left porcine LD muscle was divided to 2 sections (L1 and L2) at 24 h *p.m.* A slice of ~ 5 cm was discarded by both cranial and caudal end (shown in grey). Two chops of 20 cm thick each was then cut near cranial (L1) and caudal ends (L2). b) Division of L1 (or L2) at 24 h post mortem. A slice of 2.5 cm towards the caudal end was divided for NMR measurements, and a chop of 12 cm towards cranial end was divided for purge measurements. c) After 9 days of chilled storage, the muscle was divided for different measurements. A slice of 2.5 cm (towards caudal end) was cut for NMR measurements, and another slice of 2.5 cm (towards cranial end) was cut for color measurements (L*, a* and b*).

Figure 2. Correlations between T_{21} (a) and T_{22} (b) on day 1 (D1) and day 9 (D9) post mortem, respectively. Purge values (%) were marked above each data point. The correlation coefficients were shown in Table 2.

Figure 3. Relaxation time distribution (2 components) of water in meat as a function of storage time during 9 days of chilled storage, as derived by inverse integral transformation of the observed CPMG response curve. The figures are shown in a color scale from the start of experiment (dark blue) towards the end of the experiment (red).

Figure 4. a). T_{21} and its area, b). T_{22} and its area along storage time. c). Decrease in total area (%) of storage on each day compare to storage on day 1. In each figure, three phases are marked according to water movement: (1). exchange between intra-and extra-myofibrillar water; (2). extra-myofibrillar water moves out as drip; (3). water inflow from extra-myofibrillar domain to intra-myofibrillar domain.

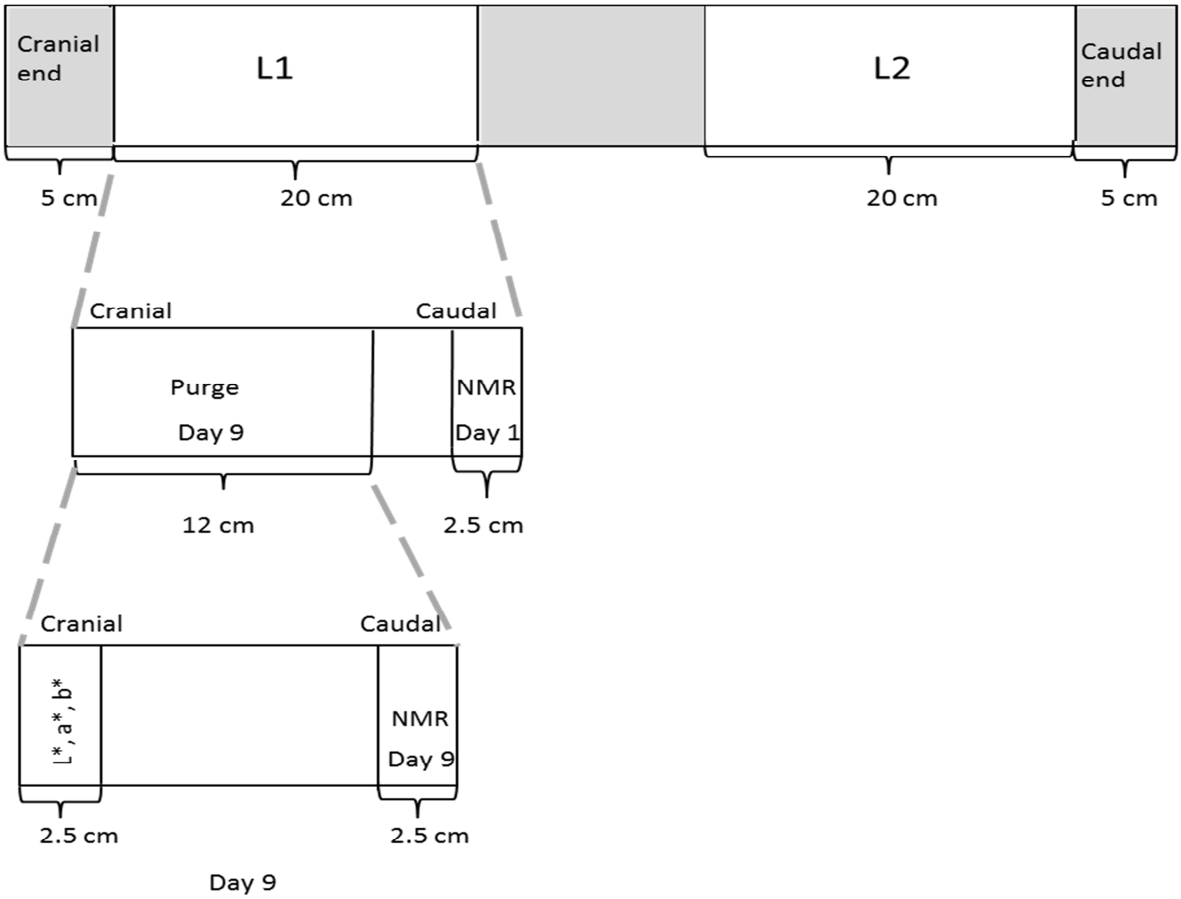
Cranial end
L1
L2
Caudal end
5 cm
20 cm
20 cm
5 cm
Cranial
Caudal
Purge
Day 9
NMR
Day 1
12 cm
2.5 cm
Cranial
Caudal
L*, a*, b*
NMR
Day 9
2.5 cm
2.5 cm
Day 9

Figure 1

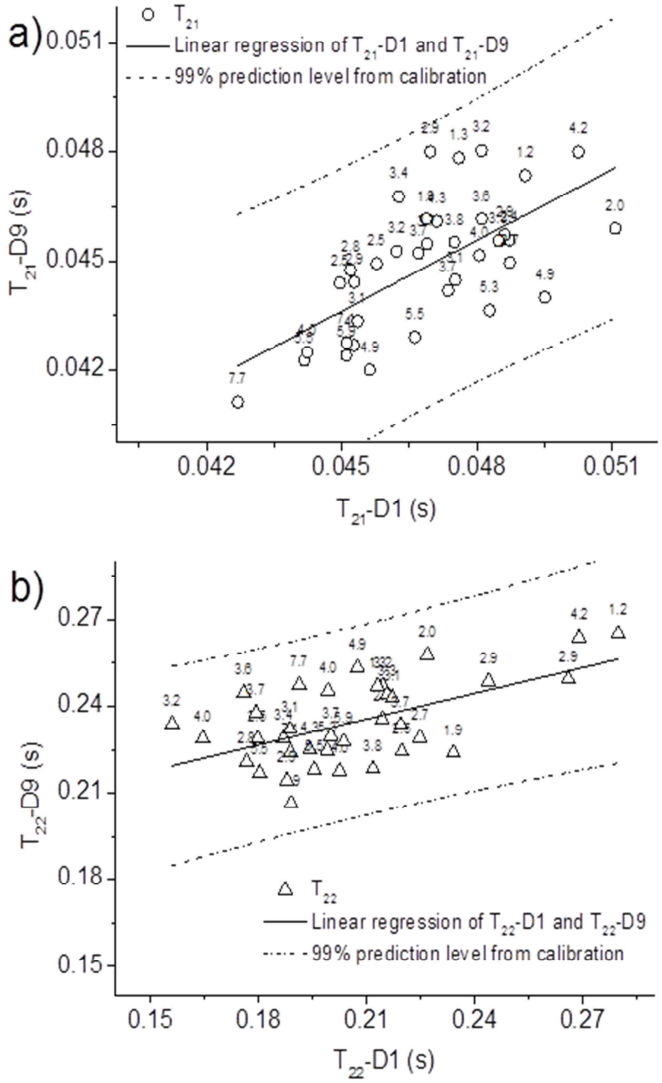
a)
T_{21}
Linear regression of T_{21}-D1 and T_{21}-D9
99% prediction level from calibration
T_{21}-D9 (s)
T_{21}-D1 (s)
0.042
0.045
0.048
0.051
b)
T_{22}
Linear regression of T_{22}-D1 and T_{22}-D9
99% prediction level from calibration
T_{22}-D9 (s)
T_{22}-D1 (s)
0.15
0.18
0.21
0.24
0.27

Figure 2

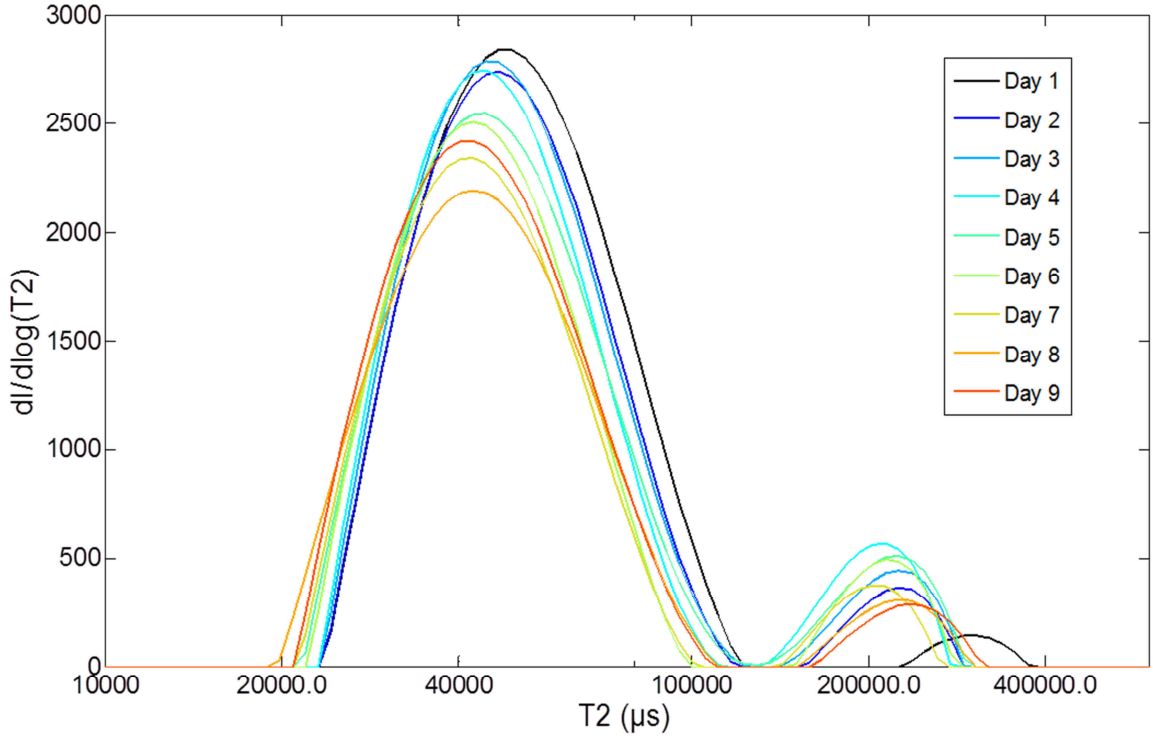
3000
2500
2000
1500
1000
500
0
dI/dlog(T2)
10000
20000.0
40000
100000
200000.0
400000.0
T2 (µs)
Day 1
Day 2
Day 3
Day 4
Day 5
Day 6
Day 7
Day 8
Day 9

Figure 3

290

291

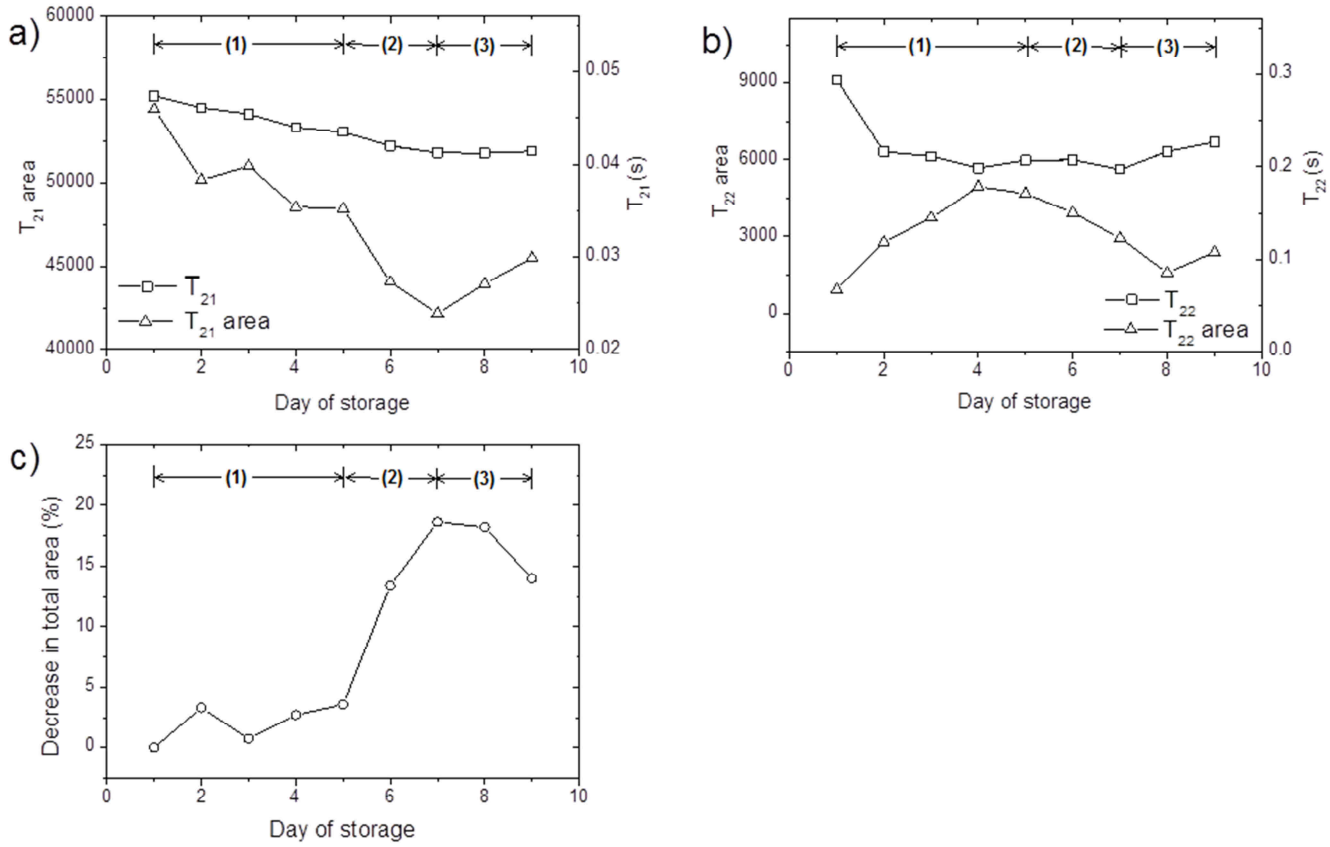

292

293 Figure 4